

2
2007



This is to certify that the
dissertation entitled

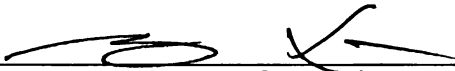
MODELING AND CONTROL FOR MICRO AND NANO
MANIPULATION

presented by

UCHECHUKWU C. WEJINYA

has been accepted towards fulfillment
of the requirements for the

Ph.D. degree in ELECTRICAL AND
COMPUTER ENGINEERING


Major Professor's Signature

8/22/07
Date

PLACE IN RETURN BOX to remove this checkout from your record.
TO AVOID FINES return on or before date due.
MAY BE RECALLED with earlier due date if requested.

DATE DUE	DATE DUE	DATE DUE

MODELING AND CONTROL FOR MICRO AND NANO MANIPULATION

By

Uchechukwu C. Wejinya

A DISSERTATION

Submitted to
Michigan State University
in partial fulfillment of the requirements
for the degree of

DOCTOR OF PHILOSOPHY

Department of Electrical and Computer Engineering

2007

ABSTRACT

MODELING AND CONTROL FOR MICRO AND NANO MANIPULATION

By

Uchechukwu C. Wejinya

Manipulation of micro and nano entities implies the movement of micro and nano entities from an initial position (location) to the desire position (location). This operation is not only necessary, but a required task with great precision. The tools needed for the manipulation needs to be chosen properly because the capabilities of the human hand are very restricted. Smart micro and nano manipulation are becoming of great interest in many applications including medicine and industry. In industry, high precision manipulation systems are especially needed for mass production of both micro and nano systems which consist of different component in respective scales. The transition from assembling and manipulating micro and nano entities manually to mass products with high quality is only attainable by automated assembly and manipulation systems. An example is the testing of integrated circuits which can be carried out by exchanging the manipulation tool by an electric probe. Furthermore, in medical research it is customary to pick up a single cell (human, plant, or animal), and carry it to another device which is used to further analyze the cell. Consequently, the cell of interest has to be separated from the other cells and picked up using the appropriate micro/nano tool. Hence it becomes absolutely necessary that the appropriate tool be used for specific micro or nano entity manipulation and assembly.

In this research, we focus on developing micro tool for manipulating micro and nano entities in liquid environment using a micro fluidic end effector system with *in-situ* Polyvinylidene Fluoride (PVDF) sensing. The microfluidic end effector system

consists of a DC micro-diaphragm pump and compressor, one region of flexible latex tube, a Polyvinylidene Fluoride (PVDF) sensor for *in-situ* measurement of micro drag force, and a micro pipette. The micro pipette of the novel microfluidic end effector system has an internal diameter (ID) smaller than $20\mu m$ used for microfluidic handling and deposition of micro and nano entities such as carbon nanotubes (CNT), DNA, and for droplet control. The novel microfluidic end effector system with force sensing can significantly improve the success rate for handling/depositing micro/nano entities in the case of carbon nanotubes between micro electrodes. The design, calibration, and experimental implementation of the novel microfluidic end effector is carried out in this research. The experimental results show the success rate for carbon nanotube(s) deposition between micro electrodes can reach close to 80%.

Furthermore, carbon nanotubes are of particular interest because they are good candidates for many electronics and sensing applications. The interests in using carbon nanotubes to manufacture electronics and sensors have increased in recent years because of the increase need for making electronics smaller, and their excellent electrical and mechanical properties. These potentials can be achieved if CNTs with semiconducting and metallic band structure can be successfully deposited and separated. The use of dielectrophoresis (DEP) has been established as a course towards the efficient deposition and separation of metallic carbon nanotubes from semiconducting carbon nanotubes. For this reason, this research presents a new mathematical model for dielectrophoresis and electrorotation of carbon nanotubes. Simulation results are presented in this research to validate the developed model.

The combination of both the micro robotic manipulation system and the atomic force microscopy (AFM) based nano-robotic system will provide a powerful tool for micro and nano manipulation. Additional applications of this research are endless considering the rapid development of micro and nano technologies.

*To my parents, BobLuke Wejinya, and Hannah Mordi,
and to my siblings, for their love and support*

ACKNOWLEDGMENTS

Foremost, I thank God for his blessings and guidance, and for giving me the strength and wisdom to complete this dissertation.

I would like to express my deepest gratitude to my advisor, Dr. Ning Xi, without whom the completion of this dissertation would not have been possible, for providing acute insights during our numerous discussion session in his office, at conferences, and over the telephone. I cannot forget our many stimulating conversations about engineering as well as on diverse aspects of life including philosophy, hardwork, and politics. He always guided me with confidence. He will always be my advisor, teacher, and friend.

I would like to thank all members of my guidance committee: Dr. Percy Pierre, Dr. Hassan Khalil, Dr. Fathi Salem, Dr. Tien-Yien Li, and Dr. Chichia Chiu. At different stages of my Ph.D. studies, they offered me timely help and unfailing support. Their astute comments and suggestions have enhanced both the technical soundness and the presentation of this dissertation.

I would like to express my sincere gratitude to my friends – too many to go through the list, and colleagues from the Robotics and Automation Laboratory especially to Dr. Yantao Shen for many hours of discussions and mentoring during the period of my doctoral studies. The discussions with Dr. Yu Sun, Dr. Imad Elhajj, Dr. Jingdong Tan, Dr. Guangyong Li, Dr. King Wai Chiu Lai, Jiangbo Zhang, Mike(Quan) Shi, Yilun Luo, Hongzhi Chen, and Lianqing Liu, have substantially contributed to my work and broadened my knowledge.

I acknowledge the financial support from General Electric Faculty for the Future Fellowship (GEFFF), The US Department of Education Graduate Assistance in Areas of National Need (GAANN) Fellowship, and Michigan State University Dissertation Completion Fellowship. Without these sources of financial support, my Ph.D work

could not have been completed.

No matter how much I acknowledge the support I received from all those mentioned above, my deepest gratitude goes to my parents, BobLuke Wejinya and Hannah Mordi. They have always been my cheerleaders and supporters. This dissertation would not have been possible without their years of encouragement and continuous support. With love and gratitude, I dedicate this dissertation to them.

TABLE OF CONTENTS

LIST OF TABLES	x
LIST OF FIGURES	xi
1 Introduction	1
1.1 Motivation	1
1.2 Literature Review	2
1.2.1 Micro Manipulation	2
1.2.2 Nano Manipulation	6
1.2.3 Microfluidics	7
1.2.4 Manipulation of Carbon Nanotubes	8
1.2.5 Micro-Bio Injection	11
1.3 Objectives of This Research	14
1.3.1 Modeling and Control Methodology for Microfluidics	14
1.3.2 Modeling and Control Methodology for Carbon Nanotubes	15
1.3.3 Modeling and Sensing in Micro-Injection	15
1.4 Challenges and Difficulties In Micro and Nano Manipulation	16
1.4.1 Challenges In Modeling and Control for Micro and Nano Manipulation	16
1.4.2 Challenges In Tools Design	17
1.5 Organization of Dissertation	18
2 Physics for Micro and Nano Manipulation	21
2.1 Forces in Micro and Nano Environment	21
2.2 Modeling of the Forces in Micro and Nano Environment	24
2.2.1 Electrostatic Attraction Force	24
2.2.2 Van der Waals Force	24
2.2.3 Surface Tension	25
2.3 Chapter Summary	26
3 Modeling of Actuation for Micro and Nano Manipulation	27
3.1 Modeling of Micro and Nano Fluidics	27
3.1.1 Fundamentals of Surface Tension and Capillary Force	28
3.1.2 Poiseuille’s Law	30
3.1.3 Design and Fabrication of Microfluidic End Effector Manipulation System	33
3.2 Modeling of Dielectrophoretic Force for Micro and Nano Manipulation	37
3.2.1 Dielectrophoretic Force Modeling	37

3.2.2	Modeling of Electrorotation for Micro and Nano Manipulation	43
3.2.3	Dynamic Modeling of Rotational Motion of Carbon Nanotubes for Intelligent Manufacturing of CNT-Based Devices	45
3.2.4	Dynamic Effect of Fluid Medium on Micro and Nano Particles by Dielectrophoresis	47
3.3	Sensing and Control in Micro and Nano Manipulation	49
3.3.1	Microfluidic Sensing and Control	49
3.3.2	Modeling of Dynamic PVDF Micro-Drag Force Sensing	49
3.4	Sensing In Micro-Bio Injection	56
3.4.1	Force Sensing In Micro-Bio Injection Using Polyvinylidene Fluoride (PVDF)	57
3.4.2	Modeling of Micro-Bio Force Sensor	59
3.5	Chapter Summary	64
4	Theory for Micro Electrode and Electric Field Design for Carbon Nanotube Applications	65
4.1	Micro Electrode Design	65
4.1.1	Theory for Micro Electrode Design	66
4.2	Electric Field Design	69
4.3	Chapter Summary	70
5	Application in Micro and Nano Manipulation and Assembly	71
5.1	Microfluidics Based Micro and Nano Manipulation and Assembly	71
5.2	Validation of Poiseuille's Law	71
5.2.1	Surface Tension Calibration Results	73
5.2.2	Suction/Pressure Calibration Results	74
5.2.3	Experimental Implementation	83
5.2.4	Experimental Results on Carbon Nanotubes Implementation	84
5.3	Dielectrophoretic Force for Manipulation of Carbon Nanotubes	88
5.3.1	Introduction	88
5.3.2	Dielectrophoretic Force: Simulation Results	90
5.3.3	Electrorotation (Torque): Simulation Results	95
5.3.4	Rotational Motion of Carbon Nanotubes: Simulation Results	96
5.4	Chapter Summary	98
6	Application in Micro-Bio Injection	101
6.1	Introduction	101
6.1.1	Integration of Micro-Bio Force Sensor with Micropipette For Bio Injection	102
6.1.2	Networked Human/Robot Micro-Bio Manipulation System	103
6.2	Experimental Implementation	105

6.2.1	Force Measurement of Living Drosophila Embryo	105
6.2.2	Preparation of Drosophila Embryo	105
6.2.3	Micro-Bio Injection and Manipulation Configuration	106
6.3	Experimental Results	107
6.3.1	Force Profile of Micro-Bio Injection and Manipulation of Living Drosophila Embryos	107
6.3.2	Directional Micro-Bio Injection Force Comparison	111
6.3.3	Quantitative Relationship Between Micro-Bio Force and Mem- brane Deformation of Living Drosophila Embryo in Different Stages	112
6.4	Chapter Summary	113
7	Conclusions	115
8	Future Work and Research Directions	118
8.1	General Overview	118
8.2	Experimental Studies	120
8.2.1	Hardware Implementation	120
8.3	Inverse Problem	121
8.4	Chapter Summary	122
A	Matlab Simulation Code for Dielectrophoretic Force and Electroro- tation of Carbon Nanotubes	123
	APPENDICES	123
B	Matlab Simulation Code for Rotation Motion of Carbon Nanotubes In Acetone	126
	BIBLIOGRAPHY	132

LIST OF TABLES

5.1	Experimental Trials of Carbon Nanotube (CNT) Manufacturing . . .	88
6.1	Time table of embryogenesis. From [1]	105

LIST OF FIGURES

1.1	System used in performing micromanipulation and micro-assembly tasks	4
1.2	Carbon nanotube structure showing both the single-walled and multi-walled[2]	9
1.3	Manipulation in macro and micro scales[3]	17
2.1	Components of Adhesion Forces[4]	22
2.2	Sticking effects during manipulation operation in micro/nano environments	23
3.1	AFM image illustrating nano entities. The scanning range is $10\mu m \times 10\mu m$	29
3.2	Capillary rise due to surface tension	29
3.3	Viscous flow in a horizontal, circular tube	31
3.4	Design and working principle of pneumatic end effector system	35
3.5	Micropump for micro and nano fluidics and tools handling	36
3.6	Illustration of dielectrophoresis	37
3.7	Polarizability of dielectric particles in medium	38
3.8	Illustration of carbon nanotube as a line	40
3.9	Schematic showing how induced dipole moment of a particle lags behind a rotating applied electric field	44
3.10	Illustration of double-end fixed PVDF sensing beam inside the sensing buffer	50
3.11	Schematics of the developed electronic interface circuit of the PVDF sensor [5, 6].	55
3.12	Illustration of the 2-D PVDF micro-force sensing tool	57
3.13	Illustration of the equivalent Y axis PVDF force sensing tool[7, 8].	58
4.1	Micro electrode design for carbon nanotube implementation	66
5.1	AFM image illustrating nano entities. The scanning range is $10\mu m \times 10\mu m$	72
5.2	Relationship between pressure and volume flow rate	73
5.3	3D plot showing the relationship between volume flow rate, radius of tube and pressure difference	74
5.4	Calibration of surface tension	75
5.5	Calibration setup	76
5.6	Experimental setup	78
5.7	Frequency response of PVDF beam	78
5.8	Height change behavior due to suction	79
5.9	Suction force of developed end effector system	80

5.10	System behavior: Step response (height change) of suction activity . . .	81
5.11	System behavior: Velocity change during suction/release	82
5.12	Experimental implementation setup for carbon nanotube deposition . .	83
5.13	CNT deposition region	84
5.14	Procedure for manufacturing of nano devices	85
5.15	AFM image of experimental results. The scanning range is $5\mu m \times 5\mu m$.	86
5.16	Microscope image depicting the sequence of depositing carbon nanotubes between micro electrodes	87
5.17	AFM image of CNT deposition result. The scanning range is $5\mu m \times 5\mu m$.	87
5.18	Clausius-Mossotti factor for DEP analysis (Metallic MWCNT in Acetone)	91
5.19	Clausius-Mossotti factor for DEP analysis (Metallic MWCNT in acetone and ethanol)	91
5.20	3D plots showing the relationship between electric field and its gradient as a function of electrode size	92
5.21	Electric field as a function of applied voltage	93
5.22	Relationship between voltage and micro electrode gap for constant electric field	94
5.23	3D plots showing the relationship between electric field and its gradient as a function of frequency and voltage	95
5.24	Dielectrophoretic force F_{DEP} on metallic MWCNT in acetone	96
5.25	Spatial variation of the electric field and its gradient on micro electrodes for CNT manipulation and separation	97
5.26	Electrorotation (torque) acting on metallic MWCNT in acetone	98
5.27	Rotation angle and velocity of CNT in acetone with initial condition $(0, 0)$	99
5.28	Rotation angle and velocity of CNT in acetone with initial condition $(\pi/2, 0)$	100
6.1	PVDF sensing tool for micro injection.	102
6.2	Networked human/robot biomanipulation work-cell at MSU.	104
6.3	The prepared Drosophila embryos for micro injection.	106
6.4	Experimental configuration of micro injection of Drosophila embryos. . . .	107
6.5	The sequence of penetrating fresh embryo through one membrane.	108
6.6	Force profile of penetrating one membrane of fresh embryo.	109
6.7	The sequence of penetrating two membranes of living embryo.	109
6.8	Force profile of penetrating two membranes of living embryo.	110
6.9	Force profile of complex operation of living embryo	110
6.10	Dorsal-ventral and anterior-posterior directions	111
6.11	Penetration forces along the dorsal-ventral and anterior-posterior directions	112

6.12	Quantitative relationship between force and membrane deformation of living embryo in different stages.	113
8.1	Proposed AC electric field for DEP implementation	121
8.2	Proposed inverse problem solution method	122

CHAPTER 1

Introduction

1.1 Motivation

In the past two decades, the development of micro and nano technology platforms have made life better in so many different ways. It has also made the engineering of micro and nano devices and system possible. For instance, the development of implantable microchips, assembling micro machines, manipulating cell, micro surgery, imaging of micro and nano devices and systems, etc. are all possible due to micro and nano technology platforms available today.

Manipulation of micro and nano entities implies the movement of micro and nano entities from an initial position (location) to the desire position (location). This operation is not only necessary, but a required task with great precision and accuracy since the dominant force on the micro and nano scale is not gravity as it is the case on the macro scale level. Since the capabilities of the human hands are very restricted in the micro and nano world, the tools needed for the manipulation needs to be designed and chosen properly.

The tasks involved in micro and nano manipulation are as follows: (1) Preparation of parts, (2) Transportation of parts, (3) Positioning and fixing of parts, (3)

Connecting the parts, (4) Testing and measuring the assembled micro and nano devices. Hence it is important to design a gripper (end effector) that is capable of manipulating micro and nano objects with great precision and accuracy.

Micro and nano entities can be of hydrophobic or hydrophilic. For hydrophobic micro and nano entities, adhesion forces are dominant during manipulation compared to the gravitational force. For hydrophilic micro and nano entities, surface tension is dominant compare to gravity. Therefore, designing the tools necessary for manipulation becomes absolutely important.

In this research, we focus on developing a novel micro tool for manipulating micro and nano entities in liquid environment using a micro fluidic end-effector system with *in-situ* Polyvinylidene Fluoride (PVDF) sensing. The novel microfluidic end effector system with force sensing can significantly improve the success rate for handling and depositing micro and nano entities in the case of carbon nanotubes between micro electrodes. Furthermore, carbon nanotubes are of particular interest because they are good candidates for many electronics and sensing applications. The interests in using carbon nanotubes to manufacture electronics and sensors have increased in recent years because of the increase need for making electronics smaller, and their excellent electrical and mechanical properties.

By combining the functionalities of both the novel microfluidic end-effector system and AFM, carbon nanotubes can be effectively and efficiently assembled and manipulated for electronics and sensing applications.

1.2 Literature Review

1.2.1 Micro Manipulation

Manipulation of micrometer sized objects has been on the rise since the development of micro technology platforms, and has continued to grow. Manipulation means that

micro objects and particles are pushed, pulled, cut, picked and placed, positioned, oriented, assembled, bent, twisted, etc., by force control and sensory feedback. The growth has positively affected the fields of Micro-Electro-Mechanical systems (MEMS), Micro-Opto-Electro-Mechanical systems (MOEMS), micromechanics, optics, biology, medicine, etc. The size, material, geometry, the consistency of manipulated micro-objects, their surroundings, the kind of task to perform are parameters that strongly influence the design and working principles of micromanipulation and microassembly systems. These systems are widely developing because of their industrial needs, challenging engineering design and manufacturing, and most importantly, the everyday life use of more micro-sized products such as the Apple iPod.

A growing number of these micro-sized objects and products require to be manipulated or assembled in sequences $1\mu m$ to $1mm$ in size [9, 10]. Some of the applications of micromanipulation include the assembly of micromotors, microgears, microball-bearings; the assembly of hybrid components such as laser microsources, intelligent endoscopic capsules, mass microspectrometers; the manipulation of cells, in vitro fertilization, study of the behavior of *Drosophila* embryos; etc.

Today, micro-assembly is mainly performed with high precision dedicated systems that are expensive and have low flexibility. Most micromanipulation and micro-assembly systems are composed of a micromanipulator, end-effectors, sensors, perimicrorobotic systems and control systems. Figure 1.1 illustrates micromanipulation tasks and systems/tools required to perform the required tasks. The assembling tasks of micro devices involve transporting and releasing of micro parts to desired positions (and orientation) and the suitable forces have to be applied to these micro entities.

In macro object/parts handling and releasing, these problems are already solved by mechanical clamps using interaction forces or geometrically constraining grippers to hold and move the relatively heavy objects [11]. For small objects, sticking effect becomes more dominant. Compared to the adhesion and electrostatic forces, the

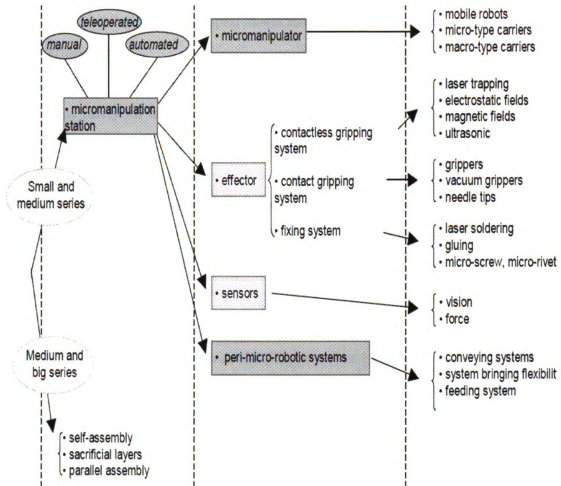


Figure 1.1. System used in performing micromanipulation and micro-assembly tasks

weight and inertia of the entity can be neglected because they scale with the cube of the size [4, 12]. A novel micromanipulator with micro gripper for micro object handling is described in [13]. A silicon MEMS sensor is used for the assembly of hybrid MEMS devices [14]. Review of recent micro gripper research indicates that micro grippers can be classified as electrostatic micro gripper, electromagnetic micro gripper, piezoelectric micro gripper, shape memory alloy micro gripper, and vacuum micro gripper[15].

Researchers have published on micro tools for microassembly and micromanipulation, but rarely on micro and nano tools for manufacturing of nano devices, and tools for microfluidic handling and transporting. For instance, in [16], Greitmann and Buser presented the microparts handling using micro tweezer. In [17], Miyazaki proposed the utilization of adhesion effects to provide the gripping force. In microbiology, very sensitive living cells are handled in a liquid environment using glass pipettes as presented in [18]. In addition, a vacuum tool and different active releasing mechanisms are presented in [19]. In [20, 21], the use of a microfluidic end effector system for microsuction, microfluidic handling, and manipulation is described.

In designing micro tools such as the gripper and end-effector, several major issues must be addressed. First, the operating target is fragile and can easily be destroyed. Therefore, the force acting on the targets must be meticulously controlled to effectively hold the target in a special environment due to sticking effect. Unlike macro objects that can be released by their self-gravitation, micro entities need to be released by an active force. Therefore, force regulation and releasing methodologies for micro tools must be considered. If the force is too strong, the intended micro object will be damaged or entirely destroyed. On the other hand, if the force is too weak, the micro target will neither be picked up nor released. Second, the structure of the micro tool must be simple and compact because of small operation workspace, and the micro and nano tool should be easily mounted on the micro system for microassem-

bly, microfluidic handling and droplet control, manufacturing of nano devices, and for micro manipulation. In addition, micro tools are very delicate, hence they have to be replaced frequently. As a result of this, efficiency of micro operation is greatly reduced. Hence, micro tools have to be simple and cheap.

1.2.2 Nano Manipulation

Nano manipulation involves the manipulation of particles and objects in the nanometer size range with a nanometer size end-effector (robot) with sub-nanometer precision. Manipulation means that nano objects and particles are pushed, pulled, cut, picked and placed, positioned, oriented, assembled, bent, twisted, etc., by force control and sensory feedback. Application of nano manipulation includes biomolecules, DNA, cells, etc.

Manipulating particles or objects in this range has been made possible today because of the development of nanotechnology platforms and tools. Some of the commercially available tools used for nano manipulation includes Scanning Electron Microscope (SEM), Transmission Electron Microscope (TEM), Scanning Tunneling Microscope (STM), and Atomic Force Microscope (AFM). All of these tool have advantages and disadvantages. However, Atomic Force Microscope (AFM) is more advantageous over other nano manipulation tools since they can operate in several environments including air, vacuum, and liquid. Most importantly, it can study biological cells when they are still alive. The image resolution from AFM often exceeds that from SEM and parallel to that from TEM.

Researchers have used AFM to manipulate nano particles and objects, and has attracted much attention among researchers in recent years and various kinds of manipulation schemes have been developed in last decade [22, 23, 24, 25]. For instance, Atomic Force Microscope (AFM) [26, 27] was used to study the behavior of nanowires under pushing condition. In [28], AFM was modified to include real-time visual feed-

back during manipulation and used to illustrate the manipulation of latex particles with diameters of $200nm$. Many of these nanoscale materials (particles and objects) do possess unique mechanical, electrical, optical, and chemical properties, and have a variety of potential applications in nanoscale devices, nano-sensors, and Nanoelectromechanical Systems (NEMS). For instance, carbon nanotubes (CNTs) are such kind of materials that have drawn much attention during the last decade.

1.2.3 Microfluidics

In the past three decades, research on microfluidics and microfluidic devices, fabricated with micromechanics technology, has contributed greatly to the fields of engineering, medicine, biology, etc. This research have ranged from gas chromatograph [29, 30] to one of the most utilized products that evolved from microfluidics, the ink jet printer [31, 32, 33]. Many different devices are have been developed, ranging from single components such as flow sensors and valves for gas pressure regulation, to complex microfluid handling systems for chemical analysis, consisting of pumps, valves, flow sensors, separation capillaries, chemical detectors etc, all integrated on a single substrate or as sandwiched modules. C.-J. Kim [34, 35] revolutionized the field of microfluidics by the development of several technologies including a pneumatically driven microcage for micro-scale object manipulation in biological liquid, and microfluidic transports, droplets, and control.

Microfluidic transport and control is important in micro/nano handling, micro/nano manipulation, and micro/nano assembly. Moving fluid through a device or channel, regardless of the application, requires a means of generating flow. The right amount of the fluid must be precisely dropped/released at the desired location. Many methods have been presented in recent years including micromechanical, electrowetting, thermocapillary pumping, and electro-osmotic flow [36, 37, 38]. However, none of these methods have feedback. To realize the maximum benefit of microfluidic

handling and manipulation, it will be necessary to generate flow using tools that are integrated with sensing and feedback.

1.2.4 Manipulation of Carbon Nanotubes

Carbon nanotubes are molecular-scale tubes of graphitic carbon with meritorious electrical and mechanical properties. They are among the stiffest and strongest fibres known, and have remarkable electronic properties and many other unique characteristics. For these reasons they have attracted huge academic and industrial interest, with thousands of papers on nanotubes being published every year. Commercial applications have been rather slow to develop, primarily because of the high production costs of the best quality nanotubes.

Carbon nanotubes (CNTs) have drawn the interest of many researchers in the field of engineering and sciences since they were discovered by Iijima [39] in 1991. The structure is shown in Fig. 1.2. This is because carbon nanotubes have extraordinary electrical and mechanical properties. Their excellent electrical properties make them to be good candidates for many electronics and sensing applications. For instance, in [40], Fukuda *et al.* summarized properties and potential applications of carbon nanotubes by emphasizing the aspects of nanoelectronics and nanoelectromechanical systems (NEMS). A fabrication method for a high-aspect-ratio nano scale pit using a carbon nanotube (CNT) as a scanning tunnelling microscope (STM) probe is described in [41, 42]. Martel *et al.* in [43] used carbon nanotube as the semiconducting channel in a field effect transistor (FET) to achieve very high mobilities comparable to or better than state-of-art silicon-based transistors.

In order to make carbon nanotubes more attractive for commercial applications, several issues need to be addressed. One of the issues is the difficulty in the deposition and integration of individual or small sets of semiconducting single walled carbon nanotubes (s-SWCNTs) and metallic single walled carbon nanotubes (m-SWCNTs)

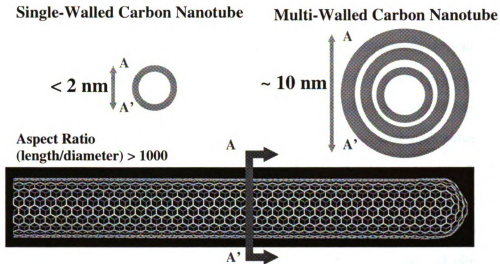


Figure 1.2. Carbon nanotube structure showing both the single-walled and multi-walled[2]

with microcircuitry. Though s-SWCNTs can be used for transistors, their metallic counterparts, m-SWCNTs, are candidates for interconnects and wires due to their low resistance and high current-carrying capability. Several groups have used different methods to assemble carbon nanotubes on micro sized electrodes. In [44], the manipulation of carbon nanotubes with an atomic force microscope was investigated and their interaction with surfaces was also reported. Wejinya *et al.* in [21] developed a microfluidic end effector for transporting and manufacturing of nano devices such as carbon nanotubes by using ac electric field. The manipulation and orientation of Actin-Myosin systems with dielectrophoresis was reported in [45]. Directed assembly of one-dimensional nanostructures into functional networks by chemically pre-patterning the substrate was investigated in [46]. Dimaki *et al.* in [47], reported numerical study calculating the probability of capturing various types of carbon nanotubes, the time frame for the assembly and the efficiency of separation, for different experimental parameter micro electrodes. The use of dielectrophoresis to manipulate and align carbon nanotubes on micro electrodes was reported in [48, 49, 50]. The

effect of ac electric field on single walled carbon nanotubes dispersed in ethanol was studied in [51]. Krupke *et al.* in [52] used dielectrophoresis to attach two ends of single walled carbon nanotubes in an e-print. In their work, they used silver (Ag) and gold (Au) electrodes spaced by $100nm$ to trap bundles of single walled carbon nanotubes dispersed in dimethylformamide (DMF). They found that nanotubes formed electrical contact with the Ag electrodes, but not with the Au electrodes. Nagahara *et al.* in [53] found similar results as in [52], but with gold (Au) electrodes spaced by $20-80nm$ or $20\mu m$. In [54], the separation of live and dead bacteria was achieved by using dielectrophoresis, and by modifying the relative responses of electrokinesis and dielectrophoresis by adjusting the magnitude of the applied voltage. It was observed that dead cells have significantly lower dielectrophoretic mobility than live cells, whereas the electrokinetic mobilities of live and dead cells were indistinguishable. In [55], the fabrication of atomic force microscope tip with a carbon nanotube using dielectrophoresis was concerned and reported. The method of dielectrophoresis is based on the ability of a nonuniform electric field to induce a dipole moment on polarizable objects, which in turn leads to a net force on the object. Secondly, separation of s-SWCNTs and m-SWCNTs is an even greater challenge. Filtration and ultrasonication was reported in [56] as a sorting method applicable for carbon nanotubes. Zheng *et al.* in [57] reported the possibility of sorting carbon nanotubes using DNA, which self-assembles on the nanotubes into a helical structure in such a way that the electrostatics of the CNTDNA hybrid depends on the tube diameter and electronic properties. Krupke *et al.* [58] used dielectrophoresis to attract predominantly m-SWCNTs to a set of microelectrodes, exploiting the fact that the magnitude of the dielectrophoretic force depends on the dielectric and conducting properties of a particle, in this case carbon nanotubes (CNTs).

1.2.5 Micro-Bio Injection

Genetic modification of *Drosophila* embryos has provided us insights that are not only scientifically interesting but also biological mechanisms to cure diseases. The fact that this type of research also has human health care implications was confirmed by the award of the 1995 Nobel Prize in Physiology or Medicine to Edward B. Lewis, Christiane Nüsslein-Volhard, and Eric F. Wieschaus for their discoveries concerning the genetic control of early embryonic development. In their work, they have used the fruit fly, *Drosophila melanogaster*, as their experimental specimen. This organism is classical in genetics. The principles found in the fruit fly, *Drosophila melanogaster*, applies to higher organisms including man [59].

The *Drosophila* genome can also provide critical information about human genes that have homologous in the fruit fly [60]. Of particular interest to medicine, several human diseases are caused by mutations in genes analogous to genes found in *Drosophila*. Genetically speaking, human and *Drosophilas* are similar. About 61% of known human disease genes have a recognizable match in the genetic code of *Drosophilas*, and 50% of *Drosophila* protein sequences have mammalian analogues [61]. *Drosophila* is being used as a genetic model for several human diseases including neurodegenerative disorders such as Parkinson's, Huntington's, and Alzheimer's diseases [62]. *Drosophila* is also being used to study mechanisms underlying immunity, diabetes, and cancer, as well as drug abuse. In addition, scientists can determine the gene function from the loss-of-function phenotype or the overexpression phenotype. Alternately, the function of human genes can be studied by inserting them into *Drosophilas* via transposable elements. Recently, Corey Goodman has been using *Drosophila* to study the wiring of the brain and nervous system [63]. His work has already led to a better understanding of how human brain develops. Consequently, the combination of the *Drosophila* genome with the well-established genetic tools in the *Drosophila* system will lead to important discoveries for human medicine, and provide

a pathway to detecting, developing, treating, and eradicating diseases in humans [64].

To implement the research on *Drosophila* genome, one of the most important approaches and tasks is the injection of substances that affect the make-up of a cell or an organism. Micro injection such as transgenes, i.e. DNA structures that often consist of a gene and a control component, results in *Drosophilas* with new characteristics, since the transgene is integrated into the *Drosophila*'s own DNA. This makes it possible to determine which genes are important for the development of the organism and which organs are affected [65]. However, most embryo injections are conducted manually. Operators often require at least one year of training to become proficient at the injection task. Even so, the operators still need to spend significant amount of time on embryo injection tasks. The success rate of a manual injection is disappointingly low, in the range of 2~4%. The reason for this is that successful micro injection is greatly dependent on injection forces, injection speed, and trajectory [66]. To improve the quality of micro injection, minimizing the damage *in vivo* caused by current injection methods, a localized, accurate, and highly efficient micro system should be developed. Although existing micromanipulators can achieve extremely high accuracy in position, the success rate of micro injection is still at the low end due to lack of an effective micro-force sensing and feedback mechanism.

Currently, there exist several developments on micro-force sensing methods used in the characterization of micro injection of different cells or embryos. Sun et al. introduced their work on the development of a microrobotic cell manipulation system, which employs a multiaxis capacitive force sensor with a tip diameter of $5\mu\text{m}$ to characterize the mechanical properties of Mouse Zona Pellucida [67]. The use of PVDF was mentioned as a sensing device in [68, 69, 70]. In [71], the mechanical behavior of the Zebrafish embryo chorion is quantitated using an unmodeled PVDF force sensor with a $14.5\mu\text{N}$ resolution. The attached injection pipette is $14.6\mu\text{m}$ in radius. The measured force is from $100\mu\text{N}$ to $800\mu\text{N}$, and an average penetration

force of $737\mu\text{N}$ is also reported in [71]. Force sensing methods in micro robotics with AFM cantilevers is described in [72]. A novel nano-probe for biological dissection and injection with complex fabrication technique is described in [73]. More recently, Zhang et al. presented a micrograting based force sensor integrated with a surface micromachined silicon-nitride probe for penetration and injection into *Drosophila* embryos [74]. In this work, they found an average penetration force of $52.5\mu\text{N}\pm 13.2\%$ with a $30\mu\text{m}$ diameter silicon tip. These works mentioned above are the valuable references in this research area. Comparing to those work, in this research, an *in situ* PVDF (Polyvinylidene Fluoride) piezoelectric two-axis micro-force sensing tool with a resolution in the range of sub- μN is developed. The tool is integrated with a glass pipette with an ultra sharp injecting tip of $1.685\mu\text{m}$ in diameter and 2.65° in angle. In addition, the dynamic model of this tool is developed based on the piezoelectric electro-mechanical effect of PVDF and the distributed parameter model of beam by incorporating the piezoelectric electro-mechanical relationship into the Bernoulli-Euler beam equation. Using this modeled high sensitivity and high resolution force sensing tool, the effects of much smaller forces in a minimally invasive area during micro injection of *Drosophila* embryos so as to minimize the damage to the embryos as well as to further ensure the studies of developmental biology and genetics can be explored. Moreover, the micro-force sensing tool can be conveniently integrated into a precision micro manipulator system and is easy to both manufacture and assemble. Without using complex MEMS technology, the developed sensing system is economical and can be widely used in characterization of mechanical properties of cell or embryos in research labs, and also has the potential for commercialization.

Furthermore, in this research, based on the developed PVDF micro-force sensing tool and the event-synchronization [75] of the video and micro-force, we further developed a networked human/robot cooperative biomanipulation system which attempts to reach complete heterogenous integration of human and robot functions for achiev-

ing reliable, accurate, and efficient biomanipulation or micro injection of cell/embryos. This system can be applied to single or multiple remote work-cells through LAN or Internet.

1.3 Objectives of This Research

The goal of this research is to develop tools for micro and nano manipulation that is capable of transporting micro and nano entities in liquid environment, and sensing in bio environments for biomanipulation and bioinjection. In order to achieve this goal, some objectives concerning microfluidic design, sensor design, and modeling in micro and nano environments have to be accomplished during the research.

1.3.1 Modeling and Control Methodology for Microfluidics

This worked is focused on exploring and developing an effective and efficient solution for micro/nano fluidic handling, droplet control, micro/nano assembly, and micro/nano manipulation. Based on a new microfluidic vacuum/pressure mechanism, a micro end-effector, which is made from a micro pipette with ID smaller than $20\mu m$, is designed. The micro end-effector (the micro pipette) is connected with the inlet/outlet of an effective micro-diaphragm air pump through the tiny tube. When voltage is applied to the air pump, the tube end can generate micro suction, or pressure force, due to vacuum or pressure action provided by the pump. The DC micro-diaphragm pump is automatically controlled using a voltage driver interfaced with a computer in order to effectively and efficiently control suction force and pressure during microfluidic handling, droplet control, and nano manufacturing. Also a high sensitivity PVDF beam sensing buffer for micro force/flow rate measurement is built between the micro pipette and micro pump. The new micro pipette based end-effector, micro pump, and PVDF sensing buffer can be integrated into a closed-loop

system to provide the precision controlled micro force, flow rate, for fine microfluidic handling, droplet control, micro/nano manipulation, micro/nano assembly, and handling of nano devices.

1.3.2 Modeling and Control Methodology for Carbon Nanotubes

This research work is focused on developing a new mathematical model for dielectrophoresis and electrorotation of carbon nanotubes. Dielectrophoresis is inherently capable of solving both the separation and assembly problems associated with the fabrication of large-scale carbon nanotube based electronics and sensors, without having to contaminate the carbon nanotubes with chemicals. Therefore, accurate model of dielectrophoresis becomes essential and critical. The derivation is followed with simulation results to preliminarily validate the model. Our model reasonably assumes that carbon nanotubes are a bunch of particles that after undergoing dielectrophoresis, forms a line shape structure. The model gives a qualitative insight into the relation between electrode design, dimensions of the carbon nanotubes, and experimentally controllable parameters such as frequency and fluid velocity. Based on these calculations we are able to give recommendations for the optimization of nanotube assembly and separation.

1.3.3 Modeling and Sensing in Micro-Injection

The goal of this research work is to address both the measurement of injection force behavior and the characterization of mechanical properties of living *Drosophila* embryos using a well modeled *in situ* PVDF (Polyvinylidene Fluoride) piezoelectric micro-force sensing tool with a resolution in the range of sub- μ N. *Drosophila* embryo is one of the most studied organisms currently in genetics and developmental

biology, and also has strong implications in the human medical study. In this research, we focus on the development of a sensorized biomanipulation tool based on the high sensitivity PVDF film and the minimally invasive pipette injector. Using this tool, close monitoring of the magnitude and direction of micro injection and other biomanipulation forces acting on the embryo during the injecting process becomes a reality. In addition, a networked micro-robotic biomanipulation platform integrating this developed two-axis (2-D) PVDF micro-force sensing tool is built. By employing the event-synchronization for the feedback of injection video and micro-force, the developed networked microrobotic platform can greatly advance operations in micro injection of living *Drosophila* embryos. Several experimental results have clearly demonstrated the quantitative relationships between the applied force and membrane structural deformation of embryos in the different stages of embryogenesis, as well as the force behaviors of micro injection .

1.4 Challenges and Difficulties In Micro and Nano Manipulation

1.4.1 Challenges In Modeling and Control for Micro and Nano Manipulation

During micro and nano manipulation, the tasks involved includes (1) Preparation of parts, (2) Transportation of parts, (3) Positioning and fixing of parts, (4) Connecting the parts, (5) Testing and measuring the assembled micro and nano devices. Currently, microassembly is performed largely by humans with tweezers and microscopes or with high precision pick-and-place robots. Both methods are inherently serial. Furthermore, the entities to be handled are less than $100\mu m$ in size on the micro scale and $1\mu m$ (with part dimensions in the molecular scale) in size on the nano scale. In

this case, surface forces work as the adhesive force. These forces are not negligible during manipulation in the micro and nano world. Figure 1.3 shows the challenges faced in micromanipulation [3]. As shown in Fig. 1.3, a piece of micro part adheres to the gripper surface during manipulation by the adhesive forces, making it difficult if not impossible to manipulate the micro part. In the macro world, manipulation is quite easy since gravity is the dominant force.

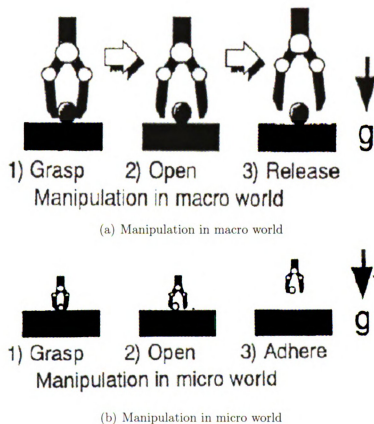


Figure 1.3. Manipulation in macro and micro scales[3]

1.4.2 Challenges In Tools Design

In designing micro and nano tools such as the grippers and end-effectors, several major issues must be addressed. First, the operating target is fragile and can easily be

destroyed. Therefore, the force acting on the micro and nano tool must be meticulously controlled to effectively hold the target. Unlike macro objects that can be released by their self-gravitation, micro and nano objects need to be released by an active force as the negative pressure vanished. This makes it important that a micro and nano tool exerts an appropriate amount of force on a micro and nano target. If the force is too strong, the intended micro or nano object will be damaged or entirely destroyed. On the other hand, if the force is too weak, the micro or nano target will neither be picked up nor released. Second, the structure of the micro/nano tool must be simple and compact because of small operation workspace. Finally, the micro/nano tool should be easily mounted on the micro/nano robot for microassembly, microfluidic handling/droplet, manufacturing of nano devices, and micro/nano manipulation. In addition, micro/nano tools are very delicate, hence they have to be replaced frequently. As a result of this, efficiency during micro and nano assembly, micro/nano fluidic handling/droplet, handling of nano devices, and micro/nano manipulation is greatly reduced. For this reason, micro/nano tools have to be simple and cheap.

1.5 Organization of Dissertation

The scope of this dissertation is to develop tools for micro and nano manipulation that is capable of transporting micro and nano entities in liquid environment, and sensing in bio environments for biomanipulation and bioinjection. The work is divided into four parts - namely design, analysis, modeling, control, and experimental verification.

Chapter 1: This chapter introduced the motivation for the research - problem background and application.

Chapter 2: In this chapter, physics for micro and nano manipulation is thoroughly examined and presented. Since adhesion forces dominates in micro and nano

scale manipulation, the physics and the mathematics describing these forces are also examined and presented.

Chapter 3: This chapter of the dissertation presents micro and nano fluidics based manipulation. The work done towards the development of a high sensitivity sensor for sensing and control in micro-bio injection. Based on a high sensitivity micro-force piezoelectric sensor, the micro-bio injection force during micro-bio injection of *Drosophila* cells for human medical studies is realized. Furthermore, this chapter also presents the research work done towards the development of a new model for dielectrophoretic force (DEP), electrorotation, and rotational motion of carbon nanotubes in viscous medium.

Chapter 4: This chapter presents the theory for micro electrode design and electric field design for carbon nanotube applications

Chapter 5: In this chapter, application of the developed micro and nano fluidic end effector system in micro and nano manipulation and assembly is presented. Experimental setup for calibrating surface tension of water and liquid acetone is designed, and results are presented. Experiments dealing with suction and release of micro and nano fluids are also performed and results presented. Further, experimental results dealing with carbon nanotube deposition using the developed micro and nano fluidic end effector system is also performed and the results are presented. Simulation results for the developed models of dielectrophoretic force, electrorotation, and rotational motion of carbon nanotubes in viscous medium are presented in this chapter.

Chapter 6: The application of the developed high sensitivity PVDF-based micro-bio force sensor for sensing and control in micro-bio injection is demonstrated in this chapter. The developed micro-bio force sensor is integrated with a micropipette and a networked human/robot micro-bio manipulation system for micro-bio injection of *Drosophila* (fruit fly) cells. Experimental results of the micro-bio injection are

demonstrated in this chapter. This work has the potential to significantly increase the efficiency of biocellular studies, bio-agriculture, genetic modification, etc.

Chapter 7: This chapter concludes the research work done in this dissertation and summarizes the contributions of the dissertation.

Chapter 8: This chapter looks at future work and research directions relating to all of the work carried out in this dissertation.

CHAPTER 2

Physics for Micro and Nano Manipulation

2.1 Forces in Micro and Nano Environment

The sequence of operation in micro and nano manipulation includes pick, transport, and place (release). Since parts in the micro and nano environment are less than a millimeter for micro entities and less than a micrometer for nano entities, and masses are less than 10^{-6} Kg for micro entities, and less than 10^{-9} Kg for nano entities, gravitational and inertial forces may become insignificant compared to adhesion forces, which are generally proportional to the surface area. In addition, when parts become very small (in the case of micro and nano entities), adhesion forces can prevent release of the part from the gripper or end effector.

The adhesion of particles to substrates has received substantial study for problems such as particulate contamination in semiconductor manufacturing [76, 77, 78]. The adhesion force is typically divided into three major components as illustrated in Fig. 2.1. The components are electrostatic attraction, Van der Waals force, and surface tension. For accurate placement of micro and nano entities during manipulation and

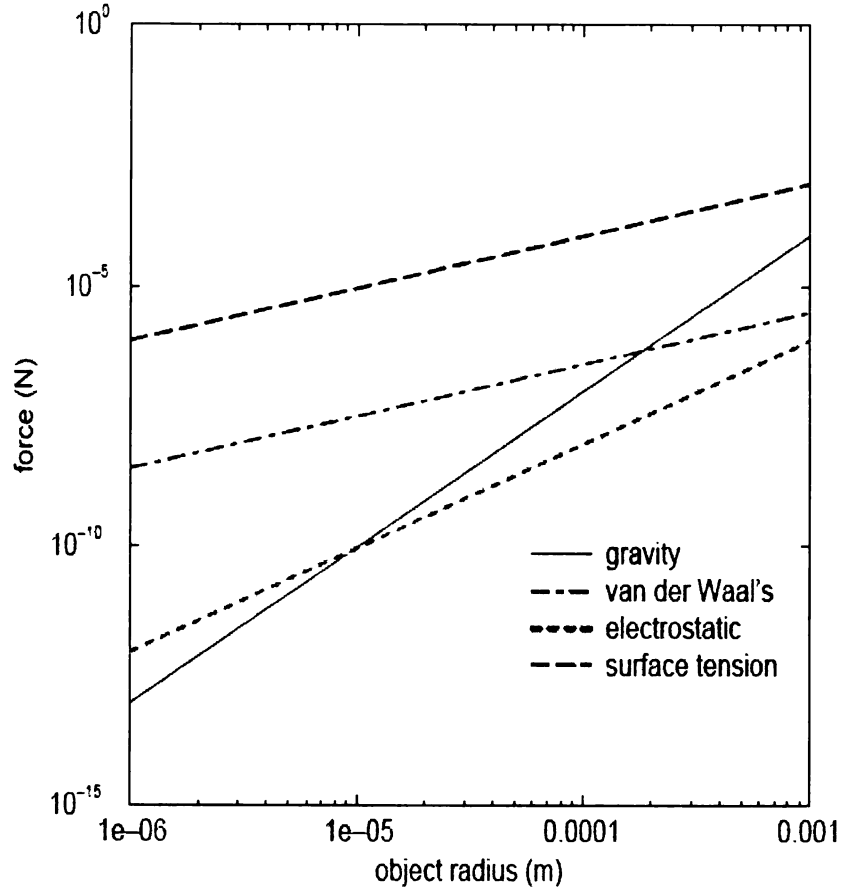
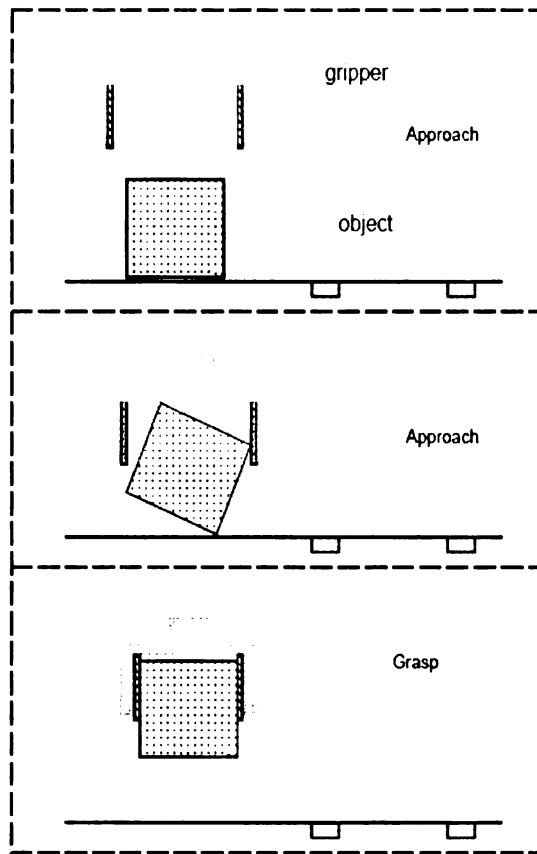


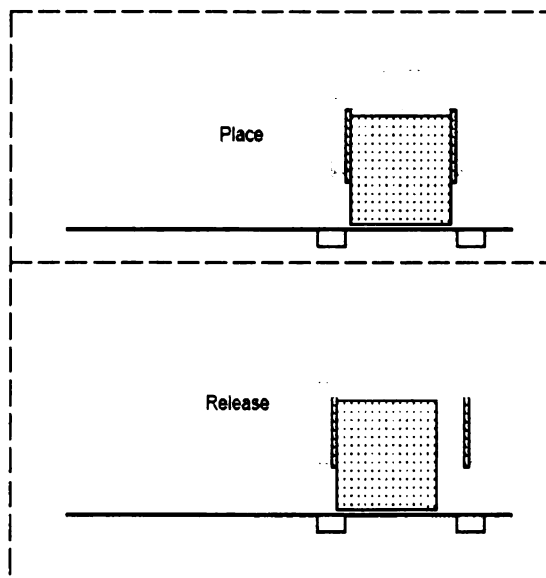
Figure 2.1. Components of Adhesion Forces[4]

assembly, adhesion forces should be an order of magnitude less than gravitational forces.

In Fig. 2.2, the effects which can be seen when attempting to manipulate micro/nano entities is demonstrated [4]. As illustrated in Fig. 2.2, micro/nano entities can be attracted to the gripper or end effector during the approach and release phase, causing inaccurate placement of the micro/nano parts. As the gripper approaches the part, electrostatic attraction may cause the part to jump off the surface into the gripper. Furthermore, when the part is placed to a desired location, it may adhere better to the gripper than the substrate, preventing accurate placement. Hence, efficiency



(a) Sticking effects in micro/nano manipulation during grasping



(b) Sticking effects in micro/nano manipulation during release

Figure 2.2. Sticking effects during manipulation operation in micro/nano environments

and high yield during manipulation operation is greatly reduced.

2.2 Modeling of the Forces in Micro and Nano Environment

In section 2.1, the adhesion forces in micro and nano manipulation are described. The components of these forces are due to electrostatic forces, van der Waals forces, and surface tension. These force components dominate during manipulation of micro and nano entities. The mathematics governing these force components are hereby described.

2.2.1 Electrostatic Attraction Force

Electrostatic attraction (and also repulsion) F_{el} is based on Coulomb forces between electrically charged bodies [11]. It also arises from charge generation or charge transfer during contact in micro and nano manipulation and assembly. The electrostatic force F_{el} between a charged sphere and an uncharged plane is described in [12] as follows.

$$F_{el} = \frac{\pi}{4 * \epsilon_0} \cdot \frac{\epsilon - \epsilon_0}{\epsilon + \epsilon_0} \cdot d^2 \cdot \sigma^2 \quad (2.1)$$

where σ is the charge density of the surface, ϵ_0 and ϵ are the air's and the plane's dielectric constants respectively, and d is the diameter of the object. In order to minimize electrostatic effects, conducting surfaces or ionization of the surrounding medium can be used.

2.2.2 Van der Waals Force

The Van der Waals force is an intermolecular force caused by momentary movements of electrons. It is also defined as forces due to instantaneous polarization of atoms and molecules due to quantum mechanical effects [79]. Van der Waals forces can start to

be significant (with smooth surfaces) at about $100\mu m$ radius, and generated electric charges from contacts could prevent dry manipulation of parts less than $10\mu m$ in size[4]. This phenomenon is described mathematically by [12] as follows.

$$F_{vdw} = \frac{H \cdot d}{12 \cdot z^2} \quad (2.2)$$

where H is the Hamaker constant, d is the diameter of the object, and z is the distance between the object and the plane. Here, $z \ll d$. On rough surfaces, the effective distance z will be increased, therefore causing F_{vdw} , the Van der Waals force to decrease.

2.2.3 Surface Tension

Surface tension effects arise from interactions of layers of adsorbed moisture on the two surfaces[4]. For instance, in a high humidity environment, or environment with hydrophilic surfaces, there may be a liquid film between the spherical object and planar surface contributing a large capillary force (force due to surface tension). This force is describes as[4, 80]

$$F_{tens} = \frac{\gamma(\cos \theta_1 + \cos \theta_2)A}{d} \quad (2.3)$$

where γ is the is the surface tension, A is the shared area, d is the gap between surfaces, θ_1 , and θ_2 are the the contact angles between the liquid and the surfaces. For hydrophilic surfaces and a separation distance much smaller than the object radius, the force due to surface tension is described as [4, 77, 81]. Furthermore, actual contact with a liquid layer has to be made for surface tension to be significant.

$$F_{tens} = 4\pi r\gamma \quad (2.4)$$

where r is the radius of the object.

2.3 Chapter Summary

The forces in micro and nano manipulation are described and summarized in this chapter. Furthermore, the mathematics describing these forces is also discussed and summarized. Although, these forces cannot be totally eliminated, they could be minimized either by designing better micro and nano manipulation tools, or by treating micro and nano manipulation tools after they have been designed. Furthermore, these forces can also be minimized by accurately modeling the micro and nano manipulation tools.

CHAPTER 3

Modeling of Actuation for Micro and Nano Manipulation

3.1 Modeling of Micro and Nano Fluidics

Biotechnology is increasingly about large numbers of experiments, such as analysis of DNA or of drugs, screening of patients, taking specimen samples, etc. All of these procedures require handling and manipulation of fluids in the micro and nano scale levels. As the number of experiments have grown, the devices used to carry them out have shrunk, and the strategy of “smaller is better” has begun to transform the world of micro and nano fluidics as it has transformed the world of electronics.

Micro and nano fluidics transporting, handling, and manipulation have stimulated three new areas of research: (1) Development of new methods for fabricating fluidic systems, (2) Invention of components from which to assemble functionally complex fluidic devices, and (3) Examination of the fundamental behavior of fluids in small channels[82]. Developments in micro and nano fluidic technology are also contributing to new experiments in fundamental biology, materials science, engineering, forensic analysis, and physical chemistry.

Interest in micro and nano fluidics have been largely motivated by applications, and dimensions and fluids are dictated by these applications [36, 83]. The most mature microfluidic technology is ink-jet printing, which uses orifices less than $100\mu m$ in diameter for the generation of drops of ink. To realize the maximum benefit of micro/nano fluidic handling and manipulation, it will be necessary to generate flow using tools that are integrated with sensing and feedback. Hence, this chapter is focused on exploring and developing an effective and efficient solution for micro/nano fluidic handling, droplet control, micro/nano assembly, and micro/nano manipulation with sensing and feedback capabilities. Based on a new pneumatic vacuum/pressure mechanism, a micro end-effector, which is made from a micro pipette with ID smaller than $20\mu m$, is designed for micro and nano fluidic handling and manipulation application.

An application of the new pneumatic end effector is to handle nano devices such as carbon nanotubes (CNTs) and silver cubes as illustrated in Fig. 5.1. In this research, experiments focusing on handling carbon nano tubes in liquid acetone, and carbon nanotube deposition between electrodes for manufacturing of nano sensor/electronics are demonstrated. The results verify the effectiveness of the new pneumatic end effector. That is, precisely and automatically placing carbon nanotube(s) in the center of two electrodes separated by a few microns.

To better understand micro and nano fluidic phenomena, some of its properties such as surface tension and capillary force, and its behavior (flow speed and flow rate) is be discussed.

3.1.1 Fundamentals of Surface Tension and Capillary Force

Surface tension is a property of liquids arising from unbalanced molecular cohesive forces at or near the surface. Surface tension will always exist whenever there is a density discontinuity as, for example, between water and air or water and oil. The magnitude of the surface tension will depend upon the nature of both substances,

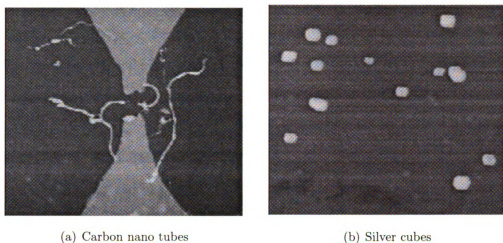


Figure 3.1. AFM image illustrating nano entities. The scanning range is $10\mu m \times 10\mu m$.

liquid and liquid, or liquid and gas. In general, surface tension is a function of temperature and pressure. Surface tension of some common pairs of fluids at $25^\circ C$ can be found in [84] The force that results from the surface tension is known as

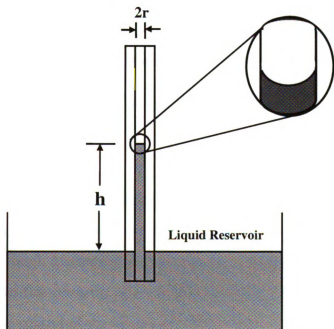


Figure 3.2. Capillary rise due to surface tension

capillary force. Fig. 3.2 illustrates capillary rise due to surface tension in which the end of the capillary tube of radius r , is immersed in liquid [85]. For sufficiently small capillaries, a substantial rise of liquid to height h in the capillary is observed because of the force exerted on the liquid due to surface tension. This force is known as the capillary force, F_{cap} . Equilibrium occurs when the force of gravity balances the capillary force. The balanced point can be used as a means to measure the surface tension and is described in [85] as:

$$\gamma(2\pi r) = \rho h(\pi r^2)g \quad (3.1)$$

where γ is the surface tension of the liquid, ρ is the density of the liquid, and g is the acceleration due to gravity. The expression for the surface tension is obtained by rearranging equation (3.1) as

$$\gamma = \frac{1}{2}\rho g r h \quad (3.2)$$

As shown in Fig. 3.2, the surface of the capillary is not perfectly flat. Instead it curves up, sometimes down at the wall to form a meniscus as illustrated in the inset in Fig. 3.2. Taking into account that the material in this region also contributes to the force of gravity, equation (3.2) (the surface tension) is expressed as

$$\gamma = \frac{1}{2}\rho g r \left(h + \frac{r}{3}\right) \quad (3.3)$$

3.1.2 Poiseuille's Law

Poiseuille's law describes the relationship between pressure, flow, and resistance (viscosity) for liquid flowing through a cylindrical tube. For instance, blood flowing through a blood vessel. Measuring fluid flow is one of the most important aspects of process control. In this research, accurate flow measurement is critical to determining the pneumatic control of the developed end-effector. Two of the important flow measurements is the flow speed and flow rate. Usually, flow is generally measured inferentially by measuring velocity (flow speed) through a known area.

The Navier-Stokes equations are the basic differential equations describing the flow of incompressible Newtonian fluids [84, 86].

The best known exact solutions to Navier-Stokes equations is for steady, incompressible, laminar flow through a straight circular tube of constant cross section [86]. This type of flow is generally known as Poiseuille flow.

Considering the flow through a horizontal circular tube of radius R as shown in Fig. 3.3. Because of the cylindrical geometry, it is convenient to use cylindrical

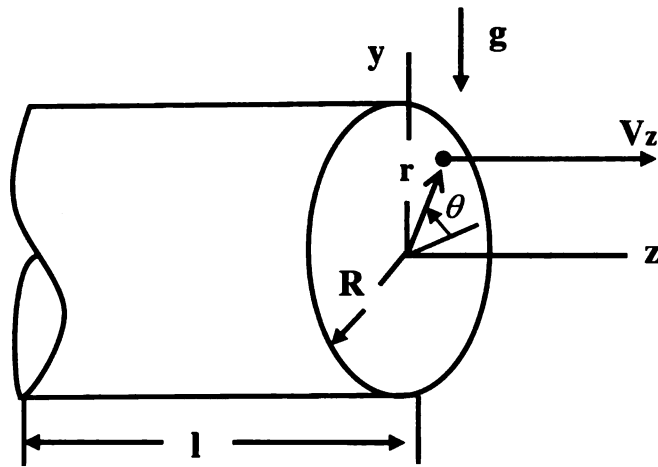


Figure 3.3. Viscous flow in a horizontal, circular tube

coordinates. From continuity equation [86],

$$\frac{\partial v_z}{\partial z} = 0 \quad (3.4)$$

Also, for steady, asymmetric flow, v_z is not a function of t or θ , so the velocity, v_z is only a function of the radial position within the tube. That is

$$v_z = v_z(r) \quad (3.5)$$

Under the conditions described above, the Navier-Stokes equations reduce to the following [86]:

$$-\frac{\partial p}{\partial z} + \mu \left[\frac{1}{r} \frac{\partial}{\partial r} \left(r \frac{\partial v_z}{\partial r} \right) \right] = 0 \quad (3.6)$$

Continually, after integrating equation (3.6), and using the fact that $\partial p/\partial z$ is a constant, the equation of motion in the z direction as illustrated in Fig.3.3 is obtained as

$$v_z = \frac{1}{4\mu} \left(\frac{\partial p}{\partial z} \right) r^2 + c_1 \ln(r) + c_2 \quad (3.7)$$

where c_2 is due to the standard condition of zero velocity of the fluid at the boundary.

Since we want v_z to be finite at the center of the tube ($r=0$), it follows that $c_1=0$, hence c_2 can be expressed as

$$c_2 = -\frac{1}{4\mu} \left(\frac{\partial p}{\partial z} \right) R^2 \quad (3.8)$$

The volume flow rate through the circular tube is given by

$$Q_v = Av \quad (3.9)$$

where A is the area of the circular tube, v is the flow velocity.

Continually, the volume flow rate through the differential area is given by

$$dQ_v = v_z(2\pi r)dr \quad (3.10)$$

Combining equations (3.8) and (3.7), and substituting into equation (3.10), then integrating over the radius of the tube, the expression for volume flow rate as a function of pressure difference is given as

$$Q = \frac{\pi R^4 \Delta p}{8\mu l} \quad (3.11)$$

where μ is the viscosity of the liquid, l is the length over pressure difference (pressure drop) along the tube.

Simulation results are presented to validate Poiseuille's law based on the parameters of the micro-diaphragm pump.

3.1.3 Design and Fabrication of Microfluidic End Effector Manipulation System

Researchers have designed extensively on micro fluidic systems and the tools for micromanipulation/microassembly, micro and nano manufacturing, bio-manipulation, and biological/chemical analysis. However, the effective and efficient micro system with reliable and high precision sensing and feedback control methodology is still an open problem. In this type of micro system, several major difficulties and challenges related to micro/nano object handling/manipulation, biological/chemical analysis, and precision droplet control have slowed down the application progress of the micro systems.

Firstly, since the integrations of micro flow/force sensors or actuators are difficult in micro scale systems as well as the effective micro flow/force sensors are currently not mature, as a result, the micro systems generally lack micro force/flow rate sensing and feedback. Even if it is possible to pack numerous sensors and actuators into a tiny volumes, however, there is a large amount of dynamic, geometric, and parametric uncertainty in micro systems, micro flow/force control in the system is still difficult so that the operating target is often lost or destroyed as well as the input/output droplet is usually inaccurate. Therefore, developing a micro flow/force sensing and closed loop control techniques that have high accuracy, precision, stability, and efficiency is one of the most challenging problem in this type of micro system. Furthermore, the sticking effects or capillary phenomenon affect the operation of micro systems apparently, how to overcome those effects so as to effectively handle/release the micro objects such as MEMS devices, micro droplet, even nano scale entities is another difficult point.

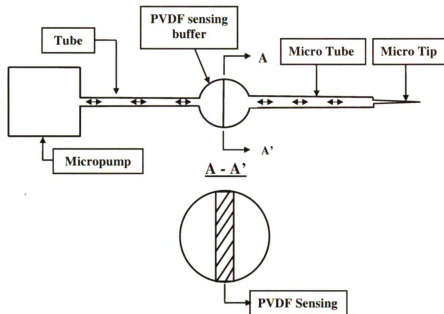
Figure 3.4 shows the developed pneumatic end-effector system for micro and nano fluidic handling and manipulation. It also illustrates the design and working principle of the pneumatic end effector. The end effector system consists of a micropump, inflow micro tube, a PVDF micro-drag force sensor, and a micro tip.

The working principle of the system is as follows. When voltage is applied to the micropump, the free tube end can generate micro suction or pressure force due to vacuum or pressure action provided by the micropump. In addition to detecting the sucking/presuring force, a high sensitivity PVDF beam sensing buffer is built between the micro tube end and micropump. As a result, the micro tube based end-effector, micropump, and PVDF sensing buffer can be integrated into a closed-loop system to provide the precision controlled micro-force for fine micromanipulation and microassembly.

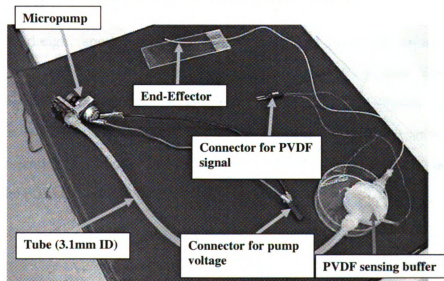
In Fig. 3.4, the micro tube used is a polytetrafluoroethylene (PTFE) micro tube. It is sometimes referred to as Teflon(R). Its internal diameter (ID) is $254\mu m$. It is very lightweight, semi-flexible, and is used for a variety of laboratory applications. The micro tube is heat resistant to $500\text{ }^{\circ}\text{C}$ continuous. It is highly valued for its toughness and insulating qualities as well as high dielectric strength over a wide range of frequencies. Most importantly, the micro tube is also non-absorbent to water and unaffected by acids and alkalis. Detail description and physical properties of the micro tube can be found in [87].

In this system, most importantly, the micropump should be chosen properly. The micropump used is shown in [88]. It is manufactured by KNF Neuberger Inc. The model is NMP05. One of the most important application of this micropump is pick and place (manipulation) of parts for integrated circuit (IC) wafers. Integrated circuit parts have sizes ranging from micrometer to millimeter.

This micropump is a reciprocating displacement micropump in which the moving surface is a diaphragm. It is also known as membrane pump or diaphragm pump. Pressure force is exerted on the working fluid through one or more moving boundaries. The low power consumption makes it ideal for use in operation where performance, power consumption, minimal weight, and size are important. The micropump's features include excellent mechanical stability, flexible mounting, low current, smooth



(a) Design and fabrication of the end effector



(b) Pneumatic end effector system

Figure 3.4. Design and working principle of pneumatic end effector system

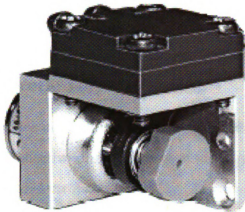


Figure 3.5. Micropump for micro and nano fluidics and tools handling

running, and efficiency. The maximum operating voltage of the micropump is 6V. The operating temperature range of the micropump is 5 °C to 40 °C, and the weight is $20 \times 10^{-3}Kg$.

In the design, specially, we use a PVDF sensing buffer to detect the suction/pressure force generated by the micropump due to the flow rates. The detected force is related to the suction/pressure force acting at the end-effector (tube end). Therefore, it is necessary to achieve the PVDF sensing model for the system, as well as it is essential to integrate the PVDF sensing beam to the system to in order to obtain the precision controlled micro-force.

3.2 Modeling of Dielectrophoretic Force for Micro and Nano Manipulation

3.2.1 Dielectrophoretic Force Modeling

Dielectrophoresis is the motion of a particle produced by the interaction of nonuniform electric field with induced effective dipole moment \mathbf{p} of the particle[89, 90]. Figure 3.6 shows the schematic of dielectrophoresis. In Fig. 3.6, the direction of the arrows exemplifies the direction of the electric field and the length of the arrows represents the magnitude of the electric field.

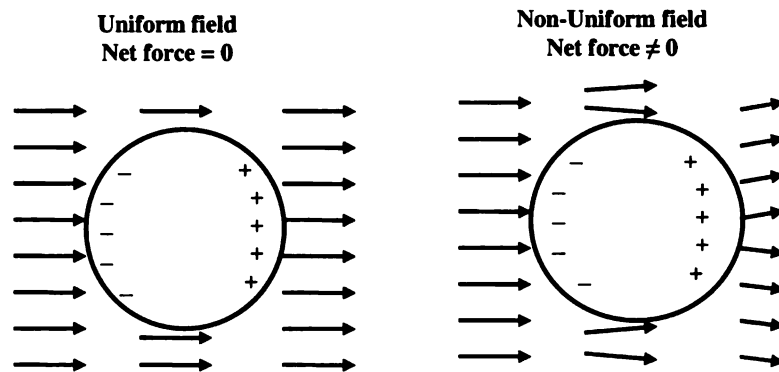


Figure 3.6. Illustration of dielectrophoresis

If the electric field is uniform, the force on each of the two poles of the dipole is equal and opposite, therefore the net force is zero and there is no movement. On the other hand, if the electric field is nonuniform, the force on each of the two poles of the dipole are not equal, therefore the net force is not equal to zero and there is movement of the particle. Furthermore, when a polarizable object is subjected to an electric field, a dipole moment is induced. If the electric field is inhomogeneous, the field strength and thus the force acting on each side of the particle will be different, causing the particle to move with respect to the medium. Depending on the polarizability of the particle compared to that of the medium, the force could push the

particle towards high electric field regions, or low electric field regions. Furthermore, if the particles have a higher polarizability (conductivity) than their immersion medium, they move toward regions of high electric field. Conversely, if the particles have lower conductivity than the medium, they move away from regions of high electric field and toward regions of low electric field. The movement of the particle towards high electric field region is called positive dielectrophoresis (+DEP) and the movement of the particle towards low electric field region is called negative dielectrophoresis (-DEP) [55, 91, 92]. In the case of an alternating electric field, the direction of the force and thus the direction of motion will remain the same even upon field reversal, because the dipole moment will be inverted as well. Furthermore, positive and negative dielectrophoresis can be achieved by choosing appropriate frequencies. The frequency at which there is no force acting on the particle or particles is known as the crossover frequency [45].

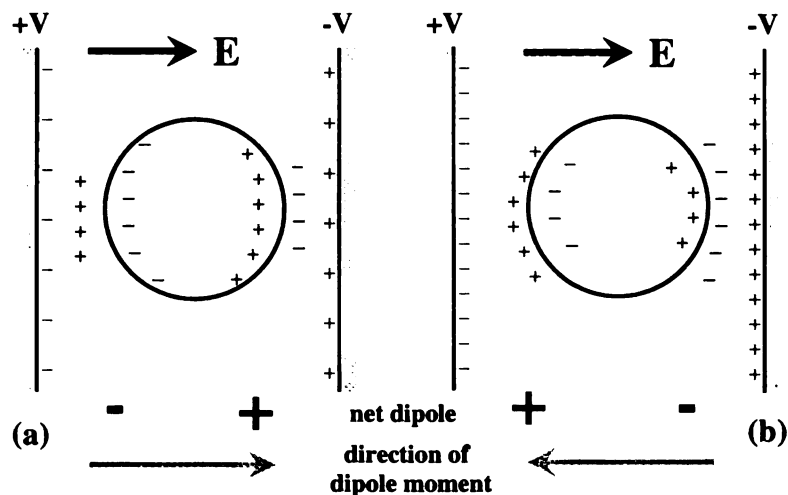


Figure 3.7. Polarizability of dielectric particles in medium

Figure 3.7 illustrates how different dielectric particles polarize. Figure 3.7(a) shows particle with much higher polarizability than the suspending medium, and Fig. 3.7(b) shows particle with much lower polarizability than the suspending medium. If the polarizability is higher, more charges are produced on the inside of the particle/fluid

interface and there is a net dipole across the particle that is parallel to the applied electric field. If the polarizability is lower, more charges are produced on the outside of the particle/fluid interface and the net dipole points in the opposite direction, against the field.

Hence, the force exerted by an electric field \mathbf{E} on a dipole with dipole moment \mathbf{p} [78, 90] is given by

$$F = (\mathbf{p} \bullet \nabla) \mathbf{E} \quad (3.12)$$

where ∇ is the del operator. The effective dipole moment of a particle is given by

$$\mathbf{p} = v \tilde{\alpha} \mathbf{E} \quad (3.13)$$

where v is the volume of the particle, and $\tilde{\alpha}$ is the complex effective polarizability. The complex effective polarizability is defined as

$$\begin{aligned} \tilde{\alpha} &= 3\epsilon_m \underbrace{\left(\frac{\tilde{\epsilon}_p - \tilde{\epsilon}_m}{\tilde{\epsilon}_p + 2\tilde{\epsilon}_m} \right)}_{\tilde{f}_{CM}} \\ &= 3\epsilon_m \tilde{f}_{CM} \end{aligned} \quad (3.14)$$

where $\tilde{\epsilon}_p$ and $\tilde{\epsilon}_m$ refers to the complex permittivity of the particle and the medium respectively defined by

$$\tilde{\epsilon}_{m,p} = \epsilon - j \frac{\sigma}{\omega} \quad (3.15)$$

Here σ is the conductivity, ϵ is the real permittivity of both the particle and the medium respectively. $\omega = 2\pi f$ is the angular frequency of the applied electric field.

The magnitude of the polarizability and the effective dipole moment of the particle is frequency dependent. This dependence is define by \tilde{f}_{CM} in equation (3.14), and it

is referred to as the *Clausius-Mossotti factor*. It is complex, describing a relaxation in the effective permittivity or polarizability of the particle with a relaxation time described in [90] as follows.

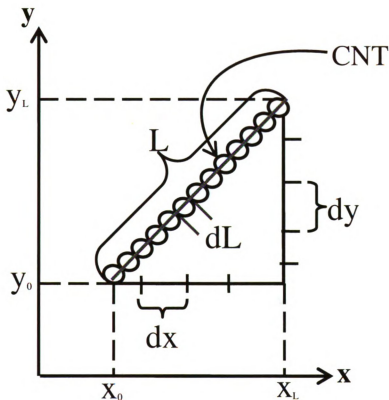


Figure 3.8. Illustration of carbon nanotube as a line

$$\tau_{MW} = \frac{\varepsilon_p + 2\varepsilon_m}{\sigma_p + 2\sigma_m} \quad (3.16)$$

Combining equations (3.72) and (3.13), the force exerted by an electric field \mathbf{E} on a dipole with dipole moment \mathbf{p} can be written as

$$F = (v\hat{\alpha}\mathbf{E} \cdot \nabla)\mathbf{E} \quad (3.17)$$

On the basis of dielectrophoresis theory, to model the DEP force distribution for manipulating CNTs, we reasonably assumed that carbon nanotube form a particle

by particle line structure after undergoing AC electric field. Our derivation is based on this assumption and as described in Fig. 3.8.

Following the geometry of Fig. 3.8, we write the volume of carbon nanotube particles as

$$v = \pi r^2 dL \quad (3.18)$$

where r is the radius of the carbon nanotube particles, dL is the change in length of carbon nanotube. By Pythagorean theorem, dL can be written as

$$dL = \sqrt{dx^2 + dy^2} \quad (3.19)$$

Hence equation (3.17) is written as

$$\begin{aligned} dF_{DEP} &= (\pi r^2 dL \tilde{\alpha} \mathbf{E} \bullet \nabla) \mathbf{E} \\ &= (\pi r^2 dL \tilde{\alpha}) (\mathbf{E} \bullet \nabla) \mathbf{E} \end{aligned} \quad (3.20)$$

By employing vector calculus and the fact that the electric field is irrotational, i.e, a vector field whose curl is zero, ($\nabla \times \mathbf{E} = 0$), equation (3.20) becomes

$$dF_{DEP} = \frac{1}{2} \pi r^2 dL \text{Re}\{\tilde{\alpha}\} \nabla |\mathbf{E}|^2 \quad (3.21)$$

where $\text{Re}\{\tilde{\alpha}\}$ is the real part of the complex effective polarizability of both the particle (CNT) and the medium.

Assuming that CNT is a 2-D object, and following the geometry of CNT in Fig. 3.8 we define the following.

$$L : y = f(x) \quad (3.22)$$

By differentiating equation (3.22), we get the following

$$dy = f'(x) dx \quad (3.23)$$

Combining equations (3.19) and (3.23), dL become

$$dL = \sqrt{(f'(x)dx)^2 + dx^2} \quad (3.24)$$

Simplifying equation (3.24), we get the following equation.

$$dL = \sqrt{1 + (f'(x))^2} dx \quad (3.25)$$

Substituting equation (3.25) into equation (3.21), we obtain the following DEP equation:

$$dF_{DEP} = \frac{1}{2} \pi r^2 \sqrt{1 + (f'(x))^2} Re\{\tilde{\alpha}\} \nabla |\mathbf{E}|^2 dx \quad (3.26)$$

Integrating both sides of equation (3.26), the dielectrophoretic force on a whole CNT particle structure under AC electric field is as follows

$$F_{DEP} = \int_{x_0}^{x_L} \frac{1}{2} \pi r^2 \sqrt{1 + (f'(x))^2} Re\{\tilde{\alpha}\} \nabla |\mathbf{E}|^2 dx \quad (3.27)$$

It can be seen from equation (3.27), the electric field function now becomes a function of one variable x rather than two variables x, y .

Substituting equation (3.14) into equation (3.27) and simplifying, equation (3.27) becomes

$$F_{DEP} = \frac{3}{2} \pi r^2 \varepsilon_m Re\{\tilde{f}_{CM}\} \int_{x_0}^{x_L} \sqrt{1 + (f'(x))^2} \nabla |\mathbf{E}|^2 dx \quad (3.28)$$

It can be seen from equation (3.28) that the derived dielectrophoretic force, F_{DEP} model for carbon nanotubes depends on the real part of Clausius-Mossotti \tilde{f}_{CM} factor, and therefore on the permittivity and conductivity of both the carbon nanotube particles and the suspending medium, as well as the frequency of the applied electric field.

Furthermore, the DEP force is proportional to the size of the particle. For small carbon nanotubes, the DEP force can be overpowered by thermal motion. To trap

CNT particles, DEP potential has to exceed thermal energy. This condition is expressed in [55] as

$$F_{DEP} \geq \frac{3}{2}kT \quad (3.29)$$

where k is the Boltzmann's constant, and T is temperature.

3.2.2 Modeling of Electrorotation for Micro and Nano Manipulation

The action of an externally applied electric field on a polarized particle results in the formation of an induced dipole moment [90]. When the dipole sits in a uniform electric field, each charge on the dipole experiences an equal and opposite force tending to align the dipole parallel to the electric field, i.e, it experiences a torque. There is usually a time delay that exists between the establishment of the electric field and the formation of the dipole. Consequently, if the field vector changes direction, the induced dipole moment vector must realign itself with the electric field vector, causing particle rotation.

Generally, the torque (electrorotation) experienced by the polarizable particle due to applied electric field can be defined in [90] as

$$\mathbf{T} = \frac{1}{2}Re[\mathbf{p} \times \mathbf{E}] \quad (3.30)$$

where \mathbf{p} and \mathbf{E} are the effective dipole moment and electric field respectively. Following the definition of the effective dipole moment given in equation (3.13), the torque can be written as

$$\begin{aligned} \mathbf{T} &= \frac{1}{2}vRe[\tilde{\alpha}(\mathbf{E} \times \mathbf{E})] \\ &= -vIm[\tilde{\alpha}](Re[\mathbf{E}] \times Im[\mathbf{E}]) \end{aligned} \quad (3.31)$$

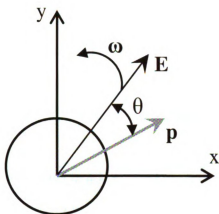


Figure 3.9. Schematic showing how induced dipole moment of a particle lags behind a rotating applied electric field

As shown in Fig. 3.9, the torque is zero when the phase angle θ between the particle's polarization vector \mathbf{p} and the applied electric field \mathbf{E} is zero. On the other hand, the torque is maximum when the phase angle is $\pm 90^\circ$. If the induced dipole moment lags behind the electric field, then the direction of rotation is with the electric field and vice versa for the induced dipole moment that leads the electric field.

Then, the torque equation can be written as

$$\mathbf{T} = -v \text{Im}[\tilde{\alpha}] |\mathbf{E}|^2 \quad (3.32)$$

Following the derivation of dielectrophoretic force, we model the electrorotation (torque) of the CNT particles by making the the following assumptions.

1. We assume carbon nanotube to be a particle line as illustrated in Fig. 3.8
2. Torque on the carbon nanotube is the sum of the segmented (dL) torque as described in Fig. 3.8

Hence, by combining equations (3.14), (3.18), (3.19), and equations (3.22)~(3.25), equation (3.32) becomes

$$d\mathbf{T} = -3\pi r^2 \varepsilon_m \text{Im}\{\tilde{f}_{CM}\} \sqrt{1 + (f'(x))^2} |\mathbf{E}|^2 dx \quad (3.33)$$

Integrating both sides of equation (3.33), we obtain the electrorotation (torque) on the carbon nanotube under AC electric field as follows

$$\mathbf{T} = -3\pi r^2 \varepsilon_m \text{Im}\{\tilde{f}_{CM}\} \int_{x_0}^{x_L} \sqrt{1 + (f'(x))^2} |\mathbf{E}|^2 dx \quad (3.34)$$

It can be seen from equation (3.34) that the derived electrorotation (torque), \mathbf{T} , model for carbon nanotubes in AC electric field depends on the imaginary part of the Clausius-Mossotti \tilde{f}_{CM} factor, and therefore on the permittivity and conductivity of both the carbon nanotube particles and the suspending medium, as well as the frequency of the applied electric field.

3.2.3 Dynamic Modeling of Rotational Motion of Carbon Nanotubes for Intelligent Manufacturing of CNT-Based Devices

When a particle rotates, it experiences a drag torque. This drag torque is characterized by a friction coefficient. The friction coefficient depends on the viscosity of the medium and the geometry of the surface properties of the particle, such as the length and the radius.

For carbon nanotube particles, which we will define as a long and very thin rod, we derived the torque due to rotation through the center of the carbon nanotube as follows.

$$I\ddot{\theta}(\omega) - \frac{L}{2}k\dot{\theta}(\omega) = \mathbf{T} \quad (3.35)$$

In equation (3.35),

I is the moment of inertia at the center of carbon nanotube particles assuming a line

model described in Fig. 3.8

$\ddot{\theta}(\omega)$ is the angular acceleration of carbon nanotube particles

$\dot{\theta}(\omega)$ is the angular velocity of carbon nanotube particles

L is the length of carbon nanotube particles

k is the rotational friction coefficient of carbon nanotube structure

\mathbf{T} is the torque due to electrorotation described in equation (3.34)

For CNT-like structures, the rotational friction coefficient k is given as follows [93, 94, 95].

$$k = \frac{\pi\eta L^3}{3\ln(L/r)} \quad (3.36)$$

where η is the viscosity of the medium, L , r are the length and the radius of CNT respectively.

Furthermore, in equation (3.35), the moment of inertia I is given as [96].

$$I = \frac{1}{12}mL^2 \quad (3.37)$$

where m is the mass of carbon nanotubes, and L is the length of CNT.

In equation (3.34), the electric field function depends on the electrode geometry as well as number of electrodes. For this derivation, we use two pairs of micro electrodes since applications involving intelligent sensor manufacturing using carbon nanotubes are conducted on two or more pairs of micro electrodes.

By defining the appropriate electric field function, equation (3.35) can be solve numerically to obtain the rotation angle and rotational velocity of carbon nanotubes in viscous medium for varying frequencies, consequently leading to an effective and efficient method of manufacturing carbon nanotube based devices.

3.2.4 Dynamic Effect of Fluid Medium on Micro and Nano Particles by Dielectrophoresis

Since carbon nanotube are disbursed in fluidic medium, it becomes very important that the dynamic effect of the fluidic medium on the CNT particles be analyzed.

When CNT particles move in a fluid, the viscous force which is proportional to its velocity retards the particles, and the particles are accelerated by a deterministic force. In this case, the deterministic force is the dielectrophoretic F_{DEP} force, and the particles experience an increasing drag force. For a constant applied force F_{DEP} , the particles reach a terminal velocity beyond which it does not accelerate. If the fluid medium is in motion itself, this terminal velocity also depends on the fluid's velocity. The dynamics of this system can be examined by employing Newton's second law of motion as follows.

$$m \frac{d\mathbf{v}}{dt} = F_{DEP} \quad (3.38)$$

where m is the mass of CNT particles, \mathbf{v} is the velocity of the particles.

When DEP force is applied to the CNT particles where the fluid is moving with velocity \mathbf{u} , the drag force experienced by the particles is proportional to its velocity due to the fluid. The drag force is expressed in [90] as

$$F_{\eta} = f(\mathbf{u} - \mathbf{v}) \quad (3.39)$$

where f is referred to as the friction factor and depends on the range of particle parameters such as size, shape, surface characteristics, and viscosity of the fluid. For a prolate ellipsoid (an ellipsoid formed by the rotation of an ellipse about its major axis) such as CNT that moves in a random direction, the friction factor f is given in [90] as

$$f = \frac{6\pi\eta l}{\ln(2l/r)} \quad (3.40)$$

where η , l , and r are the viscosity of the fluid, the length of the CNT, and the radius of CNT respectively.

Continually, equation (3.38) becomes

$$m \frac{d\mathbf{v}}{dt} = F_{DEP} + f(\mathbf{u} - \mathbf{v}) \quad (3.41)$$

We write equation (3.41) as

$$\frac{d\mathbf{v}}{dt} + \frac{f}{m}\mathbf{v} = \frac{F_{DEP}}{m} + \frac{f}{m}\mathbf{u} \quad (3.42)$$

Recognizing that equation (3.42) is a first order differential equation, and assuming that the CNT particles are initially at rest, i.e, $\mathbf{v}(0) = 0$, the solution to equation (3.42) is

$$\mathbf{v}(t) = \left(\frac{F_{DEP}}{f} + \mathbf{u}\right)(1 - e^{-(f/m)t}), \quad t > 0 \quad (3.43)$$

The acceleration of the CNT particles is described by the exponential term of equation (3.43), and it has a characteristic time constant, $\tau = m/f$. With respect to a CNT in a viscous medium, the order of τ is much smaller than the timescale that we are considering, and carbon nanotube particles reaches its terminal velocity as soon as it is exposed to AC electric field. For times greater than τ , the particles move at terminal velocity given by

$$\mathbf{v}_T = \frac{F_{DEP}}{f} + \mathbf{u} \quad (3.44)$$

With no fluidic motion, CNT particles move with terminal velocity, given by

$$\mathbf{v}_T = \frac{F_{DEP}}{f} \quad (3.45)$$

3.3 Sensing and Control in Micro and Nano Manipulation

3.3.1 Microfluidic Sensing and Control

PVDF micro-drag force sensing buffer is built to detect the fluid flow during suction and release of micro fluids. Based on the high sensitivity of the PVDF film, we built a double-end fixed PVDF sensing beam (with composite structure: one PVDF layer, one polyester layer) for detecting the suction/pressure force/flow rate caused by the fluidic flow effects. The deformation of the sensor beam is caused by the flow stream acting on the whole beam in the sensing buffer. The resulting deformation can also be equivalently made by a drag force (suction/pressure) f_c acting at the middle of the double-end fixed beam strip(s) in the sensing buffer. The design of the double-end fixed sensing beam is shown in Fig. 3.10.

3.3.2 Modeling of Dynamic PVDF Micro-Drag Force Sensing

Following the geometry characteristic of the PVDF strip, since the beam is much wider and longer than the thickness, the strain s_y along the width of the beam can be assumed to be zero. With the above descriptions, based on piezoelectric transverse effect, the unit piezoelectric equation is: (without considering the inverse piezoelectric and pyroelectric effects)[97].

$$D_3(r, t) = d_{31}\sigma_s(r, t) \quad (3.46)$$

where $D_3(r, t)$ is the normal electric displacement of PVDF film, $0 \leq r \leq L$. d_{31} is the transverse piezoelectric coefficient. $\sigma_s(r, t)$ denotes the unit stress on the PVDF strip along the length.

The surface area polarization gives a charge $Q_s(t)$ across the PVDF sensing surface

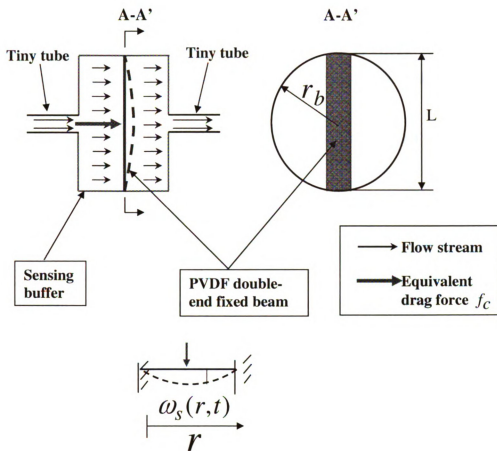


Figure 3.10. Illustration of double-end fixed PVDF sensing beam inside the sensing buffer

area S_A ($L \times W$):

$$\begin{aligned}
 Q_s(t) &= \int D_3(r, t) dS_A \\
 &= \iint_{S_A} D_3(r, t) dy dr.
 \end{aligned} \tag{3.47}$$

Using the mechanics of materials for beam, as shown in Fig. 3.10, the unit stress on the surface of the half PVDF sensing beam can be obtained if the external force $f_c(t)$ acts at the middle of the beam in the sensing buffer.

$$\sigma_s(r, t) = -cE_p \frac{\partial^2 \omega_s(r, t)}{\partial r^2} \tag{3.48}$$

According to Fig. 3.10, notice that we omit the effect of thin electrode layers at the

top and bottom surfaces of PVDF layer. c is the distance between the middle of the PVDF sensing layer and the neutral axis c_n of the beam. $\omega_s(r, t)$, the elastic deflection of the flexible composite beam caused by the micro force $f_c(t)$ at the middle of the beam.

Since the bending charge is the same along the width of PVDF ($s_y=0$), we can rewrite equation (3.47) as:

$$\begin{aligned} Q_s(t) &= \int_0^L d_{31}\sigma_s(r, t)W dr \\ &= -cE_p d_{31}W \frac{\partial \omega_s(r, t)}{\partial r} \Big|_0^L. \end{aligned} \quad (3.49)$$

Continually, a simplified and effective equivalent circuit model of a capacitor C_P can be used to represent the model of the PVDF sensing layer. The output voltage $V_s(t)$ of the PVDF sensing layer caused by the micro force can be described by

$$V_s(t) = -\frac{Q_s(t)}{C_P}. \quad (3.50)$$

By Laplace transformation, the electrical open-circuit transfer function of the PVDF sensing layer is given as:

$$V_s(s) = -\frac{Q_s(s)}{C_P}. \quad (3.51)$$

To find the dynamic relationship between the sensing output V_s and the micro suction/pressure force f_c acting at the middle of the beam, we first to describe a dynamic model of the flexible PVDF sensor beam based on the partial differential equation. Here the PDE describing the elastic deflection of the flexible PVDF sensor is a Bernoulli-Euler equation as follows:

$$EI \frac{\partial^4 \omega_s(r, t)}{\partial r^4} + \rho A \frac{\partial^2 \omega_s(r, t)}{\partial t^2} = f_c(t) \delta(r - \frac{L}{2}) \quad (3.52)$$

where E, I, L and ρ represent the Young's modulus, inertia moment, length of beam, and linear mass density of the beam. $f_c(t)$ is the external suction/pressure force

acting at the middle of the beam, which can be detected by the PVDF sensing strip. $\delta(\cdot)$ denotes the Dirac delta function.

The boundary conditions for the above equation are:

$$\omega_s(0, t) = 0 \quad (3.53)$$

$$EI \frac{\partial \omega_s^2(0, t)}{\partial r^2} = 0 \quad (3.54)$$

$$\omega_s(L, t) = 0 \quad (3.55)$$

$$EI \frac{\partial \omega_s^2(L, t)}{\partial r^2} = 0 \quad (3.56)$$

By using the modal analysis method[98], we assume that the deformation of the beam has infinite shape modes, then the deflection $\omega_s(r, t)$ can be expressed as an infinite series in the following form :

$$\omega_s(r, t) = \sum_{i=1}^{\infty} \Phi_i(r) q_{si}(t) \quad (3.57)$$

where $\Phi_i(r)$ are the eigenfunction satisfying the ordinary differential equation and $q_{si}(t)$ are the modal displacements caused by the micro force. Then the deflection mode shapes are assumed to be[98]:

$$\begin{aligned} \Phi_i(r) = & C_1 \sin(\alpha_i r) + C_2 \cos(\alpha_i r) \\ & + C_3 \sinh(\alpha_i r) + C_4 \cosh(\alpha_i r) \end{aligned} \quad (3.58)$$

Substituting the above equations (3.85) and (3.58) into the boundary conditions (3.81)~(3.84), then we found α_i are the infinite set of eigenvalues yielded by

$$\alpha_i L = i\pi \quad i = 1, 2, \dots \quad (3.59)$$

and also, the natural frequencies ω_i of the sensor beam correspond to the α_i by

$$\omega_i = (i\pi)^2 \sqrt{\frac{EI}{\rho AL^4}} \quad (3.60)$$

In order to determine the dynamics of the system, we use Lagrange's equation of motion by

$$\frac{d}{dt} \frac{\partial (E_{sk} - E_{sp})}{\partial \dot{q}_{si}} - \frac{\partial (E_{sk} - E_{sp})}{\partial q_{si}} = Q_i. \quad (3.61)$$

Here, E_{sk} is the kinetic energy, E_{sp} represents the potential energy and Q_i is the generalized nonconservative forces related to the external micro force. They are

$$E_{sk} = \frac{1}{2} \int_0^L \dot{\omega}_s(r, t)^2 \rho A dr \quad (3.62)$$

$$E_{sp} = \frac{1}{2} \int_0^L EI \omega_s''(r, t)^2 dr \quad (3.63)$$

$$Q_i = f_c(t) \Phi_i\left(\frac{L}{2}\right) \quad (3.64)$$

where a prime indicates the derivative with respect to position and a dot denotes the derivative with respect to time.

Using the Lagrange's equation of motion (3.61) and (3.87), we have the differential equation corresponding to each shape mode of the sensor beam to be

$$EI \alpha_i^4 q_{si}(t) + \rho A \ddot{q}_{si}(t) = f_c(t) \Phi_i\left(\frac{L}{2}\right) \quad (3.65)$$

Then by the Laplace transformation of the above equation, the dynamic relationship between the modal displacements $q_{si}(s)$ and the external micro force is given as

$$q_{si}(s) = \frac{f_c(s) \Phi_i\left(\frac{L}{2}\right)}{\rho A (s^2 + \omega_i^2)}. \quad (3.66)$$

Based on equations (3.77) and (3.79), since $\omega_s(r, s) = \sum_{i=1}^{\infty} \Phi_i(r) q_{si}(s)$, by Laplace transform of equation (3.77), $Q_s(s)$ can be represented as

$$\begin{aligned} Q_s(s) &= -c E_p d_{31} W \omega_s'(r, s) \Big|_0^L \\ &= -c E_p d_{31} W \sum_{i=1}^{\infty} [\Phi_i'(L) - \Phi_i'(0)] q_{si}(s). \end{aligned} \quad (3.67)$$

Substituting equation (3.89) into equation (3.79), then we have

$$V_s(s) = C_s \sum_{i=1}^{\infty} [\Phi_i'(L) - \Phi_i'(0)] q_{si}(s). \quad (3.68)$$

where $C_s = \frac{-c E_p d_{31} W}{C_p}$.

Subsequently, by combining equations (3.88) and (3.90), we have the dynamic sensing model, which denotes the dynamic relationship between the output voltage V_s of PVDF sensing beam and the external micro suction/pressure force f_c at the middle of the beam in the sensing buffer as follows:

$$\frac{V_s(s)}{f_c(s)} = C_s \sum_{i=1}^{\infty} \left\{ \frac{[\Phi'_i(L) - \Phi'_i(0)]\Phi_i(\frac{L}{2})}{\rho A(s^2 + \omega_i^2)} \right\}. \quad (3.69)$$

To achieve the sensing voltage V_s , the PVDF sensing beam is interfaced with the analog/digital input/output board PCI-DAS4020/12 in the PC through an instrumental amplifier circuit illustrated in Fig. 3.11. The circuit is constructed using the ultralow input bias current operational amplifier AD549 with a high input impedance $R_{in} = 10^{13}\Omega$ and low bias current $150fA$ [99]. Notice that $R_3 = R_4$ and $R_1 = R_2$. The amplifier circuit is used to buffer the open circuit voltage V_s of the sensing beam, and can convert the high impedance signal generated by the PVDF sensing beam to a low impedance voltage suitable for convenient coupling to the acquisition board PCI-DAS4020/12. The circuit output V_{so} is an amplified and filtered approximation of the voltage V_s and can be sampled by PCI-DAS4020/12 board to the PC. The transfer function between V_{so} and V_s can be represented as:

$$\frac{V_{so}(s)}{V_s(s)} = \frac{R_3}{R_1} \underbrace{\frac{sR_{in}C_P}{1 + sR_{in}C_P}}_{C_b}. \quad (3.70)$$

To further remove the 60Hz noise from the data acquisition system, a zero phase notch filter is added in the data collection system.

Finally, by considering the whole sensing system, the global transfer function is given as:

$$\frac{V_{so}(s)}{f_c(s)} = C_b C_s \sum_{i=1}^{\infty} \left\{ \frac{[\Phi'_i(L) - \Phi'_i(0)]\Phi_i(\frac{L}{2})}{\rho A(s^2 + \omega_i^2)} \right\}. \quad (3.71)$$

Based on this dynamic equation, we can obtain the micro suction/pressure force $f_c(t)$

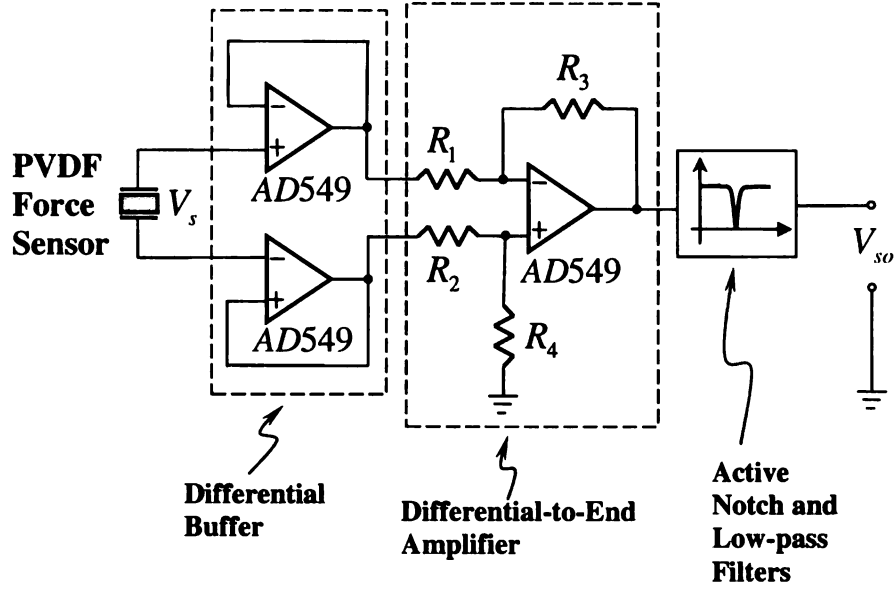


Figure 3.11. Schematics of the developed electronic interface circuit of the PVDF sensor [5, 6].

by measuring the output voltage $V_{so}(t)$ of the sensing beam when the initial values $f_c(t_0)$ and $V_{so}(t_0)$ are known.

In addition, the force achieved from equation (3.93) is the suction/pressure force in the sensing buffer. In order to get the suction/pressure force at the end-effector (tube end), we assume the air pressure P caused by the pump is the same in the tube end and in the sensing buffer. The following equations can be written based on the the assumptions.

$$P = \frac{F_s}{A_s}, \quad P = \frac{f_c}{A_c}. \quad (3.72)$$

Rearranging equation (3.72) and solving for the suction/pressure force F_s at the free tube end (end-effector), we have

$$F_s = \frac{A_s}{A_c} f_c. \quad (3.73)$$

where A_s is the cross section area of the inner tube end, and A_c is the cross section area of the sensing buffer, and f_c is the micro suction/pressure force at the middle

of the beam in the sensing buffer. Equation (3.73) can be used for detecting the suction/pressure force at the tube end (end-effector).

3.4 Sensing In Micro-Bio Injection

In micro-bio injection, the lack of effective force sensing and feedback mechanism have dramatically reduced the success rate during injection and manipulation. Hence this work addresses both the measurement of injection force behavior and the characterization of mechanical properties of living *Drosophila* embryos using a well modeled *in situ* PVDF (Polyvinylidene Fluoride) piezoelectric micro-force sensing tool with a resolution in the range of sub- μN . *Drosophila* embryo is one of the most studied organisms currently in genetics and developmental biology, and also has strong implications in the human medical study. In this work, we focus on the development of a sensorized biomanipulation tool based on the high sensitivity PVDF film and the minimally invasive pipette injector. Using this tool, close monitoring of the magnitude and direction of micro injection and other biomanipulation forces acting on the embryo during the injecting process becomes a reality. In addition, a networked microrobotic biomanipulation platform integrating this developed two-axis (2-D) PVDF micro-force sensing tool is built. By employing the event-synchronization for the feedback of injection video and micro-force, the developed networked microrobotic platform can greatly advance operations in micro injection of living *Drosophila* embryos. Several experimental results have clearly demonstrated the quantitative relationships between the applied force and membrane structural deformation of embryos in the different stages of embryogenesis, as well as the force behaviors of micro injection .

Ultimately, the technology will provide a critical and major step towards the development of automated micro-bio manipulation for batch micro injection and even microsurgery of living embryos for potential human medical study, which will facilitate

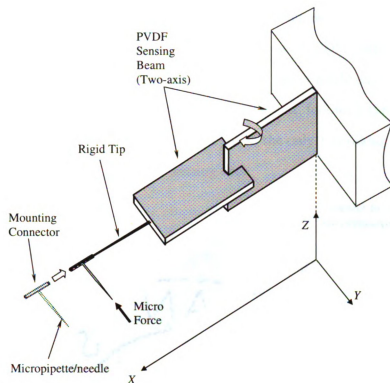


Figure 3.12. Illustration of the 2-D PVDF micro-force sensing tool [7, 8]

the development of medicine for the cure of human diseases.

3.4.1 Force Sensing In Micro-Bio Injection Using Polyvinylidene Fluoride (PVDF)

For effective biomanipulation and micro injection, a self-decoupling two-axis (2-D) PVDF force sensing tool has been developed as shown in Figure 3.12.

The 2-D sensing tool is designed based on a serial connecting structure. In each direction, a PVDF composite beam is constructed. Notice that the composite beam is basically a two layer structure whose piezoelectric layer acts as a sensing device bonded to a support beam layer made from polyester. It can also be seen that this structure provides a decoupled force measurement in the Y and Z axis, which is due to

the two PVDF composite beams' orthogonal configuration, as well as the strong shear forces along the Y and Z axis existing between the two PVDF beams. At the free end of the sensing tool, a rigid steel tip is attached, and a modified micropipette or needle is assembled to the end of the rigid tip. Notice that, following the configuration shown in Fig. 3.12, for micro injection in this work, the only 1-D (along Y axis) micro injection force is measured using the sensing tool.

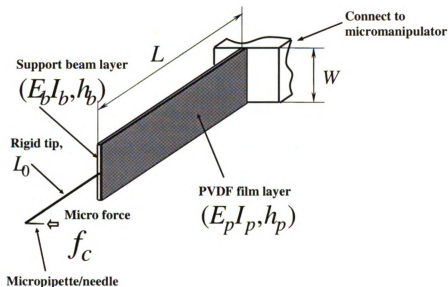


Figure 3.13. Illustration of the equivalent Y axis PVDF force sensing tool[7, 8].

Subject to the super flexibility of the cantilever base micro-force sensor, development of a dynamic sensing model for achieving accurate micro-force measurement becomes necessary [100]. In this research work, the dynamic force modeling along one of the force axes (Y axis) is described in detail as follows. To conveniently model the Y axis force sensing, an equivalent and simplified 1-D structure is shown in Fig. 3.13. In this figure, the deformation of the sensor beam is caused by the applied force acting along the micropipette at the end of the rigid tip.

3.4.2 Modeling of Micro-Bio Force Sensor

In order to achieve accurate force information during micro-bio injection and manipulation, it becomes necessary to model the developed micro-bio force sensor.

Following the geometry characteristic of the PVDF sensing layer, since the beam is much wider and longer than the thickness, the strain s_y along the width of the beam can be assumed to be zero [101]. With the above descriptions, based on the piezoelectric transverse effect, the unit piezoelectric equation is: (without considering the pyroelectric effects due to use at stable temperature environment.) [97, 102].

$$D_3(r, t) = d_{31}\sigma_s(r, t) \quad (3.74)$$

where $D_3(r, t)$ is the normal electric displacement of PVDF film. d_{31} is the transverse piezoelectric coefficient. $\sigma_s(r, t)$ denotes the unit stress of the PVDF sensing layer along the beam length, and $0 \leq r \leq L$.

The surface area polarization gives a charge $Q_s(t)$ across the PVDF sensing layer surface area S_A ($L \times W$):

$$\begin{aligned} Q_s(t) &= \int D_3(r, t) dS_A \\ &= \iint_{S_A} D_3(r, t) dy dr. \end{aligned} \quad (3.75)$$

Using the mechanics of materials for a cantilever beam [103], as shown in Fig.3.13, the unit stress on the surface of the PVDF sensing layer can be obtained if the external load $f_c(t)$ acts along the micropipette

$$\sigma_s(r, t) = -cE_p \frac{\partial^2 \omega_s(r, t)}{\partial r^2} \quad (3.76)$$

According to Fig.3.13, notice that since two-layer composite beam is considered (we omit the effect of very thin and low Young's modulus electrode layers at the top and bottom surfaces of PVDF layer.). c is the distance between the middle of the PVDF sensing layer and the neutral axis c_n of the composite beam. $\omega_s(r, t)$, the elastic

deflection of the flexible composite beam caused by the micro force $f_c(t)$ along the micropipette. E_p is the Young's modulus of the PVDF sensing layer.

Since the bending charge is the same along the width of PVDF ($s_y=0$), we can rewrite equation (3.75) as:

$$\begin{aligned} Q_s(t) &= \int_0^L d_{31}\sigma_s(r,t)Wdr \\ &= -cE_p d_{31}W \frac{\partial\omega_s(r,t)}{\partial r} \Big|_0^L. \end{aligned} \quad (3.77)$$

A simplified and effective equivalent circuit model of a capacitor C_P can be used to represent the model of the PVDF sensing layer. And the output voltage $V_s(t)$ of the PVDF sensing layer caused by the micro force can be described by

$$V_s(t) = \frac{Q_s(t)}{C_P}. \quad (3.78)$$

By Laplace transformation, the electrical open-circuit transfer function of the sensing layer is given as:

$$V_s(s) = \frac{Q_s(s)}{C_P}. \quad (3.79)$$

To find the dynamic relationship between the sensing output V_s and the micro force f_c acting along the micropipette, we first describe a dynamic model of the flexible PVDF sensing beam based on the partial differential equation (PDE). Here the PDE describing the elastic deflection of the flexible composite PVDF sensing beam is a Bernoulli-Euler equation with additional terms due to the external force and moment at the free end of sensing beam as follows:

$$\begin{aligned} EI \frac{\partial^4\omega_s(r,t)}{\partial r^4} + \rho A \frac{\partial^2\omega_s(r,t)}{\partial t^2} &= f_c(t)\delta(r-L) \\ &+ f_c(t)L_0 \frac{\partial(\delta(r-0) - \delta(r-L))}{\partial r} \end{aligned} \quad (3.80)$$

where E, I, L, L_0 and ρ represent the Young's modulus, inertia moment, length of beam, length of the rigid tip, and linear mass density of the composite beam respectively. We assume that $EI = E_b I_b + E_p I_p$ is the flexural rigidity of the composite

sensing beam and $\rho A = \rho_b W h_b + \rho_p W h_p$ is mass per unit length of the sensing beam. It is important to note that E_b, I_b represents the Young's modulus and inertia moment of the polyester layer, and I_p represents the inertia moment of the PVDF sensing layer. ρ_b, h_b represents the mass per unit density and the thickness of the polyester layer, and ρ_p, h_p represents the mass per unit density and the thickness of the PVDF sensing layer. $\delta(\cdot)$ denotes the Dirac delta function.

The boundary conditions for the above equation are:

$$\omega_s(0, t) = 0 \quad (3.81)$$

$$EI \frac{\partial \omega_s(0, t)}{\partial r} = 0 \quad (3.82)$$

$$EI \frac{\partial \omega_s^2(L, t)}{\partial r^2} = f_c L_0 \quad (3.83)$$

$$EI \frac{\partial \omega_s^3(L, t)}{\partial r^3} = f_c. \quad (3.84)$$

By using the modal analysis method [98], and assuming that the deformation of the beam has infinite shape modes, the deflection $\omega_s(r, t)$ can be expressed as an infinite series in the following form :

$$\omega_s(r, t) = \sum_{i=1}^{\infty} \Phi_i(r) q_{si}(t) \quad (3.85)$$

where $\Phi_i(r)$ are the eigenfunction satisfying the ordinary differential equation and $q_{si}(t)$ are the modal displacements caused by the micro force.

Using the Lagrange's equation of motion and orthogonality conditions [98], we have the differential equation corresponding to each shape mode of the composite beam of the sensing tool to be

$$\begin{aligned} EI \alpha_i^4 q_{si}(t) + \rho A \ddot{q}_{si}(t) &= f_c(t) \Phi_i(L) \\ &+ f_c(t) L_0 [\Phi_i'(L) - \Phi_i'(0)] \end{aligned} \quad (3.86)$$

where a prime indicates the derivative with respect to position and a dot denotes the derivative with respect to time. α_i are the infinite set of eigenvalues. The natural

frequencies ω_i of the composite sensing beam correspond to the α_i by

$$\omega_i = \alpha_i^2 \sqrt{\frac{EI}{\rho A}} \quad (3.87)$$

Then by the Laplace transformation of the above equation, the dynamic relationship between the modal displacements $q_{si}(s)$ and the external micro force is given as

$$q_{si}(s) = \frac{f_c(s)(\Phi_i(L) + L_0[\Phi_i'(L) - \Phi_i'(0)])}{\rho A(s^2 + \omega_i^2)}. \quad (3.88)$$

Based on equations (3.77) and (3.79), since $\omega_s(r, s) = \sum_{i=1}^{\infty} \Phi_i(r)q_{si}(s)$, by Laplace transform of equation (3.77), $Q_s(s)$ can be represented as

$$\begin{aligned} Q_s(s) &= -cE_p d_{31} W \omega_s'(r, s) \Big|_0^L \\ &= -cE_p d_{31} W \sum_{i=1}^{\infty} [\Phi_i'(L) - \Phi_i'(0)] q_{si}(s). \end{aligned} \quad (3.89)$$

Substituting equation (3.89) into equation (3.79), we have

$$V_s(s) = C_s \sum_{i=1}^{\infty} [\Phi_i'(L) - \Phi_i'(0)] q_{si}(s). \quad (3.90)$$

where $C_s = \frac{-cE_p d_{31} W}{C_P}$.

Subsequently, by combining equations (3.88) and (3.90), we have the dynamic sensing model, which denotes the dynamic relationship between the output voltage V_s of the PVDF sensing layer and the external micro force f_c along the Y axis (micro pipette) as follows:

$$\begin{aligned} \frac{V_s(s)}{f_c(s)} &= C_s \sum_{i=1}^{\infty} \left\{ \frac{[\Phi_i'(L) - \Phi_i'(0)]\Phi_i(L)}{\rho A(s^2 + \omega_i^2)} \right. \\ &\quad \left. + \frac{L_0[\Phi_i'(L) - \Phi_i'(0)]^2}{\rho A(s^2 + \omega_i^2)} \right\}. \end{aligned} \quad (3.91)$$

To achieve the sensing voltage V_s , the PVDF sensing layer is interfaced with the PCI-DAS4020/12 analog/digital input/output board (Measurement & Computing

Co.) in the PC through a developed instrumental amplifier circuit illustrated in [7, 5]. The circuit was constructed using the AD549 ultralow input bias current operational amplifier (Analog Devices Co.) with a high input impedance $R_{in} = 10^{13}\Omega$ and low bias current $150fA$. Notice that $R_3 = R_4$ and $R_1 = R_2$. The amplifier circuit is used to buffer the open circuit voltage V_s of the PVDF sensing layer, and can convert the high impedance signal generated by the PVDF sensing layer to a low impedance voltage suitable for convenient coupling to the PCI-DAS4020/12 acquisition board. The circuit output V_{so} is an amplified and filtered approximation of the voltage V_s and can be sampled by the PCI-DAS4020/12 board. The maximum sampling frequency of PCI-DAS4020/12 is 20MHz with 12-bit AD resolution. The loop time of the force sensing and acquisition is about $60\mu s$. The transfer function between V_{so} and V_s can be represented as:

$$\frac{V_{so}(s)}{V_s(s)} = \frac{R_3}{R_1} \underbrace{\frac{sR_{in}C_P}{1 + sR_{in}C_P}}_{C_b}. \quad (3.92)$$

To further remove the $60Hz$ noise from the data acquisition system, a zero phase notch filter is added in the data collection system.

Finally, by considering the whole sensing system, the global transfer function is found

$$\frac{V_{so}(s)}{f_c(s)} = C_b C_s \sum_{i=1}^{\infty} \left\{ \frac{[\Phi'_i(L) - \Phi'_i(0)]\Phi_i(L)}{\rho A(s^2 + \omega_i^2)} + \frac{L_0[\Phi'_i(L) - \Phi'_i(0)]^2}{\rho A(s^2 + \omega_i^2)} \right\}. \quad (3.93)$$

Based on this dynamic equation, we can obtain the micro force $f_c(t)$ by measuring the output voltage $V_{so}(t)$ from the sensing PVDF when the initial values $f_c(t_0)$ and $V_{so}(t_0)$ are known.

3.5 Chapter Summary

In this research work, the development of a micro pneumatic end effector technology with in-situ PVDF beam force sensing for micro robotic manipulators and for the manufacturing of nano devices such as carbon nanotube(s) is presented. The dynamic PVDF force sensing model is developed based on a beam fixed at both ends. The PVDF sensing beam can measure/detect the suction/pressure force/flow rate caused by the micro pump. Then the corresponding flow rate or force at the tube end (end-effector) can be determined by the measured flow rate and force. As a result, the micro tube based end-effector, micro pump, and PVDF sensing buffer can be integrated into a closed-loop bi-directional pneumatic driving platform to provide the precision controlled micro suction/pressure force or bi-directional flow rates for fine micro/nano scale assembly, manipulation, manufacturing, and droplet control. Furthermore, in this research work, the modeling and control for manipulating carbon nanotubes using dielectrophoretic force is presented. The dielectrophoretic force model is derived assuming CNT to be a particle line structure after undergoing AC electric field. The electrorotation (torque) model on CNT is also derived and presented by the assumption that carbon nanotubes form a line shape after undergoing AC electric field compare to existing model that assumes carbon nanotubes to be one particle. In addition, the mathematical model describing precisely the rotational motion of carbon nanotubes in viscous medium (acetone) is derived and presented. All of these mathematics have ground breaking potential in the field of nanotechnology.

CHAPTER 4

Theory for Micro Electrode and Electric Field Design for Carbon Nanotube Applications

4.1 Micro Electrode Design

In order to effectively deposit, manipulate, and implement carbon nanotubes using dielectrophoresis as described in chapter 3 on micro electrodes, it become necessary to mathematically describe the micro electrode geometry. The micro electrode design is based on the assumption that the electrical potential at any point (x,y,z) created by a micro electrode of interest is defined by a polynomial that obeys Laplace's equation[104]. The solution to to Laplace's equation are also known as potential theory. By substituting this polynomial into Laplace's equation the corresponding equipotentials can therefore be determined, and these in turn can be used to define the required micro electrode boundaries for use in carbon nanotube deposition, manipulation, and implementation using dielectrophoresis. Furthermore, the micro electrodes design method can readily be applied to three-dimensional micro electrode

design, for the sake of simplicity and the fact that carbon nanotube deposition and manipulation is carried out on two dimensional micro electrode array, the theoretical development is restricted to two dimensional micro electrode design.

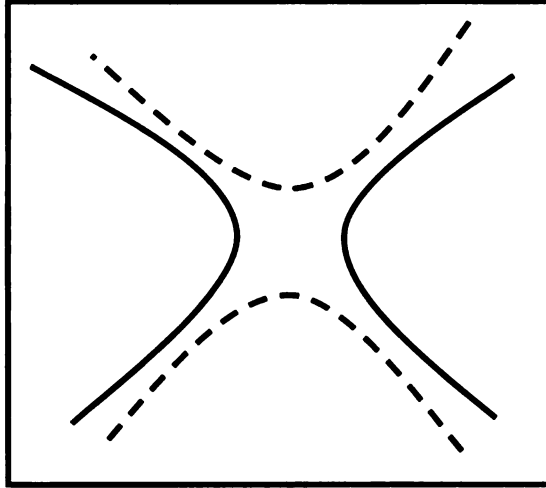


Figure 4.1. Micro electrode design for carbon nanotube implementation

Figure 4.1 shows the micro electrodes design for carbon nanotube deposition, manipulation, and implementation using dielectrophoresis as described in chapter 3. It is worth noting that the design is not restricted to the one depicted in Fig. 4.1. Notice that in Fig. 4.1, the number of micro electrode pairs is two, hence a second order polynomial is employed to derive the necessary boundary conditions and applied potential between any pair of the micro electrode.

4.1.1 Theory for Micro Electrode Design

In designing micro electrodes for deposition, manipulation, and implementation of carbon nanotubes using dielectrophoresis, an electric potential defined by a second-order Laplace's polynomial is considered. We defined this polynomial as follows.

$$f_2(x, y) = a_1x^2 + a_2xy + a_3y^2 \quad (4.1)$$

In equation (4.1), the subscript 2 in $f_2(x, y)$ indicates the order n , of the polynomial. Since electrodes are in pairs, and we are defining a second-order polynomial for electrode geometry, then there will be $2n$ electrodes. Here we'll have four electrodes or two pairs of electrodes as depicted in Fig.4.1.

From equation (4.1), and in general, there will be a total number of C_{n+1}^n coefficients. In our case, there will be C_3^2 coefficients.

Following Laplace's equation, i.e

$$\frac{\partial^2 f_2(x, y)}{\partial x^2} + \frac{\partial^2 f_2(x, y)}{\partial y^2} = 0, \quad (4.2)$$

we get the following.

$$\frac{\partial^2 f_2(x, y)}{\partial x^2} = 2a_1 \quad (4.3)$$

and

$$\frac{\partial^2 f_2(x, y)}{\partial y^2} = 2a_3 \quad (4.4)$$

Substituting equations (4.3) and (4.4) into the Laplace's equation, equation (4.2), we get the following.

$$2a_1 + 2a_3 = 0 \quad (4.5)$$

Simplifying equation (4.5), we get the following

$$a_3 = -a_1 \quad (4.6)$$

Hence equation (4.1) can be expressed generally as

$$f_2(x, y) = a_1x^2 + a_2xy - a_1y^2 \quad (4.7)$$

where a_1 and a_2 are independent parameters and $f_2(x, y)$ is the linear combination of the following two independent functions.

$$\begin{aligned} f_{2a} &= x^2 - y^2 \\ f_{2b} &= xy \end{aligned} \tag{4.8}$$

Furthermore, since the electric potential function based on f_{2a} is $f_2(x, y) = a_1(x^2 - y^2)$, it can be used to define the equipotentials in the the electric field. For instance, equipotentials can be constructed using the following equations.

$$\begin{aligned} k &= x^2 - y^2 \\ -k &= x^2 - y^2 \end{aligned} \tag{4.9}$$

Equation (4.9) is clearly represented in Fig.4.1 for both positive and negative polarities.

Furthermore, if the electrodes are shaped according to equipotential lines depicted in Fig.4.1, and positive and negative potentials of $+v$ and $-v$ are applied, then the potential $f_2(x, y)$ at any point (x, y) in the inter-electrode space is given by the following equation.

$$f_2(x, y) = \frac{v}{k}(x^2 - y^2) \tag{4.10}$$

It is important to note that the constant k , in equation (4.9) used to determine of equipotentials can be chosen arbitrarily and will not affect the final electric field pattern established by the electrode. On the other hand, it's value does determine the size of the designed electrode.

4.2 Electric Field Design

The use of dielectrophoresis defined by [89, 90] as the motion of a particle produced by the interaction of nonuniform electric field with induced effective dipole moment \mathbf{p} of the particle, to trap and manipulate carbon nanotubes on micro electrodes was described in chapter 3. However, for controlled and predictable applications of dielectrophoresis, a knowledge of the non-uniform electric field distribution established by the micro electrode geometry becomes absolutely critical and necessary. In the section 4.1.1, the theory for micro electrode design was developed in detail. This theory also governs electric potentials for the designed micro electrodes.

In chapter 3, we derived a new mathematical model for application of dielectrophoresis on carbon nanotubes for implementation on carbon nanotubes. The derived model takes into account the spatial variation of both the electric field and the gradient of the electric field on micro electrodes. Therefore, the spatial variations of the electric field, $|E|$ and $\nabla|E|^2$ described in the dielectrophoretic force model (DEP) in chapter 3 is choosing for a second order polynomial micro electrode geometry derived in section 4.1.1.

In equation (4.1), the micro electrode structure is in two dimension, i.e (x, y) . Hence the electric field would comprise of two components, E_x , and E_y . These field components are determined by taking the partial differential of the potential function $f_n(x, y)$. In this case $n = 2$ as described in equation (4.1). It is important to note that for $n = 1$, the electric field is uniform, hence $\nabla|E|^2 = 0$ and no DEP force is exerted on carbon nanotube particles located between the micro electrodes. For $n > 1$, then $\nabla|E|^2$ becomes a function of position (x, y) and n . Without loss of generality, in [104], $\nabla|E|^2$ varies as $(x^2 + y^2)^{n-1.5}$. Hence electric field function is chosen based on the above derivation and as a function of position (x, y) on the designed micro electrodes.

4.3 Chapter Summary

This chapter presents the mathematics describing the design of micro electrodes geometry for effective deposition, manipulation, and implementation of carbon nanotubes using dielectrophoresis as described in chapter 3. The mathematics describing the electric field design for dielectrophoresis application on carbon nanotubes on micro electrodes is also described. The micro electrode design and the electric field function design are based on the assumption that the electrical potential at any point (x,y,z) created by a micro electrode of interest is defined by a polynomial that obeys Laplace's equation. For this application, a second-order polynomial was employed to formulate the design of the micro electrodes and electrical field function candidates.

CHAPTER 5

Application in Micro and Nano Manipulation and Assembly

5.1 Microfluidics Based Micro and Nano Manipulation and Assembly

An application of the new microfluidic end effector is to handle nano devices such as carbon nanotubes (CNTs) and silver cubes as illustrated in Fig. 5.1. In this work, experiments focusing on handling carbon nano tubes in liquid acetone, and carbon nanotube deposition between micro electrodes for manufacturing of nano sensor/electronics are demonstrated. The results verify the effectiveness of the new microfluidic end effector. That is, precisely and automatically placing carbon nanotube(s) in the center of two micro electrodes separated by a few microns.

5.2 Validation of Poiseuille's Law

The developed micro microfluidic end effector system consists of a DC micro-diaphragm pump. To validate Poiseuille's law, a simulation was done using the pa-

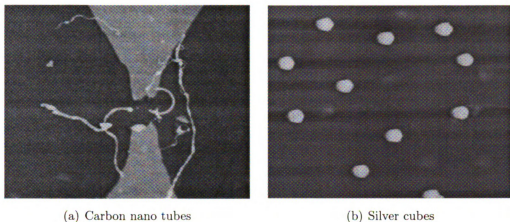


Figure 5.1. AFM image illustrating nano entities. The scanning range is $10\mu m \times 10\mu m$.

rameters of the DC micro-diaphragm pump. The DC micro-diaphragm pump model used is NMP05. Details can be found in [20, 88]. Based on the micro pump parameters, and using Poiseuille's law, equation (3.11), we can get the relationship between volume flow rate and differential pressure as illustrated in Fig. 5.2. In Fig. 5.2, the blue solid line represents the relationship between volume flow rate and differential pressure for liquid water, while the red dashed line depicts the relationship between volume flow rate and differential pressure for liquid acetone. The length and diameter of the micro pipette used for the simulation are $1mm$ and $20\mu m$ respectively. The results verify the model. Fig. 5.3 shows a 3D plot showing the relationship between volume flow rate, radius of tube and pressure difference. The simulation was done using the parameters of two liquids, water and acetone respectively. The viscosities of water and acetone are $890 \times 10^{-6}Ns/m^2$ and $300 \times 10^{-6}Ns/m^2$ respectively. The pressure difference required to disburse acetone is much lower than water because the viscosity of water is much higher than the viscosity of acetone. The simulation result verifies the model. In our experiments, two different pipettes with different internal diameters were employed to deposit carbon nanotubes between micro electrodes.

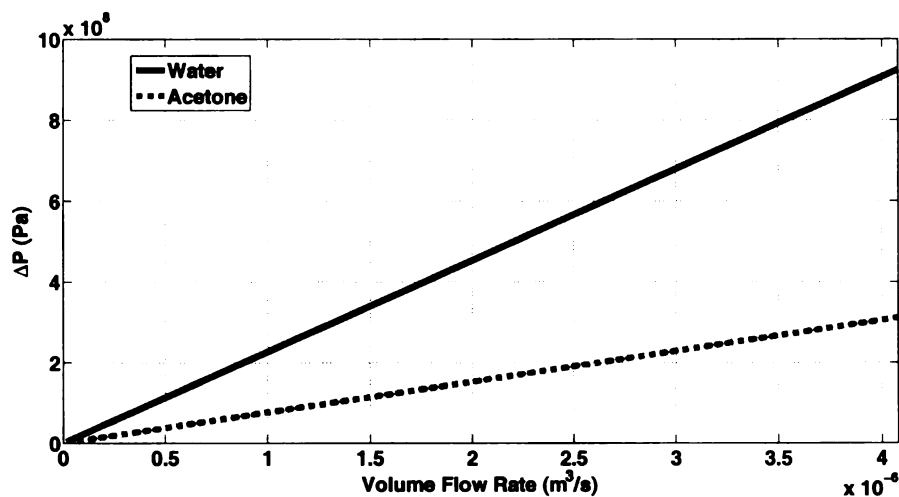
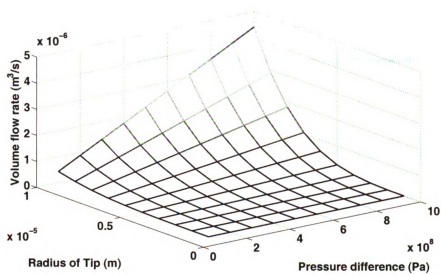


Figure 5.2. Relationship between pressure and volume flow rate

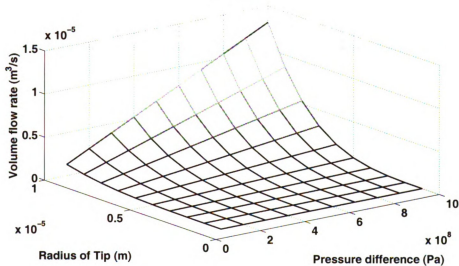
5.2.1 Surface Tension Calibration Results

In addition, to achieve accurate experimental results, surface tension calibrations are performed on water and acetone. Since experiments will focus on carbon nanotubes deposition, and carbon nanotubes are dispersed in liquid acetone, it becomes necessary to have accurate surface tension calibration for liquid acetone under experimental condition. Based on equation (3.3), the calibrations are conducted for both water and liquid acetone.

Figure. 5.4 shows two results of surface tension calibration. Figure. 5.4(a) illustrates the surface tension for water at 28 °C and Fig. 5.4(b) illustrates acetone at 29 °C. In Fig. 5.4, the best fit (blue line) of the results were obtained by using least square method. The results match the the surface tension of both liquids in literature. The calibration results show that the calibration setup is an effective setup for calibrating both liquids.



(a) Water

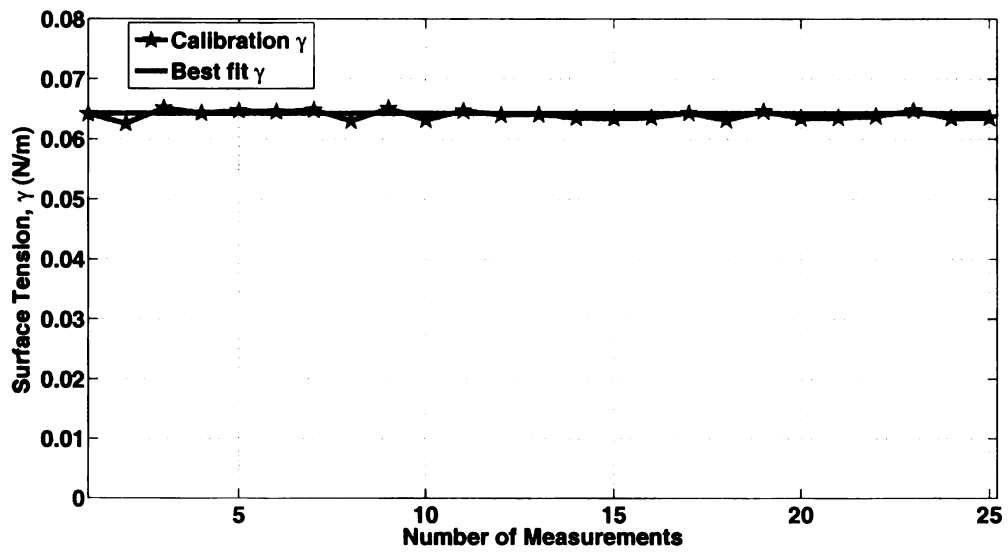


(b) Acetone

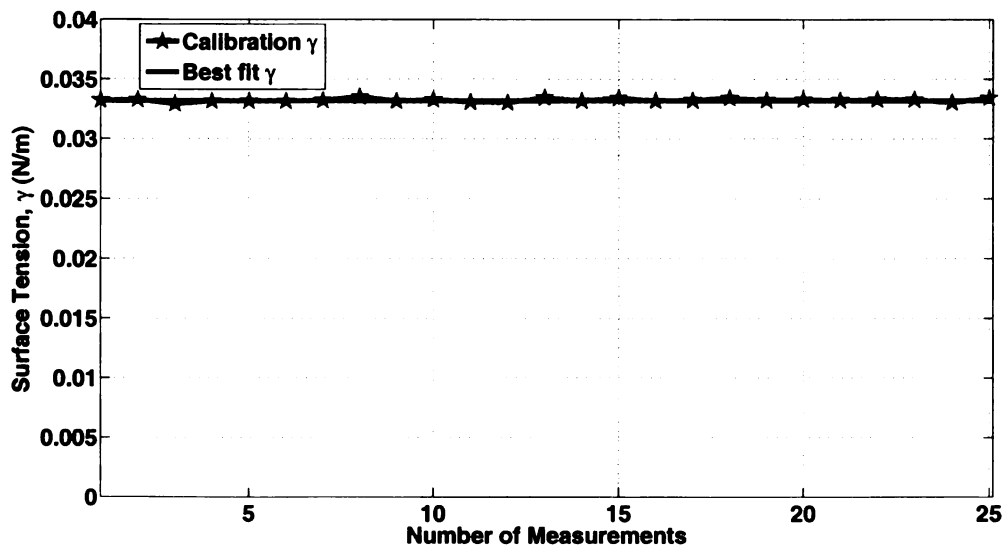
Figure 5.3. 3D plot showing the relationship between volume flow rate, radius of tube and pressure difference

5.2.2 Suction/Pressure Calibration Results

To calibrate the suction/pressure behavior of the system, a novel calibration setup is built as shown in Fig. 5.5. In Fig. 5.5, the tube is vertically aligned into the water container. Both the tube and the container are under the microscope. In order to



(a) Water



(b) Acetone

Figure 5.4. Calibration of surface tension

observe the water column surface change inside the tube due to the suction/pressure, a 45° reflective mirror is set aside the vertical tube. The light source is in the left to emit the light to the setup. At the reflection of the mirror, the height change of the water/acetone column inside the tube will be observed by the microscope. In Fig. 5.5, h_0 represents the pre-load height due to the capillary force before suction/pressure.

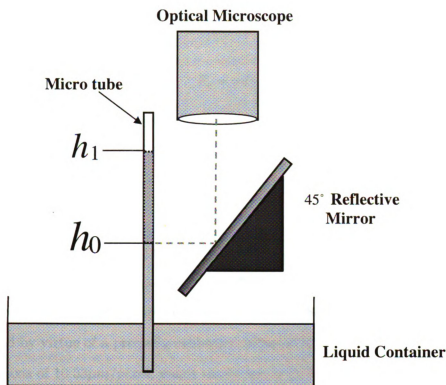


Figure 5.5. Calibration setup

h_1 is the height change due to the suction (vacuum action of pump). Based on the observed height change of water column, we have the following equation to calibrate the suction/pressure force F_s as

$$F_s = W(h_1) - F_c \quad (5.1)$$

where $W(h_1)$ is the column weigh of water/acetone column h_1 , F_c is the capillary force between the tube material and water column.

The weight of the water/acetone column $W(h_1)$ is expressed as

$$W_{h_1} = \rho \pi r^2 h_1 g \quad (5.2)$$

where ρ is the density of water, r is the radius of the end-effector, g is acceleration due to gravity.

Similarly, the capillary force between the tube material and the water/acetone column F_c is expressed as

$$F_c = \pi d\gamma \quad (5.3)$$

where d is the diameter of the capillary, and γ is the surface tension of the liquid.

By combining equations (5.2) and (5.3), equation (5.1) becomes

$$F_s = \rho\pi r^2 h_1 g - 2\pi r\gamma \quad (5.4)$$

Furthermore, the suction/pressure calibration experimental tests were conducted on a micro robotic system at stable room temperature, and it is controlled by a PC-based control system. Since capillary effect contributes to the overall suction/pressure force, and by virtue of a precisely calibrated Mitutoyo 2x microscope with resolution in the x-axis of $10.53\mu m/pixel$, y-axis resolution of $13.33\mu m/pixel$, and a Sony CCD camera system, the setup for accurately measuring the change in height due to suction/pressure force and capillary effect was tested. In the test, the diameter of the end effector is $254 \times 10^{-6}m$. The micro-drag force sensing PVDF beam is shown in Fig. 3.10. The sensor beam has the following dimensions and parameters: $L = 0.0212m$, $w = 0.004m$, $h = 28\mu m$ (PVDF film), $Cp = 0.90 \times 10^{-9}F$, $E = 2 \times 10^9 N/m^2$, $\rho = 1.911 \times 10^{-3}Kg/m^2$.

To reduce the vibrations from the environment, an active vibration isolated table is used during the experiment as depicted in Fig. 5.6. The resolution of the sensor is in the range of sub- μN . The output dynamic range of the sensor is 84.3 dB. The detailed results can be found in [6].

By calibration, from the recorded video of height change of water/acetone column, we also obtained the relationship between height change and applied voltage to the micropump. The results show that the calibration setup is an effective setup for calibrating the micro suction/pressure force of the microfluidic system.

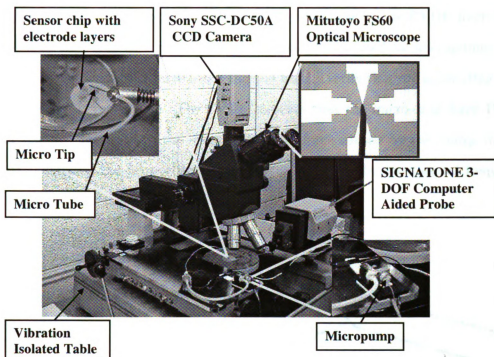


Figure 5.6. Experimental setup

Suction and Pressure Calibration Results

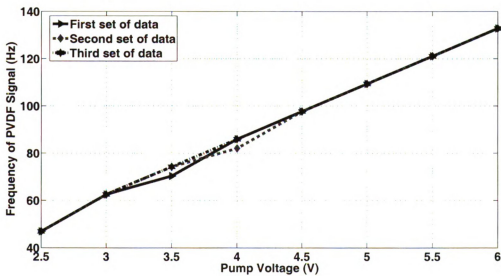


Figure 5.7. Frequency response of PVDF beam

Figure 5.7 shows the experimental frequency response of the PVDF micro-drag force sensor to the force signal. The force signal is generated by micropump. The experiment was conducted three times and the results verify that the micro-drag force PVDF sensing is repeatable. The results indicate that the micro-drag force PVDF sensor has fast response to the suction/pressure force caused by the pump voltage and demonstrates the proportional relationship between the force signal frequency and the applied voltage to pump.

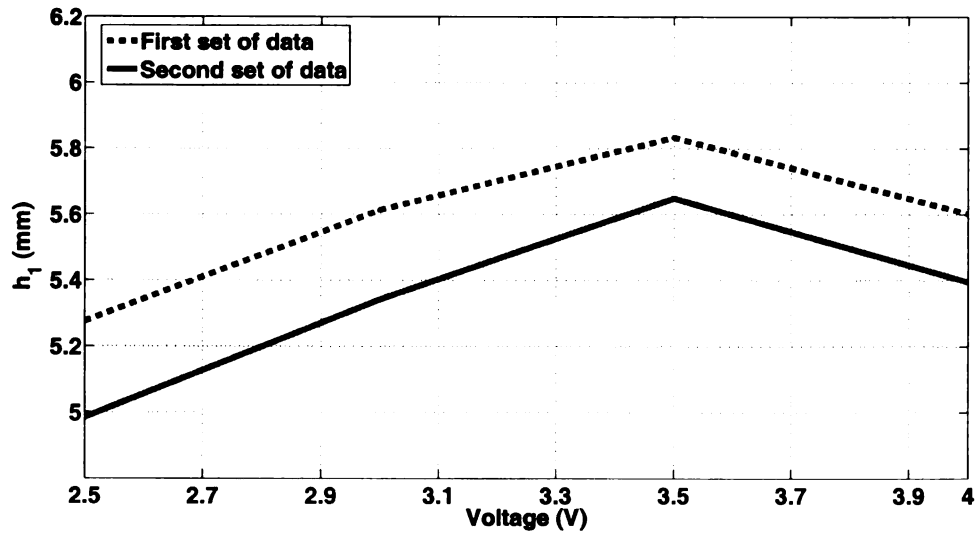


Figure 5.8. Height change behavior due to suction

Figure 5.8 demonstrates the relationship between the height change h_1 due to suction and the applied voltage of the pump based on the calibration method depicted in Fig. 5.5. The calibration experiment was conducted two times to show repeatability of the system.

Figure 5.9 shows the results of the calibrated suction/pressure force of the developed microfluidic end-effector corresponding to different applied voltage to the pump based on equation (5.4). In Fig. 5.9, the fitted curve (red dashed line) was obtained by using built-in cubic spline function in MATLAB, and can be used as the model of the suction/pressure force behavior. Based on the model, further experiments will

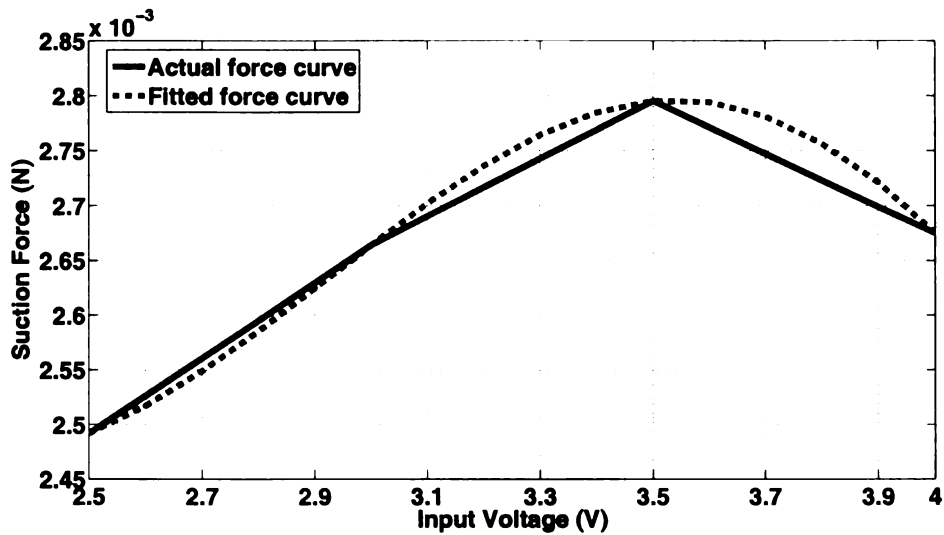


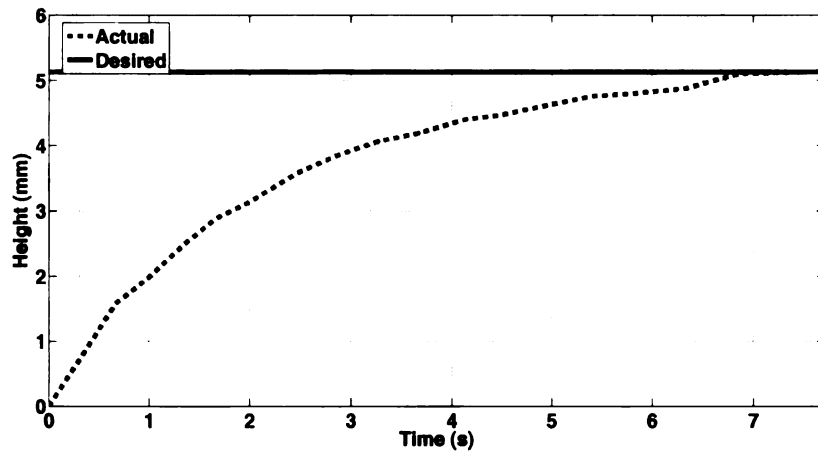
Figure 5.9. Suction force of developed end effector system

focus on verification of the developed PVDF sensing model and to refine the sensing model and parameters.

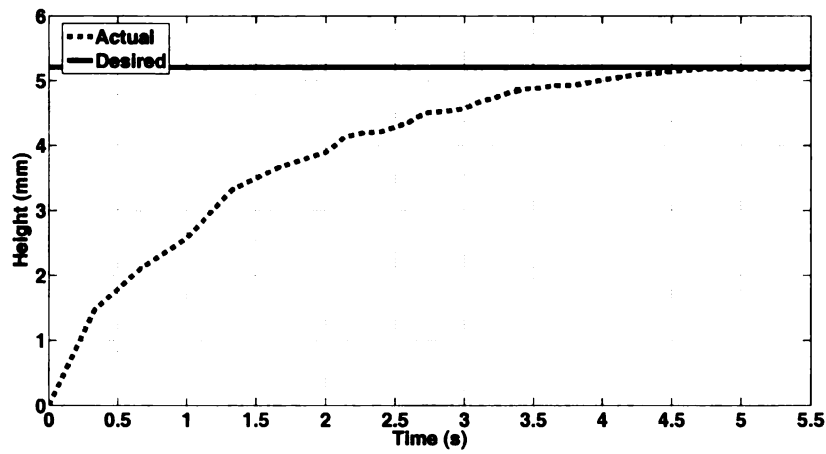
In addition, the step response of height change is also considered and the results are depicted in Fig. 5.10 for input voltage of 2.5V, 3.0V, and 3.5V respectively. In Fig. 5.10, the blue solid lines are the desired height change due to suction for each applied voltage, and the dashed red lines are the actual (step change) height due to suction for each input voltage. From Fig. 5.10, it is clear that the system response is good and the change in actual height tracks the desired height very well in a very short period of time.

The suction/release velocity for the developed microfluidic end-effector system is also considered and the results are illustrated in Fig. 5.11 for applied voltages of 2.5V, 3.0V, and 4V respectively. In Fig. 5.11, the top (red-dashed) plots are the velocity profiles due to suction, while the bottom (blue) plots represents the velocity profiles during release. The velocity profiles provide an indication of what range of voltage to applied for specific application.

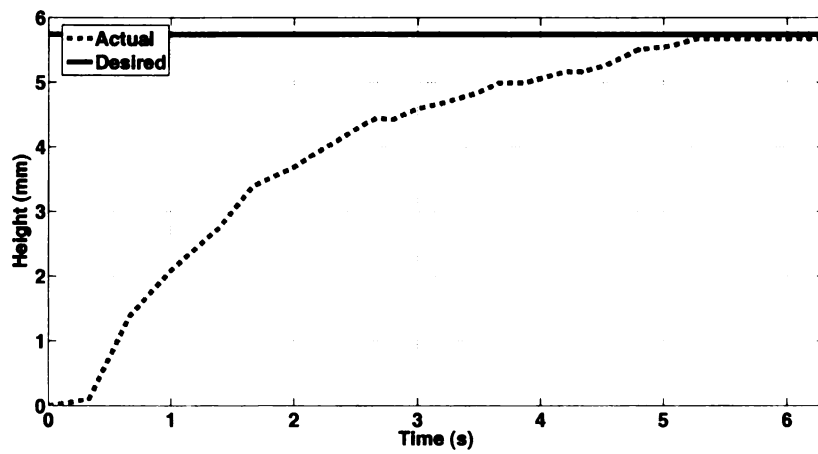
All experimental tests verify the feasibility and effectiveness of the developed sys-



(a) Step response for 2.5V

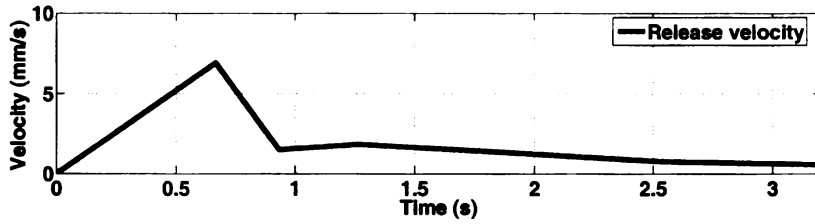
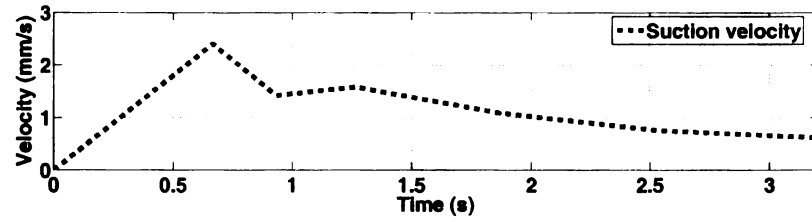


(b) Step response for 3.0V

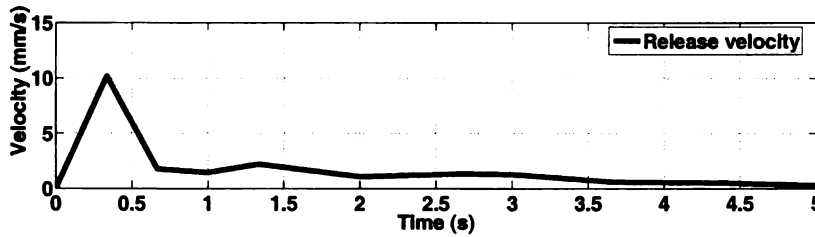
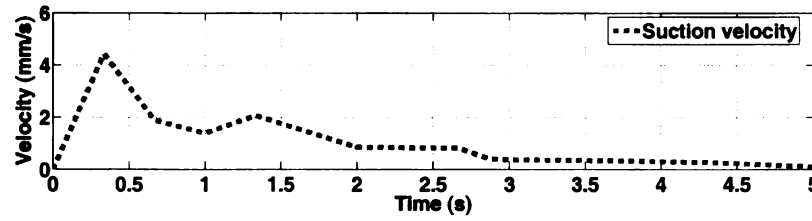


(c) Step response for 3.5V

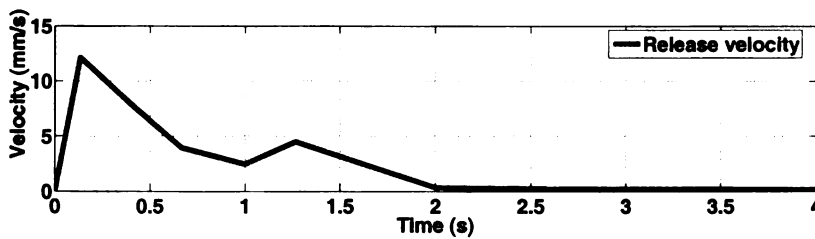
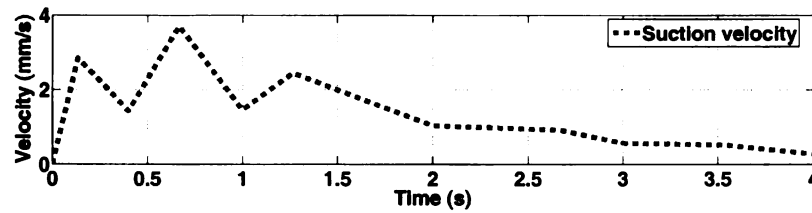
Figure 5.10. System behavior: Step response (height change) of suction activity



(a) Velocity at 2.5V



(b) Velocity at 3.0V



(c) Velocity at 4.0V

Figure 5.11. System behavior: Velocity change during suction/release

tem. That is, the suction/pressure force can be precisely controlled for fine manipulation and for controlled carbon nanotube(s) deposition between two micro electrodes for micro/nano sensors/electronics manufacturing.

5.2.3 Experimental Implementation

Figure 5.12 depicts the experimental implementation setup for handling of carbon nanotube(s) deposition. The objective of this experiment is to precisely drop carbon nanotube(s) between two micro electrodes for CNT based sensor manufacturing.

In order to achieve the bidirectional (sucking/droplet) flow, the micro pump is driven by a current driver interfaced with a PC as depicted in Fig. 5.12. The current driver is a *SN754410* quadruple high current H-bridge driver. It can provide bidirectional drive capability up to 1A at voltages up to 36V. The current driver is designed for operation from $-40\text{ }^{\circ}\text{C}$ to $85\text{ }^{\circ}\text{C}$. By using this current driver, we do not have to reverse the polarity of the micro pump during experiment for either sucking or releasing/droplet.

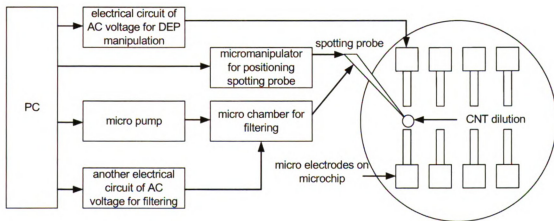


Figure 5.12. Experimental implementation setup for carbon nanotube deposition

5.2.4 Experimental Results on Carbon Nanotubes Implementation

Experiments focusing on carbon nanotube(s) deposition between micro electrodes are conducted using the developed microfluidic end-effector system. All experimental tests were conducted on a micro robotic system depicted in Fig. 5.6 at stable room temperature, and it is controlled by a PC-based control system.

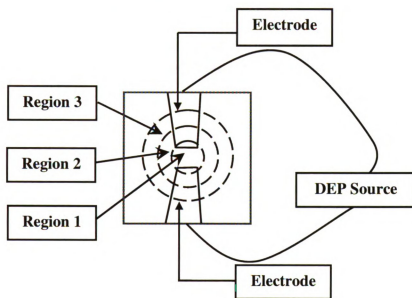


Figure 5.13. CNT deposition region

Figure 5.13 shows the regions around the micro electrodes where CNT was dropped using the new microfluidic end effector for CNT based sensor manufacturing. Regions 1, 2, and 3 have diameters $2.31\mu\text{m}$, $3.58\mu\text{m}$, and $4.77\mu\text{m}$ respectively.

Figure 5.14 depicts the procedure used for the handling of nano devices such as carbon nanotube(s). Notice that the handling procedure is automatically performed. The pipette shown in Fig. 5.14 has an internal diameter (ID) of $20\mu\text{m}$. In Fig. 5.14, (a) is the initial position of the pipette, (b) is when the pipette automatically moves to the handling position on the micro electrodes substrate, (c) is when the CNT mixed

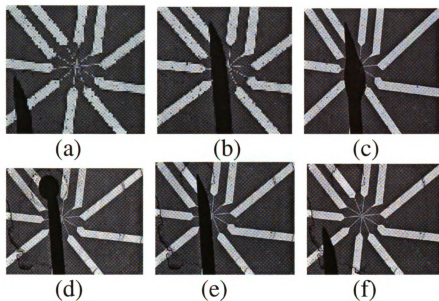


Figure 5.14. Procedure for manufacturing of nano devices

with acetone is in process of being dropped/deposited between the micro electrode , (d) shows the mixed liquid distributing around the micro electrodes, (e) shows when the CNT is dropped on the micro electrode gap, and (f) is when the micro pipette automatically comes back to the starting position.

Figure 5.15 shows the successful experimental results verifying the performance of the new microfluidic end effector system for microfluidic handling of nano devices. The microfluidic end effector is used to precisely drop carbon nanotube(s) between micro electrodes substrate. In Fig. 5.15, (a), (d), (e), and (f), the gap between the micro electrode is $2.43\mu\text{m}$, and the gap between the micro electrode in Fig. 5.15 (b) and (c), is $1.4\mu\text{m}$. Furthermore, in Fig. 5.15 (c), (d), (e), and (f), bundle carbon nanotubes are drop while in Fig. 5.15(a), single carbon nanotube is drop between the micro electrode gap.

In addition, experiments were conducted using a different size spotting probe as depicted in Fig. 5.12 to deposit CNT between micro electrodes. Figure 5.16 depicts the procedure used for the deposition of carbon nanotube between micro

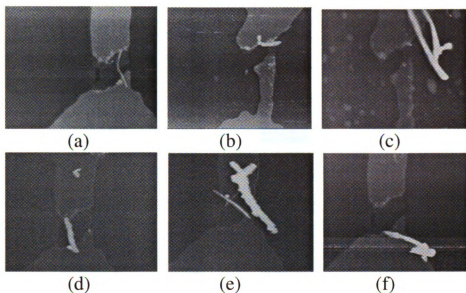


Figure 5.15. AFM image of experimental results. The scanning range is $5\mu\text{m}\times 5\mu\text{m}$.

electrodes for microfluidic handling operation. Notice that the deposition procedure is automatically performed. The spotting probe shown in Fig. 5.16 has an internal diameter (ID) of $10\mu\text{m}$. In Fig. 5.16, (a) is the initial position of the pipette, (b) is when the pipette automatically moves to the deposition position on the electrode, (c) is when the CNT mixed with acetone is in process of being delivered between the micro electrode, and (d) shows when the CNT is delivered on the micro electrode gap. The experiment was conducted under stable room temperature.

Figure 5.17 shows the successful experimental result verifying the effectiveness of the $10\mu\text{m}$ spotting probe. The spotting probe illustrated in Fig. 5.12 is used to precisely deposit CNT between micro electrodes. In Fig. 5.17, the length and diameter of CNT are $2\mu\text{m}$ and 45nm respectively. Ultimately, this technology will facilitate the manufacturing of micro/nano devices, micro/nano electronics, efficient drug delivery, and enhance micro/nano fluidic manipulation.

In summary, Table 5.1 shows the experimental trial to drop carbon nanotube(s) between two micro electrodes, and the experiments were conducted 14 times. The x in

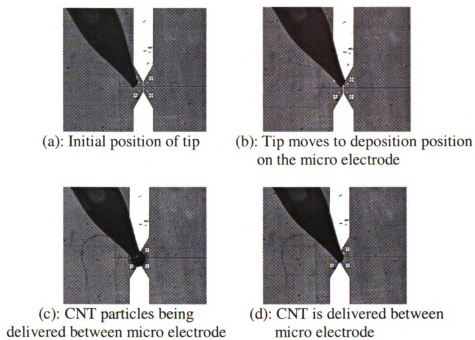


Figure 5.16. Microscope image depicting the sequence of depositing carbon nanotubes between micro electrodes

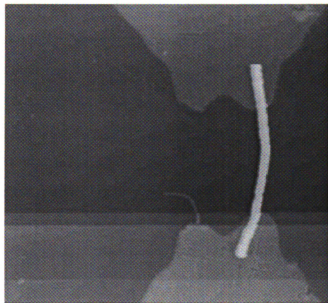


Figure 5.17. AFM image of CNT deposition result. The scanning range is $5\mu\text{m} \times 5\mu\text{m}$.

Table 5.1. Experimental Trials of Carbon Nanotube (CNT) Manufacturing

Trials	1	2	3	4	5	6	7	8	9	10	11	12	13	14
Region	x	1	1	2	3	2	1	3	3	x	2	1	x	2

the table indicates no CNT was found between the micro electrodes for that particular trial. Using the microfluidic end effector, carbon nanotube(s) were successfully drop between micro electrodes 11 times. The success rate of microfluidic handling and deposition of carbon nanotube(s) approaches 80%.

5.3 Dielectrophoretic Force for Manipulation of Carbon Nanotubes

5.3.1 Introduction

Carbon nanotubes (CNTs) have drawn the interest of many researchers in the field of engineering and sciences since they were discovered by Iijima [39] in 1991. This is because carbon nanotubes have extraordinary electrical and mechanical properties. Their excellent electrical properties make them to be good candidates for many electronics and sensing applications. For instance, in [40, 12], Fukuda *et al.* summarized properties and potential applications of carbon nanotubes by emphasizing the aspects of nanoelectronics and nanoelectromechanical systems (NEMS). Martel *et al.* in [43] used carbon nanotube as the semiconducting channel in a field effect transistor (FET) to achieve very high mobilities comparable to or better than state-of-art silicon-based transistors. These applications will require to move and orient carbon nanotubes to specific location. For example, the deposition and orientation of carbon nanotubes between micro electrodes for microelectronics fabrication.

Several issues need be to address in order for the potential applications of carbon nanotubes are realized. One of the issues is the difficulty in the transporting and deposition. This issue has been resolved to high degree of certainty by the development of a microfluidic micro and nano fluidic end effector manipulation system described in Chapter 3.

Since carbon nanotubes come in two forms - metallic and semiconducting, it becomes necessary that a system be developed for separating semiconducting CNTs from metallic CNTs. This is because semiconducting CNTs can be used for applications that may not be suitable for metallic CNTs and vice versa. Metallic carbon nanotubes are also available in different forms namely, metallic single walled carbon nanotubes (m-SWCNTs) and metallic multi walled carbon nanotubes (m-MWCNTs). The semiconducting carbon nanotubes are also available in semiconducting single walled carbon nanotubes (s-SWCNTs) and possibly semiconducting multi walled carbon nanotubes (s-MWCNTs). No research group have successfully claimed or suggested to have discovered semiconducting multi walled carbon nanotubes. Krupke *et al.* [58] used dielectrophoresis to attract predominantly m-SWCNTs to a set of micro electrodes, exploiting the fact that the magnitude of the dielectrophoretic force depends on the dielectric and conducting properties of a particle, in this case carbon nanotubes (CNTs). The drawback in [58] and other related references is that it assumed in the dielectrophoretic force model that carbon nanotubes are a particle.

In this research, we focus on developing a new mathematical model for dielectrophoresis and electrorotation of carbon nanotubes. Dielectrophoresis is inherently capable of solving both the separation and assembly problems associated with the fabrication of large-scale carbon nanotube based electronics and sensors, without having to contaminate the carbon nanotubes with chemicals. Therefore, accurate model of dielectrophoresis becomes not only essential, but critical. The derivation is followed with simulation results to preliminarily validate the model. Our model reasonably

assumes that carbon nanotubes are a bunch of particles that after undergoing dielectrophoresis, forms a line shape structure. The model gives a qualitative insight into the relation between electrode design, dimensions of the carbon nanotubes, and experimentally controllable parameters such as frequency and fluid velocity. Based on these calculations we are able to give recommendations for the optimization of nanotube assembly and separation.

5.3.2 Dielectrophoretic Force: Simulation Results

In order to obtain simulation results for the developed DEP force model, the Clausius-Mossotti factor \tilde{f}_{CM} , was obtained from equation (3.14). From equation (3.14), \tilde{f}_{CM} depends on the conductivity and the real permittivity of both the CNT and the fluidic medium. It also depends on ω , the angular frequency of the applied electric field. In the simulation, metallic multiwalled CNTs are dispersed in liquid acetone, and the parameters are described as follows.

σ_p : conductivity of metallic multiwall CNT (S/m)

ε_p : permittivity (dielectric constant) of metallic multiwall CNT

σ_m : conductivity of fluid medium, acetone (S/m)

ε_m : permittivity (dielectric constant) of fluid medium, acetone.

The value of the parameters used in the simulation at room temperature are as follows.

$$\sigma_p = 1 \times 10^8 \text{ S/m}, \varepsilon_p = 3.9, \sigma_m = 100 \times 10^{-12} \text{ S/m}, \text{ and } \varepsilon_m = 21.$$

Figure 5.18 shows the real and complex plot of the Clausius-Mossotti, \tilde{f}_{CM} factor for the given parameters of the medium acetone, and metallic MWCNT particles. Furthermore, since carbon nanotubes are also dispersed in other mediums such as ethanol, Fig. 5.19 shows the Clausius-Mossotti, \tilde{f}_{CM} factor for both acetone and ethanol. The real part of \tilde{f}_{CM} will be used to determine the DEP force while its complex part will be used to determine the electrorotation (torque) on the CNT.

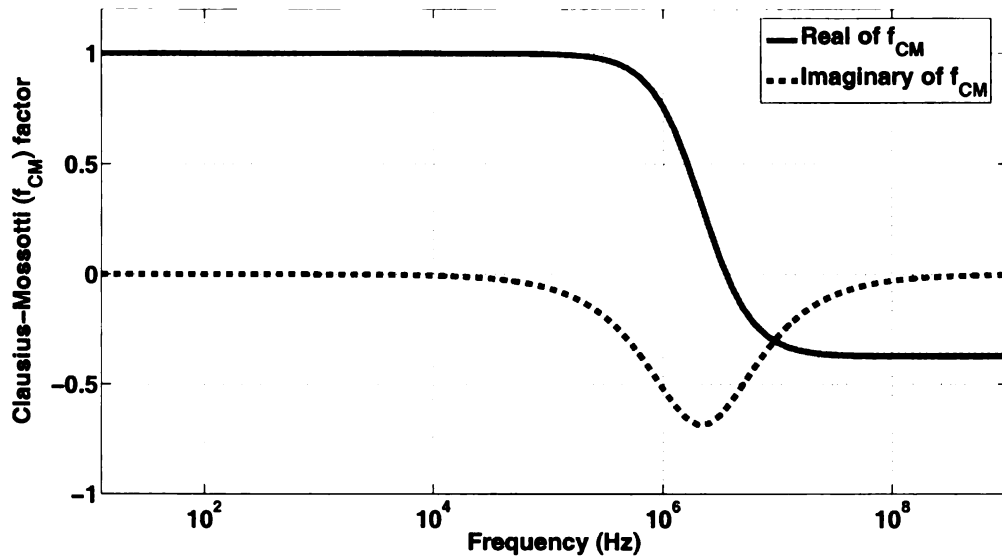


Figure 5.18. Clausius-Mossotti factor for DEP analysis (Metallic MWCNT in Acetone)

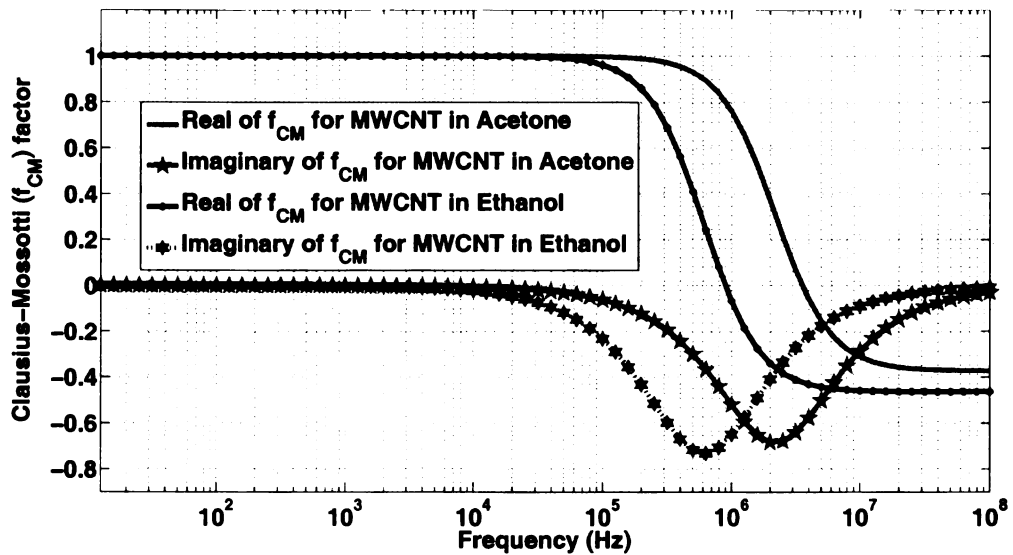
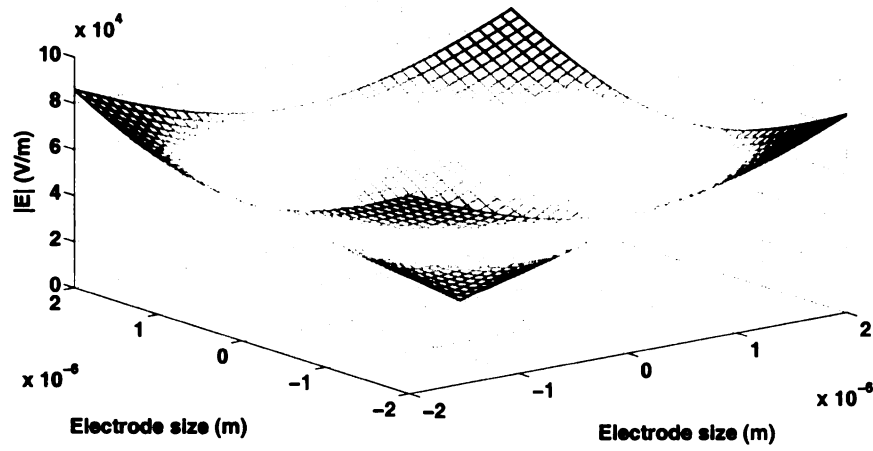
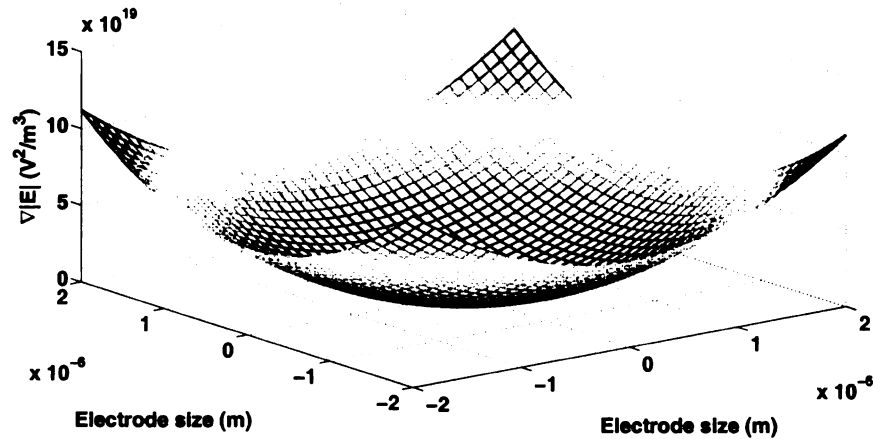


Figure 5.19. Clausius-Mossotti factor for DEP analysis (Metallic MWCNT in acetone and ethanol)

Since the DEP force highly depends on the applied electric field, it is paramount that the electric field function be chosen and investigated appropriately. Firstly, in our simulation, electric field and the square of the electric field functions are chosen based on a second order polynomial derived from Laplace's equations for defining electrode geometry as described in [104].



(a) Electric field as a function of electrode size



(b) Gradient of the electric field as a function of electrode size

Figure 5.20. 3D plots showing the relationship between electric field and its gradient as a function of electrode size

Figure 5.20 shows 3D simulation results of the chosen electric field function and its gradient. Figure 5.20(a) shows the 3D plot of the electric field as a function of the

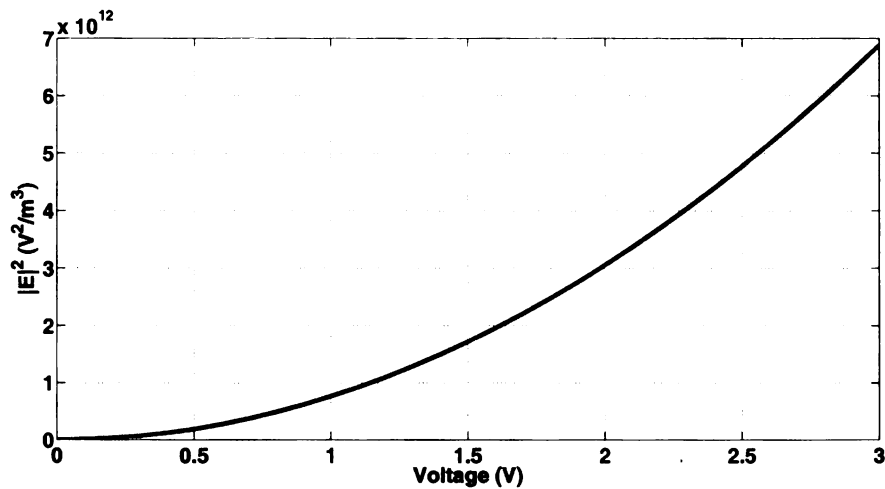


Figure 5.21. Electric field as a function of applied voltage

electrodes while Fig. 5.20(b) shows the 3-D plot of the gradient of the electric field as a function of the electrodes.

Consequently, Fig. 5.21 shows the relationship between the electric field function and applied voltage. This relationship is also based on a second order polynomial derived from Laplace's equations for defining electrode geometry as described in [104]. As the voltage increases, the electric field also increases as depicted in Fig. 5.21.

Figure 5.22, shows the relationship between voltage and the gap between micro electrode. In this figure, since carbon nanotubes will burn at voltage greater than $2V$, it becomes absolutely critical that the gap between micro electrodes be less than or equal to $2\mu m$ for applied constant electric field.

In addition, since DEP force also depends on the frequency of the AC electric field, we examined the relationship between frequency and applied electric field. Figure 5.23 shows 3D plots describing the relationship between frequency, voltage, and the electric field function. Figure 5.23(a) shows the 3D plot of the electric field, frequency, voltage, while Fig. 5.23(b) describes the relationship between the gradient of the electric field, frequency, and voltage.

Figure 5.24 shows the total dielectrophoretic force on the CNT after undergoing

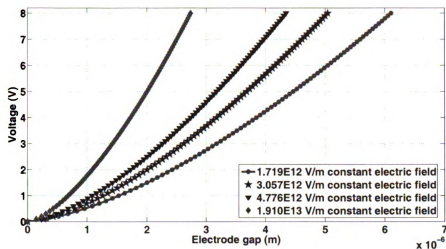
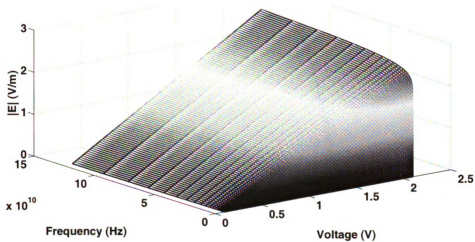


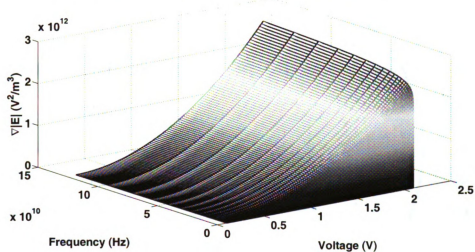
Figure 5.22. Relationship between voltage and micro electrode gap for constant electric field

AC electric field. In this figure, it is clear that F_{DEP} is a positive constant for frequencies less than 8×10^4 Hz. The magnitude of dielectrophoretic force F_{DEP} reduces between 8×10^4 Hz and 3.5×10^6 Hz for the parameters used, and it is still positive. For frequencies between 3.5×10^6 Hz and 7×10^7 Hz, the dielectrophoretic force F_{DEP} is negative. Furthermore, for frequencies greater than 7×10^7 Hz, DEP force becomes negative constant. This implies that for MWCNT, the metallic or more polarized ones will attract towards the electrode (high electric field region) while the semiconducting ones will repel the electrode (low electric field region) and possibly move toward the middle of the electrode. The semiconducting ones now can be extracted and use for electronics design exploration.

Furthermore, a simulation of the spatial variation of the electric field and its gradient was investigated. Figure 5.25 shows the electric field variation on the micro electrodes. Figure 5.25(a) shows the spacial variation of the electric field on micro electrodes, while Fig. 5.25(b) depicts the spatial variation of the gradient of the electric field on micro electrodes. This can be used to determine the direction of the moving CNTs as well as high electric field regions and low electric field regions.



(a) Electric field as a function of frequency and voltage



(b) Gradient of the electric field as a function of frequency and voltage

Figure 5.23. 3D plots showing the relationship between electric field and its gradient as a function of frequency and voltage

5.3.3 Electroration (Torque): Simulation Results

Figure 5.26 shows the electroration (torque) acting on CNT after undergoing AC electric field. In this figure, the maximum electroration occurs when the frequency is 2.1×10^6 Hz, and decreases for frequencies greater than 2.1×10^6 Hz. The electroration (torque) is positive for all frequencies of the applied electric field.

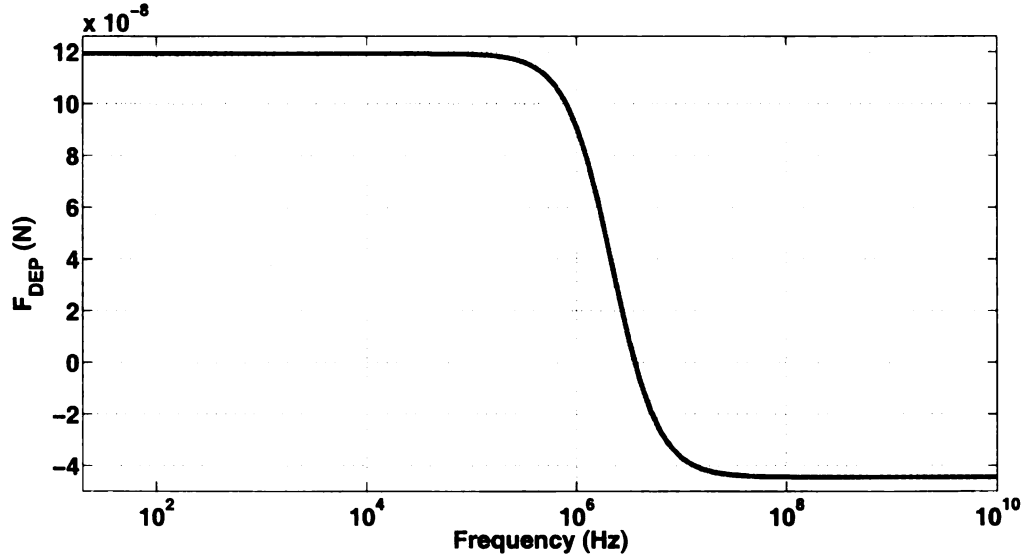


Figure 5.24. Dielectrophoretic force F_{DEP} on metallic MWCNT in acetone

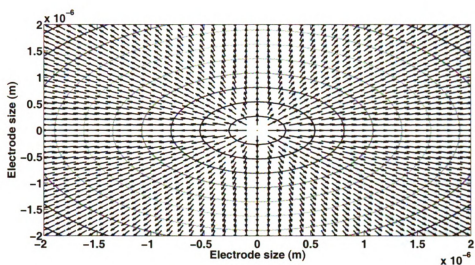
5.3.4 Rotational Motion of Carbon Nanotubes: Simulation Results

The resulting rotational dynamics of carbon nanotubes in viscous medium is giving in equation (3.35). Following equations (3.36) and (3.37), and constructing the appropriate electric field function, the governing resulting equation of motion for CNT is obtained. In order to verify this derivation, simulation was done by choosing appropriate parameters.

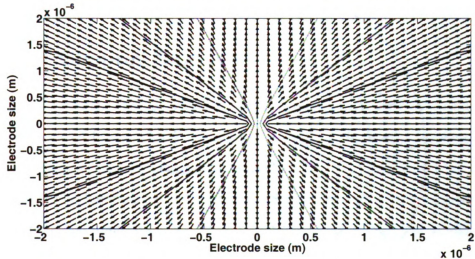
The values of some of the parameters used in the simulation at room temperature are as follows.

$$L = 2\mu m, \eta = 300 \times 10^{-6} Ns/m^2, m = 20 \times 10^{-9} Kg, \text{ and } r = 20nm.$$

Figures 5.27 and 5.28 show the simulation results of both CNT rotation angles and rotation velocities in viscous medium for different initial conditions. Figure 5.27 shows that CNT model as a line particle will continue to rotate until an external force is applied to it. This external force will result from applied electric field termed dielectrophoresis force (DEP). On the other hand Fig. 5.28 shows that CNT will stop



(a) Spatial variation of the electric field on micro electrodes



(b) Spatial variation of the gradient of the electric field on micro electrodes

Figure 5.25. Spatial variation of the electric field and its gradient on micro electrodes for CNT manipulation and separation

rotating when it is perpendicular to the the applied electric field. Hence the rotation velocity becomes zero. Based on the simulation results, the model can be used to effectively control the orientation/rotation of carbon nanotubes for application in intelligent manufacturing of CNT-base sensors and other applications such as electrical circuits, as fiber and film, computer circuits, etc.

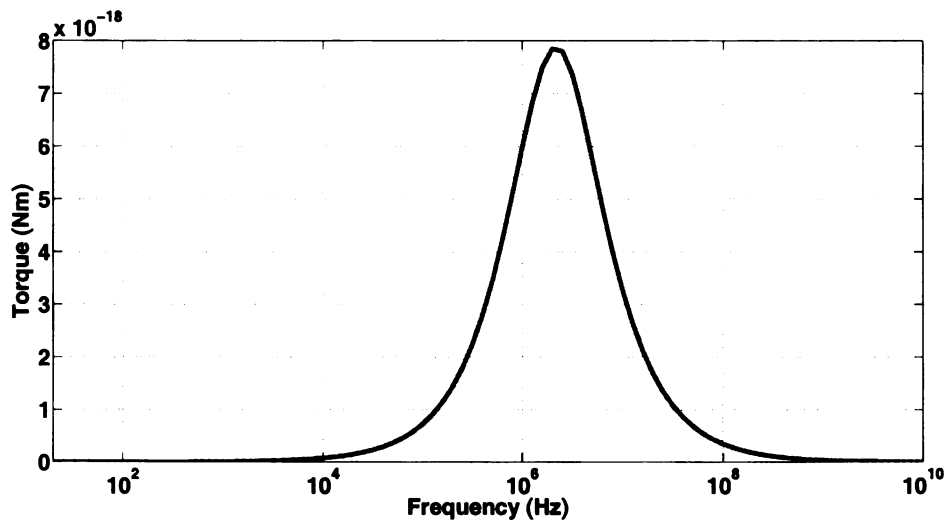
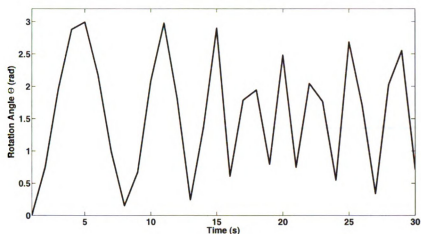


Figure 5.26. Electrorotation (torque) acting on metallic MWCNT in acetone

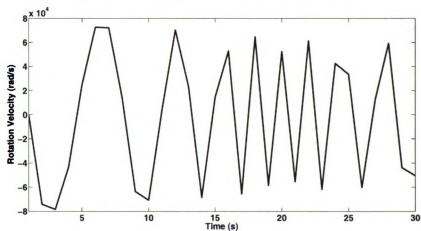
5.4 Chapter Summary

In this research, the development of a microfluidic end effector technology with a well modeled in-situ PVDF beam force sensing for deposition/handling of nano entities such as carbon nanotube(s) is presented. This unique tool is also used for microfluidic handling of nano devices, micromanipulation and microassembly, and has potential application for MEMS assembly, biomanipulation, blowing or delivering micro fluid drops, and drug delivery. Experiments focusing on the deposition of carbon nanotubes(s) between micro electrodes for manufacturing of CNT based sensors was conducted and results presented. The success rate of this experiment using the developed microfluidic end effector reach 80%. The calibration and experimental procedures are effective and efficient. Calibration and experimental results verify the performance of the new microfluidic end effector. Ultimately the technology will provide a critical and major step towards the development of automated delivering of micro fluid drops, enhance micro/nano manipulation, assembling of micro/nano devices, and nano manufacturing.

Furthermore, simulation results are presented for dielectrophoretic force model,



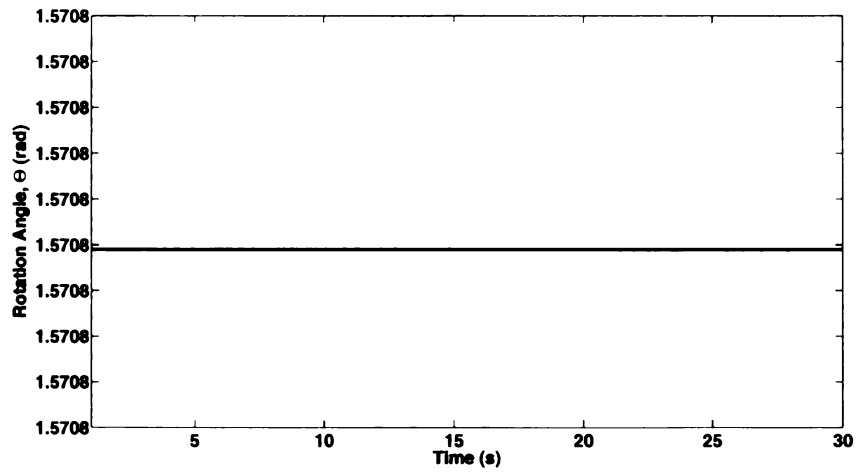
(a) Rotation angle of CNT with 0 initial condition



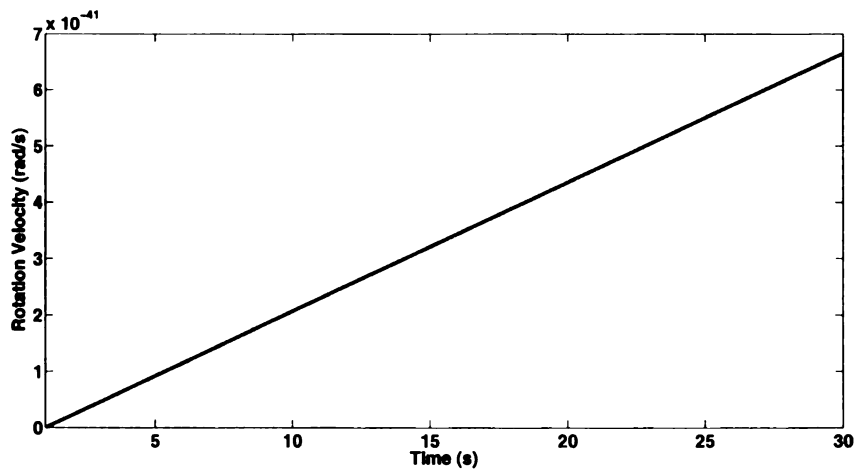
(b) Rotation velocity of CNT with 0 initial condition

Figure 5.27. Rotation angle and velocity of CNT in acetone with initial condition (0, 0)

electrorotation (torque) model, and rotation motion of carbon nanotubes for intelligent manufacturing of CNT based devices. Ultimately, the developed model will provide a critical and major step towards the use of carbon nanotubes in the manufacturing of electronics and sensors for potential use in electrical circuits, as fiber and film, computer circuits, light bulb filament, ultracapacitors, combat jackets, etc. Application of this model can range from using carbon nanotubes to detect biomolecules by forming FET (field effect transistor), as a sensor device for the detection of cancer



(a) Rotation angle of CNT with $\pi/2$ initial condition



(b) Rotation velocity of CNT with 0 initial condition

Figure 5.28. Rotation angle and velocity of CNT in acetone with initial condition $(\pi/2, 0)$

marker, etc.

CHAPTER 6

Application in Micro-Bio Injection

6.1 Introduction

In micro-bio injection, the lack of effective force sensing and feedback mechanism have dramatically reduced the success rate during injection and manipulation. Hence this work addresses both the measurement of injection force behavior and the characterization of mechanical properties of living *Drosophila* embryos using a well modeled *in situ* PVDF (Polyvinylidene Fluoride) piezoelectric micro-force sensing tool with a resolution in the range of sub- μN . In addition, a networked microrobotic biomanipulation platform integrating this developed two-axis (2-D) PVDF micro-force sensing tool is built. By employing the event-synchronization for the feedback of injection video and micro-force, the developed networked microrobotic platform can greatly advance operations in micro injection of living *Drosophila* embryos. Several experimental results have clearly demonstrated the quantitative relationships between the applied force and membrane structural deformation of embryos in the different stages of embryogenesis, as well as the force behaviors of micro injection .

6.1.1 Integration of Micro-Bio Force Sensor with Micropipette For Bio Injection

In this work, the developed two-axis PVDF sensing tool for micro injection is demonstrated in Fig. 6.1. In the sensing tool, a fine tipped micropipette with a tip diameter of $1.685\mu\text{m}$ and a tip angle of 2.65° is attached to the end of the rigid steel tip. The micropipette is made by Omega Dot capillary tubing 30-30-1 of Frederick Haer & Co Inc. The Omega Dot capillary tubing is a unique product which revolutionized micropipette filling. The tiny fiber ($100\mu\text{m}$) extruded into the capillary lumen, promotes capillary action and eliminates the need for boiling or vacuum filling of the tip. This tubing is good for single cell recording and micro injection [105].

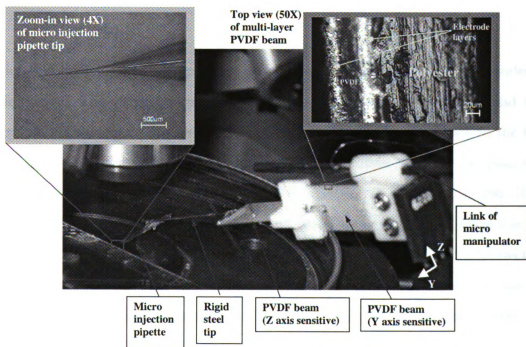


Figure 6.1. PVDF sensing tool for micro injection.

The multi-layer structure of PVDF composite beam is also shown in a 50X zoom-in microscope picture. There are four layers in the beam. Two thin layers are identical $6\mu\text{m}$ thick silver/urethane ink electrode layers with a low Young's modulus of

100MPa. The other two layers are the 30 μ m thick PVDF layer and 125 μ m thick Polyester layer, respectively, with Young's moduli of $3 \times 10^9 Pa$ and $3.8 \times 10^9 Pa$. Since the Young's modulus of the PVDF or Polyester layer is 30 times more than the electrode layers, it is reasonable to neglect the effect of the electrode layers in the model mentioned in Section IIA. The developed sensing tool has the following dimensions and related parameters: $L = 0.018348m$; $W = 0.010521m$; $L_0 = 0.05401m$; $C_P = 0.88 \times 10^{-9}F$; $d_{31} = 23 \times 10^{-12}C/N$; $c = 102.5 \times 10^{-6}m$; $h_p = 30 \times 10^{-6}m$; $h_b = 125 \times 10^{-6}m$; $E_p = 3 \times 10^9 N/m^2$; $E_b = 3.8 \times 10^9 N/m^2$; $\rho_p = 1.78 \times 10^3 Kg/m^3$; $\rho_b = 1.39 \times 10^3 Kg/m^3$; the amplified gain of the circuit is $K_a = \frac{R_3}{R_1} = 10$.

6.1.2 Networked Human/Robot Micro-Bio Manipulation System

Micro-bio injection and manipulation requires operations to be performed under a microscope. The visual information on the position of the micro injector and the surrounding workspace can be updated through real-time video feedback to the human operator. By visually observing the injection operations, a human can plan and correct the next operation so as to achieve a reliable and robust injection [106, 107]. In this work, we used both the micro-force and vision as essential action references for an integrated human/robot cooperative system. That is, the developed piezoelectric PVDF micro-bio force sensing tool with a resolution in the range of sub- μN can be integrated with a 3-DOF micromanipulator. The Mitutoyo FS60 optical microscope and a Sony SSC-DC50A CCD Color Video Camera can capture the micro-bio injection process in 30 frames/s, and feed back the visual information. Notice that, in this system, both the visual and micro-force data streams are transferred or fed back via the network. To ensure the synchronization of two data streams, an event-synchronization method proposed in [108, 75] is employed.

The developed network based biomanipulation work-cell in the Robotics and Au-

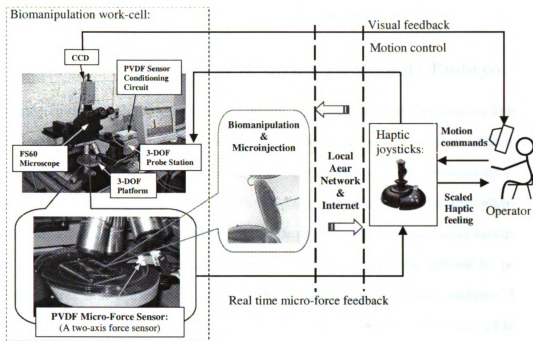


Figure 6.2. Networked human/robot biomanipulation work-cell at MSU.

tomation Laboratory at Michigan State University is shown in Fig. 6.2. It consists of a 3-DOF micromanipulator (SIGNATONE Computer Aided Probe Station, a step resolution of $32nm$), a 3-DOF platform, a Mitutoyo FS60 optical microscope and a Sony SSC-DC50A CCD Color Video Camera. The 3-D platform can be controlled to convey the embryos or cells to the working area observed by the microscope. To reduce vibrations, an active vibration isolated table is used during biomanipulation/micro injection. The joystick used in the human/robot cooperative biomanipulation system is a 3-DOF Microsoft SideWinder force feedback joystick. The 3-D movement of the joystick is sent to the 3-D micromanipulator, and the micro forces felt by the PVDF force sensing tool at the front end of micromanipulator are then fed back to operators through the joystick.

6.2 Experimental Implementation

6.2.1 Force Measurement of Living Drosophila Embryo

Usually, the Drosophila embryo is bilaterally symmetrical, and distinctions between the dorsal and ventral surfaces are indicated by differences in curvature. The dorsal side is flattened while the ventral side is somewhat convex. The dimensions of the embryos are variable, an average length is $500\mu m$, the diameter is about $180\mu m$. In addition, 17 embryonic stages in the living Drosophila embryo have been subdivided for a general reference in the embryo research. These stages are defined by prominent features that are easily distinguishable in the living Drosophila embryo. For a reference in the experimental section, Table 6.1 shows the time and events of the 17 stages at room temperature.

Table 6.1. Time table of embryogenesis. From [1]

Stage	Time	Events
1~4	0:00~2:10h	Cleavage
5	2:10~2:50h	Blastoderm
6~7	2:50~3:10h	Gastrulation
8~11	3:10~7:20h	Germ band elongation
12~13	7:20~10:20h	Germ band retraction
14~15	10:20~13:00h	Head involution and dorsal closure
16~17	13:00~22:00h	Differentiation

6.2.2 Preparation of Drosophila Embryo

The Drosophila embryos used in the experiments were prepared following a standard procedure. In this research, fresh Drosophila embryos in the early stages (usually stages 1~4, 0~130 minutes after hatching) were collected into a basket, then dechlorinated in 100% bleach for 2 minutes in order to completely remove the outer tough opaque chorion. After the dechlorination, the embryos are rinsed thoroughly in $20^{\circ}C$ water for 2 minutes to remove all traces of bleach. A soft brush is then used to uni-

formly transfer embryos to a glass slide with double stick tape. Finally, embryos on the tape were covered with Halocarbon 700 oil and ready for injection. Notice that, the adhesive force of the tape is strong enough to hold the embryos in place for injection. Approximately 50 living embryos were prepared. After the chorion removal mentioned above, those living embryos are still enclosed by an inner homogeneous vitelline membrane, which will be broken through by the sharp pipette for micro injection. Figure 6.3 shows the 10X microscope image of fresh *Drosophila* embryos.

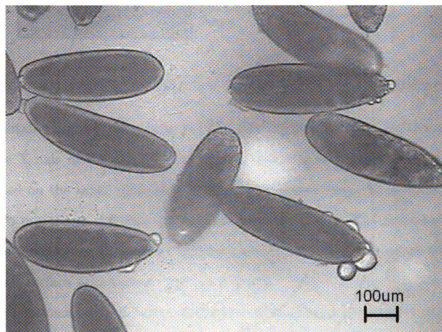


Figure 6.3. The prepared *Drosophila* embryos for micro injection.

6.2.3 Micro-Bio Injection and Manipulation Configuration

Using the developed networked human/robot micro-bio manipulation system, the micro injection configuration is shown in Fig.6.4.

In this configuration, the embryos are held in place on the stick tape of a glass slide, which is placed on the 3-DOF platform. The Y axis of force sensing tool

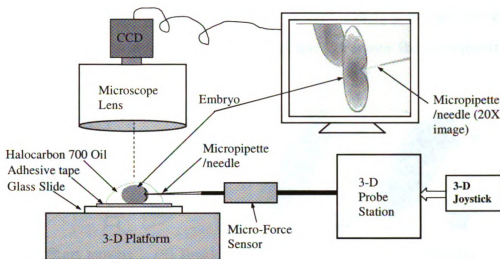


Figure 6.4. Experimental configuration of micro injection of *Drosophila* embryos.

is horizontally aligned. This ensures that only a normal injection force is applied along the Y axis of the PVDF force sensing tool. Since the prepared embryos are distributed on the taped glass slide with diverse orientations, the injection angle of the micro pipette on different *Drosophila* embryos, that is, the angle between the incidence direction of the pipette injector and the normal direction of the embryo membrane surface approached, may be different. Based on this configuration, all force measurements and the characterization of mechanical properties of the living embryos were implemented at a stable room temperature of 28°C.

6.3 Experimental Results

6.3.1 Force Profile of Micro-Bio Injection and Manipulation of Living *Drosophila* Embryos

To measure the force profile of micro injection of embryo, the general operation procedures are as follows: first, the operator drives the joystick to move the micropipette tip along the Y axis to approach the embryo for injection. Once the tip penetrates the

first membrane and goes inside of the embryo or continues to penetrate the second membrane, in order to stop the pipette tip, the operator moves the micropipette tip back along the Y axis.

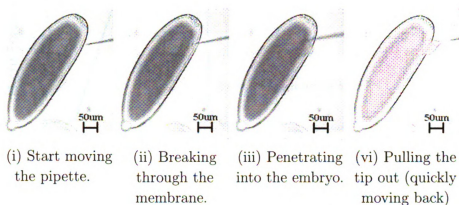


Figure 6.5. The sequence of penetrating fresh embryo through one membrane.

In Fig. 6.5, a micro-bio injection sequence of the fresh embryo is shown. In this injection, when the pipette tip penetrated the membrane of the embryo, it was moved back. As shown in Fig. 6.6, the force profile was measured by the developed PVDF sensing tool. The injection angle is 36.08° , and injection speed is about $14.254\mu\text{m/s}$. Notice that, when the pipette tip is moved back, due to the fluid frictions and the inertial effect, a negative force is shown in the force curve. The puncturing force is approximately $3.1\mu\text{N}$. The embryo used is in stage 5 (Blastoderm Stage).

The sequence in Fig. 6.7 demonstrates penetration of the whole embryo, which means two membranes at the dorsal and ventral sides are punctured. The injection angle is 17.3° , and injection speed is about $58.5\mu\text{m/s}$. Since the first penetration needs to overcome both the internal pressure of closed embryo and the membrane stress, the maximum puncturing force of $7.44\mu\text{N}$ appears in the penetration of the first membrane. The penetration force of the second membrane is $3.61\mu\text{N}$.

Figure. 6.8 shows the force profile detected by the developed micro-bio PVDF force sensing tool. Notice that, the embryo used is in Stage 10 (Germ Band Elongation

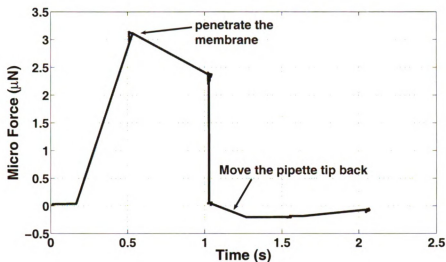


Figure 6.6. Force profile of penetrating one membrane of fresh embryo.

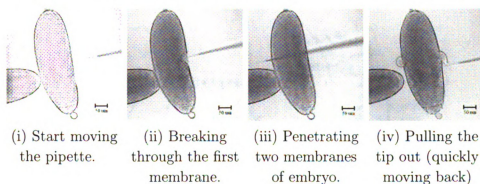


Figure 6.7. The sequence of penetrating two membranes of living embryo.

Stage). From the force profile, the penetration force and time of living embryo in Stage 10 are greater and longer than the fresh embryo in Stage 5 demonstrated above. It is reasonable because the plasticity and density of the embryo membrane are both increased when the living embryo becomes gradually mature [1].

In addition, Fig. 6.9 shows the complex force profile including 5 contact-release operations and then the penetration of the embryo. Notice that, the speeds of the 5 contacts and 5 releases are diverse. Moreover, when the tip penetrates the first membrane into the embryo, the tip continues to impact the second membrane without

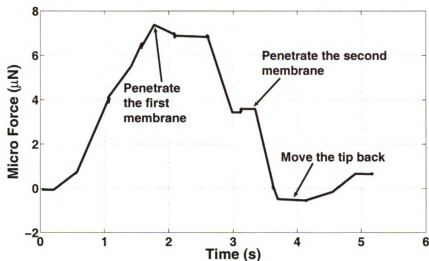


Figure 6.8. Force profile of penetrating two membranes of living embryo.

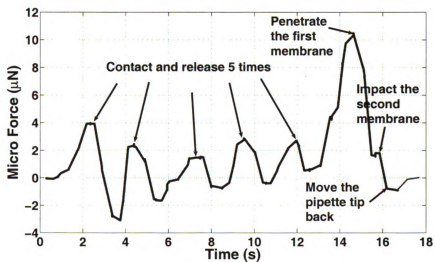


Figure 6.9. Force profile of complex operation of living embryo

puncturing it, then the tip is pulled out. These force behaviors are clearly demonstrated in Fig. 6.9. The embryo chosen is in Stage 11~12 (Stage of Germ Band Elongation and Retraction). The injection angle is 43.1° , and injection speed is about $44.4\mu\text{m}/\text{s}$. The puncturing force is approximately $9.5\mu\text{N}$.

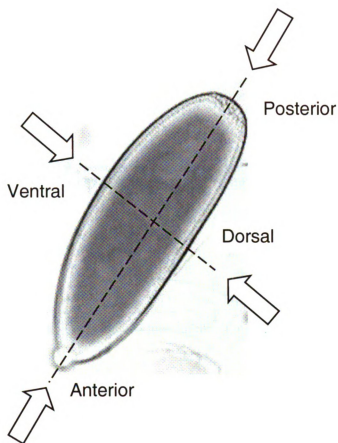


Figure 6.10. Dorsal-ventral and anterior-posterior directions

6.3.2 Directional Micro-Bio Injection Force Comparison

In this work, we also seek for the quantitative relationship of penetration forces along two directions of the embryo body. That is, the anterior-posterior and dorsal-ventral directions, which are illustrated in Fig. 6.10. Using the prepared *Drosophila* embryos between Stage 1 and 5, the penetration micro-bio forces along two directions are investigated. The results are shown in Fig. 6.11. It can be seen that the penetration force along the dorsal-ventral direction is about 3.6 times smaller than the penetrating force along the anterior-posterior direction in the case of Stage 1~5 embryos are measured.

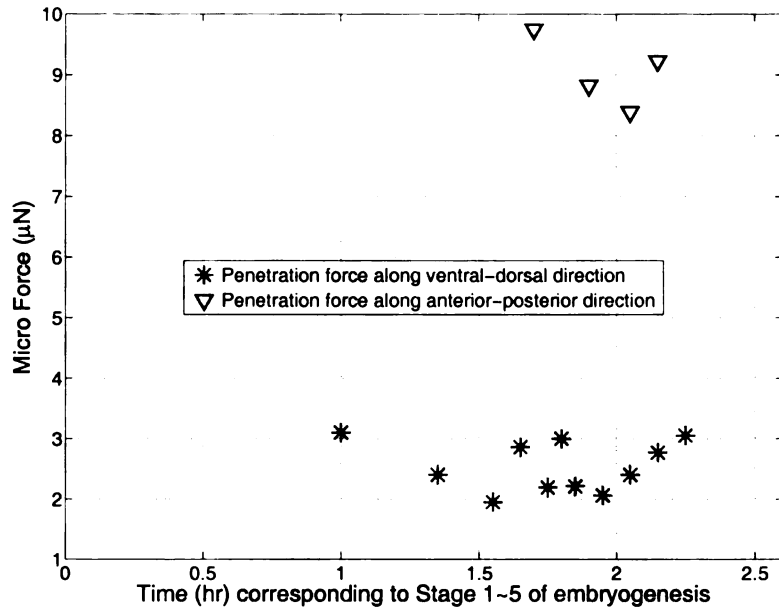


Figure 6.11. Penetration forces along the dorsal-ventral and anterior-posterior directions

6.3.3 Quantitative Relationship Between Micro-Bio Force and Membrane Deformation of Living Drosophila Embryo in Different Stages

By employing an off-line membrane deformation measurement, which is based on the microscope images with a maximum resolution of $0.702\mu\text{m}/\text{pixel}$, and the corresponding micro-bio force measurement, characterizing and quantifying the differences on mechanical properties of the living Drosophila embryos in different stages of embryogenesis is investigated. As a result, the quantitative relationship between the force and the membrane deformation is found and established.

As shown in Fig. 6.12, several relationships on force-membrane deformation of diverse embryos in different stages are demonstrated. It can be seen that membranes of living embryo in the early stages have relatively smaller deformation with respect

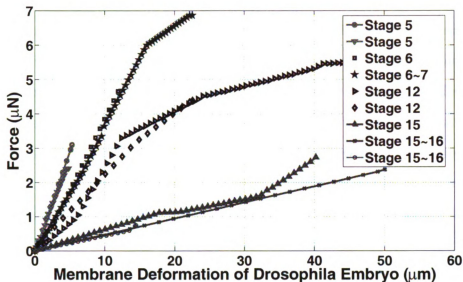


Figure 6.12. Quantitative relationship between force and membrane deformation of living embryo in different stages.

to the membranes of late stage embryos before being penetrated. In Fig. 6.12, from the early stages to the late stages, the stiffness of the embryo membrane reduces gradually. This implies that the plasticity of membrane of living *Drosophila* embryo gradually increase when the embryo becomes mature. In addition, the results in the same stage are repeatable by multiple experimentation. These quantitative results will improve the quality of micro injection for the study of the *Drosophila* genetic projects currently in existence.

6.4 Chapter Summary

In this work, we investigated and characterized the force behavior and mechanical properties of living *Drosophila* embryos using an *in situ* PVDF (Polyvinylidene Fluoride) piezoelectric micro-bio force sensing tool with a resolution in the range of sub- μN . Our objective is to realize a highly efficient and accurate micro-bio injection of genetic material into the living *Drosophila* embryo. Therefore, close monitoring of

the magnitude and direction of micro-bio injection and other biomanipulation forces acting on the embryo during the injecting process will be the important step. In this work, we developed a networked micro-robotic biomanipulation platform integrating the PVDF micro-bio force sensing tool in order to effectively implement force sensing and injection of living *Drosophila* embryos. Based on the event-synchronization for feedback of injection video and micro-bio force, the developed networked micro-robotic platform can greatly advance operation in biomanipulation and micro injection. Through experiments, quantitative relationships between the applied force and vitelline membrane structural deformation for different stages of embryogenesis and micro-bio injection force behaviors using an ultra sharp pipette tip were found. Ultimately, the technology will provide a critical and major step towards the development of automated biomanipulation for minimally invasive injection of living *Drosophila* embryos for human medical studies. The application of this work is endless, ranging from agriculture (genetic modification of crop) to forensic science, etc.

CHAPTER 7

Conclusions

Manipulation of micro and nano entities implies the movement of micro and nano entities from an initial position (location) to the desire position (location). This operation is not only necessary, but a required task with great precision. The tools needed for the manipulation needs to be chosen properly because the capabilities of the human hand are very restricted. Smart micro and nano manipulation are becoming of great interest in many applications including medicine and industry. In industry, high precision manipulation systems are especially needed for mass production of both micro and nano systems which consists of different component in respective scales.

Micro and nano entities can be hydrophobic or hydrophilic. For hydrophobic micro and nano entities, adhesion forces are dominant during manipulation compared to the gravitational force. For hydrophilic micro and nano entities, surface tension is dominant compare to gravity. Therefore, designing the tools necessary for manipulation becomes absolutely important.

In this research work, the problem of micro/nano fluidic handling and transporting has been solve by the development of a micro and nano fluidic end effector technology with in-situ PVDF beam force sensing for micro robotic manipulators and for the manufacturing of nano devices such as carbon nanotubes. The PVDF sensing

beam can measure/detect the suction/pressure force/flow rate caused by the micro pump. Then the corresponding flow rate or force at the tube end (end-effector) can be determined by the measured flow rate and force. As a result, the micro tube based end-effector, micro pump, and PVDF sensing buffer can be integrated into a closed-loop bi-directional pneumatic driving platform to provide the precision controlled micro suction/pressure force or bi-directional flow rates for fine micro/nano scale assembly, manipulation, manufacturing, and droplet control. All the experimental results show the efficacy and efficiency of the developed micro and nano fluidic end effector system.

An application of the micro and nano fluidic end effector technology with in-situ PVDF beam force sensing for micro robotic manipulators is to handle carbon nanotubes (CNTs). That is, transporting and deposition of carbon nanotubes between micro electrode for manufacturing of carbon nanotube based devices such as sensor, circuitry, etc. Since carbon nanotubes come in two forms - metallic and semiconducting, we attempt to develop a scheme to separating them for suitable applications. The most used separation method is dielectrophoresis. Hence, a new mathematical model based on the fact that carbon nanotubes form a line shape after undergoing dielectrophoresis is developed. Furthermore, model describing the electrorotation (torque) due to dielectrophoresis is also concerned and derived based on the line model assumption. The derivations is followed with simulation results to validate the models.

Furthermore, in this research work, the problem of force sensing in micro-bio injection and manipulation has been solve by the development of a highly sensitive micro-bio force sensor as described in Chapter 3. Experiments were focused on micro-bio injection of living *Drosophila* (fruit fly) cells for human medical study. The developed micro-bio force sensor is integrated with a network human/robot micro-bio manipulation system demonstrated in Chapter 5. The integration of the system with

a high precision microscope provides complete visual information on the position of the micro injector (tool) and the surrounding workspace. Our objective of realizing high efficiency and accurate micro-bio injection of genetic material into the living *Drosophila* embryo was achieved.

The combination of both the micro robotic manipulation system and the atomic force microscopy (AFM) based nano-robotic system will provide a powerful tool for manipulating and assembling nano particles, nano-wires, nanotubes, micro-bio sensors, and DNA. Additional applications of this research are endless considering the rapid development of micro and nano technologies.

CHAPTER 8

Future Work and Research Directions

8.1 General Overview

Micro and nano manipulation, manufacturing, and assembly have drawn a lot interests in many different fields including computing, engineering, biology, medicine, etc. The architecture and capabilities of micro and nano systems are still an active research area because there are still many problems to be solved. This dissertation has addressed several issues in design, modeling, and analysis of micro and nano systems. Certainly more can be done to expand on the work presented in this dissertation and even more can be done to address various other issues in micro and nano systems which have not been the topic of this dissertation.

As stated in chapter 1, the goal of this research is to develop tools for micro and nano manipulation, manufacturing, and assembly that is capable of transporting micro and nano entities in liquid environment, and sensing in bio environments for biomanipulation and micro-bio injection.

The latter goal has been achieved in this dissertation by the development of a

micro-bio force sensor for sensing micro-Newton forces during micro-bio injection of living *Drosophila* (fruit fly) cells for human medical study, and for potential application in agriculture.

The goal involving the development of a tool for micro and nano manipulation that is capable of transporting micro and nano entities in liquid environment has been achieved by the development of a micro and nano fluidic end effector system. Furthermore, the developed micro fluidic end effector system is used to successfully deposit carbon nanotubes between micro electrode for application in manufacturing of CNT based devices.

In order to to fully realize the impact of the work done in this dissertation, fabrication of the micro and nano fluidic end effector system by developing or using existing MEMS technology becomes absolutely necessary. Recently, Lai, *et al.* [109, 110] developed an automated robotic deposition process that is capable of manufacturing nano devices using existing MEMS technology. Their system is also capable of manufacturing single carbon nanotube based nano devices and can has the capability to separate metallic carbon nanotubes from semiconducting carbon nanotubes.

Since micro and nano fluidics have become increasingly essential in today's development and testing of drugs, it becomes necessary that all experiments be conducted in a "clean room" at stable room temperature and controlled humidity. These processes would dramatically improve efficiency and effectiveness of drug delivery systems, micro-bio analysis systems, etc.

During preliminary experiments, it was observed and confirmed that the applied AC electric field (dielectrophoresis) between two micro electrodes affects other micro electrode pairs on the chip. For instance, if there are two pairs of micro electrodes on a chip, and an AC electric field is applied between one pair, the other pair is affected. This is because of the spatial distribution of the AC field, and the fact that all the electrodes are conducting. Hence solving this problem will make a huge impact in

the fabrication process of CNT based devices.

Hence, I propose two possible ways to solve this problem. The first part involves the development of theoretical framework for micro electrode design and geometry. This problem has been solved in chapter 4 of this dissertation. Based on the derived theory, micro electrodes can be fabricated using existing micro fabrication process and architecture, for example electron beam lithography (EBL), or by developing a new mask for the micro electrode design. The second part will involve software implementation for the developed micro electrodes. In this case, complete logic statement (truth table) of the number of micro electrode pairs becomes essential in order to fully implement the overall system experimentally.

8.2 Experimental Studies

8.2.1 Hardware Implementation

The objective of the hardware implementation is to make sure that when an AC electric field is applied between two micro electrodes, the other pairs of micro electrodes on the chip will not be affected. In other words, the applied AC electric field should spatially distribute between the micro electrode pair in use.

Figure 8.1 shows the proposed schematic for implementing the AC field for DEP application. In Chapter 3, it was stated that the movement of the particle towards high electric field region is called positive dielectrophoresis (+DEP) and the movement of the particle towards low electric field region is called negative dielectrophoresis (-DEP) [55, 91, 92]. Hence, in Fig. 8.1, low frequency (about 1-5KHz) implies positive DEP.

The idea presented in Fig. 8.1 is that only electrode A and B would have spatial distribution of AC electric field when a low frequency AC field is applied (or a high frequency AC electric field). In either of these cases, electrodes C and D should be

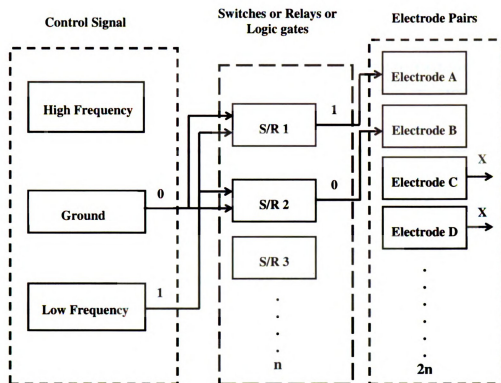


Figure 8.1. Proposed AC electric field for DEP implementation

disconnected represented by (X). In general, for $2n$ number of micro electrodes, only two should be on when AC electric field is applied between them.

A number of avenues can be pursued to carry this work further. The combination of the software and hardware implementation will provide a powerful tool for not only CNT manipulation, manufacturing, assembly, separation, and analysis, but also DNA, cells, and other biological entities.

8.3 Inverse Problem

In Chapter 3, section 3.2.3, modeling rotational motion of carbon nanotubes for intelligent manufacturing of CNT-based devices is presented. This model was possible because of prior knowledge of the electric field function and micro electrode geometry.

On the other hand, this problem can be reversed.

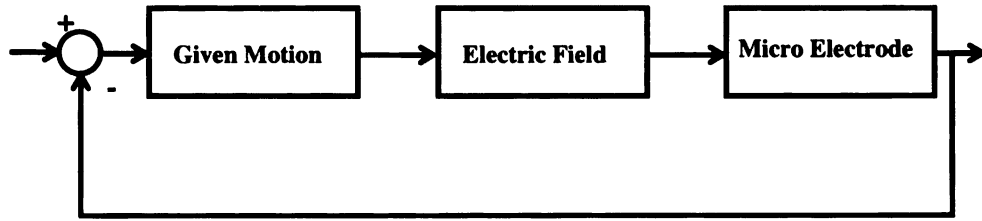


Figure 8.2. Proposed inverse problem solution method

That is, giving a random rotational motion of micro or nano particle, in this case, carbon nanotube, how can a micro electrode be designed for that particular or sets of random rotational motions? Figure 8.2 is used to illustrate a possible solution method to this inverse problem. Solving this problem will significantly improve the use of carbon nanotubes in manufacturing of intelligent CNT-based devices, and could potentially eliminate the use of nano robotic manipulation system to manipulate CNTs after undergoing dielectrophoresis.

8.4 Chapter Summary

This chapter presents future work, and research directions, and provided possible solution methods and ideas in solving these potentially ground breaking problems in micro and nano manipulation, manufacturing, and assembly.

The overall impacts of this dissertation and future work are endless given the current state of micro and nano technologies.

APPENDIX A

Matlab Simulation Code for Dielectrophoretic Force and Electrorotation of Carbon Nanotubes

```
close all
```

```
clc
```

```
clear
```

```
format(long)
```

```
 $V_0 = 2;$             Applied potential for MWCNT
```

```
 $d = 2.0 \times 10^{-6};$             Gap between electrode
```

```
 $x_0 = 0;$   $x_L = 2 \times 10^{-6};$             Initial and final length of a MWCNT
```

```
 $r = 10 \times 10^{-9};$             Radius of a MWCNT
```

```
 $em = 21;$             dielectric constant (Permittivity) of Acetone
```

$sm = 100 \times 10^{-12}$; conductivity of Acetone (T = 25 deg C)

$ep = 3.9$; dielectric constant (Permittivity) of MWCNT

$sp = 1 \times 10^8$; conductivity of MWCNT (T = 25deg)C)

for $w = 0.1:0.1:9$

$ep_1(\text{round}(10 * w)) = ep - (sp/(10^{(w+1)})) * j$;

$em_1(\text{round}(10 * w)) = em - (sm/(10^{(w+1)})) * j$;

$K1(\text{round}(10 * w)) = ((ep_1(\text{round}(w * 10)) - em_1(\text{round}(10 * w)))/(ep_1(\text{round}(w * 10)) + 2 * em_1(\text{round}(10 * w))))$; Calculating Clausius-Mossotti K(w) factor

$w1(\text{round}(10 * w)) = 10^{(w+1)}$;

end

$K1$; $R1 = \text{real}(K1)$; $I1 = \text{imag}(K1)$;

$C = 1.5 * pi * r^2 * em * R1$; The constant terms in the developed force model (WX-Formula)

$C1 = -3 * pi * r^2 * em * I1$; The constant terms in the developed torque model (WX-Formula)

$\text{syms } x$; Symbolic declaration

$a = 2$; $b = 0.5E - 6$;

$y = a * x + b$; Function definition in the force model derivation

$yd = \text{diff}(y, x)$; Derivative of y in the force model derivation

$EE = ((2 * V_0^2)/d^3) * \text{sqrt}((x^2 + y^2))$; E-field Gradient function for force calculation

$ET = (V_0^2/d^2) * (x^2 + y^2)$; E-field for Torque calculation

```

    S = sqrt(1 + yd2);
    F = int(S * EE, x, x0, xL);
    F1 = C * F; F1 = double(F1);      Total DEP Force on CNTs
    T = int(S * (abs(ET))2, x, x0, xL); T1 = C1 * T;
    T1 = double(T1);      Total Torque on CNT (Electro-rotation)

```

Check if solution is numeric

```

isnumeric(F1);      To check whether F1 is numeric
isnumeric(T1);      To check whether T1 is numeric

```

Plotting the DEP Force Result

```

figure(1)
plot(w1,F1)
grid on
xlabel(Frequency (Hz)),   ylabel(FDEP (N))
title (Dielectrophoretic Force for developed model)

```

Plotting the Electrorotation (Torque) Result

```

figure(2)
plot(w1,T1,)
grid on
colormap(hsv);
xlabel(Frequency (Hz)),   ylabel(Torque (Nm))
title (Torque (Electrorotation) on CNT)

```

APPENDIX B

Matlab Simulation Code for Rotation Motion of Carbon Nanotubes In Acetone

Rotational motion function gets called in main function for simulation.

```
function xp = CNT(t,x)

format(long)
xp = zeros(2,1);
ke = 6.586782492084132E - 11;
V = 2;           Applied potential for MWCNT
gap = 2.0 × 10-6;   Gap between electrode
dia = 20 × 10-9;   Diameter of MWCNT
L = 2 × 10-6;     Length of CNT
x0 = dia/2;  y0 = dia/2;   Initial position of CNT on micro electrode
C1 = 1.353 × 10-14;   Maximum which is at 2MHz
```

$\eta = 300 \times 10^{-6}$; Viscosity of Acetone

$m = 20 \times 10^{-9}$; Mass of CNT

$I = (1/12) * m * L^2$; Moment of inertia for a long thin rod (CNT)

$k = (\pi * \eta * L^3) / (3 * (\log(L/(dia/2))))$; Rotational friction coefficient

Based on the chosen electric field function and the analysis of the input torque, (Torque due to electrorotation), we get the following.

$$A1 = (C1 * V^2) / (3 * k_e^2);$$

$$A2 = 3 * L^2 * x_0;$$

$$A3 = 3 * L^2 * y_0;$$

$$A4 = 3 * L * (x_0^2 + y_0^2);$$

The analysis of derived rotational motion equation in Chapter 3 produces the following terms.

$$a0 = (L * k) / (2 * I);$$

$$a1 = (A1 * L^3) / I;$$

$$a2 = (A1 * A2) / I;$$

$$a3 = (A1 * A3) / I;$$

$$a4 = (A1 * A4) / I;$$

Numerical solutions to the differential equation

$$xp(1) = x(2);$$

$$xp(2) = -a0 * x(2) + (a1 + a2) * (\cos(x(1)))^3 + a3 * \sin(x(1)) * (\cos(x(1)))^2 + a4 * \cos(x(1));$$

Main Function

`format (long)`

`tspan = linspace(0, 2, 1000);` 0-3seconds, with 5000 points

`x0 = [pi/4; 0];` Initial Conditions (rotation angle, rotation velocity)

`[t, x] = ode23tb(@CNT, tspan, x0);` Matlab built in ode solver

Author's Publications

1. U.C. Wejinya, Ning Xi, Yantao Shen, and King Wai Chiu Lai, An Efficient Approach of Handling and Deposition of Micro and Nano Entities Using Sensorized Microfluidic End-Effector System, *Sensor and Actuators A: Physical*, Accepted for publication, 2007.
2. Yantao Shen, U.C. Wejinya, Ning Xi and Craig A. Pomeroy, Force Measurement and Mechanical Characterization of Living Drosophila Embryos for Human Medical Study, *Journal of Engineering in Medicine, Part H*, 221(2):99-112, January 2007.
3. Jiangbo Zhang, Ning Xi, Guangyong Li, Hohin Chan, and Wejinya, U.C., Adaptable End Effector for Atomic Force Microscopy Based Nanomanipulation. *IEEE Transactions on Nanotechnology*, 5(6), November 2006.
4. Yantao Shen, Eric Winder, Ning Xi, Craig A. Pomeroy, and Wejinya, U.C., Closed Loop Optimal Control Enabled Piezoelectric Micro-Force Sensors, *IEEE/ASME Transactions on Mechatronics*, 11(4), August 2006.
5. Wejinya, U.C., Ning Xi, Yantao Shen, and King Wai Chiu Lai, Modeling and Control of Carbon Nanotube Orientation for Nano Assembly, *Applied Physics Letters*, in preparation, 2007.
6. Wejinya, U.C., Yantao Shen, Ning Xi, and King Wai Chiu Lai, Dynamic Modeling of Rotational Motion of Carbon Nanotubes for Intelligent Manufacturing of CNT-Based Devices, *Proceedings of the 2007 IEEE/RSJ International Conference on Intelligent Robots and Systems*, 29 October - 2 November 2007.
7. Wejinya, U.C., Yantao Shen, Ning Xi, and King Wai Chiu Lai, Modeling Dielectrophoretic Force for Manipulating Carbon Nanotubes (CNTs), *Proceedings of the 2007 IEEE/ASME International Conference on Advanced Intelligent Mechatronics*, Zürich, Switzerland, September 2007
8. Wejinya, U.C., Yantao Shen, Ning Xi, and King Wai Chiu, Controlling the Orientation of Carbon Nanotubes in Nano Assembly, *The 7th IEEE International Conference on Nanotechnology*, Hong Kong, China, August 2007.

9. Wejinya, U.C., Yantao Shen, Ning Xi, and Fathi Salem, Force Measurement of Embryonic System Using In Situ PVDF Piezoelectric Sensor, *The 2006 IEEE International Midwest Symposium on Circuits and Systems Proceedings*, San Juan, Puerto Rico, August 2006.
10. Wejinya, U.C., Yantao Shen, Ning Xi, and Jiangbo Zhang, Microfluidic End Effector for Manufacturing of Nano Devices, *Proceedings of the 2006 IEEE International Conference on Robotics and Automation*, Orlando, FL, May 2006.
11. Wejinya, U.C., Yantao Shen, Ning Xi, and Eric Winder, Development of Pneumatic End Effector for Micro Robotic Manipulators, *Proceedings of the 2005 IEEE/ASME International Conference on Advanced Intelligent Mechatronics*, Monterey, CA, July 2005.
12. Yantao Shen, Wejinya, U.C., Ning Xi, Craig A. Pomeroy and Zhun Fan, Characterization of Living Drosophila Embryos Using Micro Robotic Manipulation System, *Proceedings of the 2006 IEEE/RSJ International Conference on Intelligent Robots and Systems*, Beijing, China, October 2006.
13. Yantao Shen, Ning Xi, Wejinya, U.C., Wen J. Li, and Jizhong Xiao, Infinite Dimension System Approach for Hybrid Force/Position Control in Micromanipulation, *Proceedings of the 2004 IEEE International Conference on Robotics and Automation*, New Orleans, LA, April 2004.
14. Yantao Shen, Ning Xi, Wejinya, U.C., and Wen J. Li, High Sensitivity 2-D Force Sensor for Assembly of Surface MEMS Devices, *Proceedings of the 2004 IEEE/RSJ International Conference on Intelligent Robots and Systems*, Sendai, Japan, September 28-October 2, 2004.
15. Yantao Shen, Ning Xi, Craig Pomeroy, Wejinya, U.C., and Wen J. Li, An Active Micro-Force Sensing System with Piezoelectric Servomechanism, *Proceedings of the 2005 IEEE/RSJ International Conference on Intelligent Robots and Systems*, Edmonton, Alberta, Canada, August 2005.
16. Eric Winder, Yantao Shen, Ning Xi, Wejinya, U.C., and Craig Pomeroy, Optimal Control Based Active Force Sensing System for Micromanipulation, *Proceedings of the 2005 IEEE/ASME International Conference on Advanced Intelligent Mechatronics*, Monterey, CA, July 2005.
17. King Wai Chiu Lai, Ning Xi, Wejinya, U.C., Yantao Shen, and Wen J. Li, Automated Robotic Deposition System for Manufacturing Nano Devices, *Proceedings of the 2007 IEEE/RSJ International Conference on Intelligent Robots and Systems*, 2007.
18. Blank Sebastian, Yantao Shen, Ning Xi, and Wejinya, U.C., High Precision PSD Guided Robot Localization: Design, Mapping, and Position Control, *Proceedings of the 2007 IEEE/RSJ International Conference on Intelligent Robots and Systems*, 2007.

19. King Wai Chiu Lai, Ning Xi, and Wejinya, U.C., Automated Process for Manufacturing Single Carbon Nanotube Based Nano Devices, *The 7th IEEE International Conference on Nanotechnology*, Hong Kong, China, August 2007.

BIBLIOGRAPHY

- [1] Flymove, <http://flymove.uni-muenster.de/stages/stgtabelle.html>.
- [2] <http://www.cnanotech.com>.
- [3] Fumihito Arai, Daisuke Andou, Yukio Nonoda, Toshio Fukuda, Hitoshi Iwata, and Kouichi Itoigawa. Integrated microendeffector for micromanipulation. *IEEE/ASME Transactions on Mechatronics*, 3:17–23, March 1998.
- [4] R. S. Fearing. Survey of sticking effects for micro parts handling. In *Proc. IEEE/RSJ Int. Conf. on Intelligent Robots and Systems*, pages 212–217, Pittsburgh, PA, August 1995.
- [5] Yantao Shen, Ning Xi, U. C. Wejinya, Wen J. Li, and Jizhong Xiao. Infinite dimension system approach for hybrid force/position control in micromanipulation. In *Proc. IEEE Int. Conf. on Robotics and Automation*, pages 2912–2917, New Orleans, LA, April 2004.
- [6] Y.T. Shen, N. Xi, and Wen J. Li. Force guided assembly of micro mirrors. In *Proc. IEEE/RSJ Int. Conf. on Intelligent Robots and Systems*, volume 3, pages 2149–2154, 2003.
- [7] Yantao Shen, Ning Xi, U.C. Wejinya, and Wen J. Li. High sensitivity 2-d force sensor for assembly of surface mems devices. In *Proc. of the IEEE/RSJ International Conference on Intelligent Robots and Systems*, volume 4, pages 3363–3368, Sendai, Japan, September 2004.
- [8] Uchekukwu C. Wejinya, Yantao Shen, Ning Xi, and Fathi Salem. Force measurement of embryonic system using in situ pvdv piezoelectric sensor. In *Proc. IEEE International Midwest Symposium on Circuits and Systems Proceedings*, San Juan, Puerto Rico, August 2006.
- [9] H. Van Brussel, J. Peirs, D. Reynaerts, A. Delchambre, G. Reinhart, N. Roth, M. Weck, and E. Zussman. Assembly of microsystems. *Annals of the CIRP*, 49:451–472, 2000.
- [10] J. Peirs. *Design of micromechatronic systems: scalelaws, technologies, and medical applications*. PhD thesis, K.U. Leuven, Leuven, Belgium, 2001.

- [11] Wolfgang Zesch, Markus Brunner, and Ariel Weber. Vacuum tool for handling microobjects with a nanorobot. In *Proc. IEEE Int. Conf. on Robotics and Automation*, pages 1761–1766, Albuquerque, New Mexico, April 1997.
- [12] Fumihito Arai, Daisuke Ando, and Toshio Fukuda. Micro manipulation based on micro physics. In *Proc. IEEE/RSJ Int. Conf. on Intelligent Robots and Systems*, pages 236–241, Pittsburgh, PA, August 1995.
- [13] T. Sato, K. Koyano, M. Nakao, and Y. Hatamura. Novel manipulator for micro object handlings as interface between micro and human worlds. In *Proc. IEEE/RSJ Int. Conf. on Intelligent Robots and Systems*, volume 3, pages 1674–1681, 1993.
- [14] B. Nelson, Y. Zhou, and B. Vikramaditya. Sensor-based micro-assembly of hybrid mems devices. *IEEE Control System Magazine*, 16:35–45, 1998.
- [15] Liu Min, Peng Gang, and Huang Xin-han. Research on vacuum micro-tool for handling micro-target. *O.I. Automation*, 4:9–12, 2002.
- [16] G. Greitmann and R. Buser. Tactile microgripper for automated handling of microparts. In *8th Int. Conf. on Solid-State Sensors and Actuators*, pages 372–375, Stockholm, Sweden, June 1995.
- [17] H. Miyazaki. Fabrication of three-dimensional micro structures by heaping up fine particles. In *Proc. of 72nd Annual Spring Meeting*, pages 273–276, 1995.
- [18] K.T. Brown and D.G. Flaming. *Advanced Micropipette Techniques for Cell Physiology*. John Wiley and Sons, Inc., New York, New York, USA, 1986.
- [19] Masuyaki N. and Kazuhisha I. *et al.* Prototypes of non-tweezing handling tools with releasing mechanisms. *Trans. of Japan Soc. of Mech. Engineers, C*, 6:1021–1026, 1995.
- [20] Uchechukwu C. Wejinya, Yantao Shen, Ning Xi, and Eric Winder. Development of pneumatic end effector for micro robotic manipulators. In *Proc. IEEE/ASME Int. Conf. on Advanced Intelligent Mechatronics*, pages 558–563, Monterey, CA, July 2005.
- [21] Uchechukwu C. Wejinya, Yantao Shen, Ning Xi, , and Jiangbo Zhang. Microfluidic end effector for manufacturing of nano devices. In *Proc. IEEE Int. Conf. on Robotics and Automation*, pages 1384–1389, Orlando, FL, May 2006.
- [22] D.M. Schaefer, R. Reifenberger, A. Patil, and R.P. Andres. Fabrication of two-dimensional arrays of nanometer-size clusters with the atomic force microscope. *Appl. Phys. Lett.*, 66:1012–1014, 1995.

- [23] T. Junno, K. Deppert, L. Montelius, and L. Samuelson. Controlled manipulation of nanoparticles with an atomic force microscope. *Appl. Phys. Lett.*, 66:3627–3629, 1995.
- [24] A.A.G. Requicha, C. Baur, A. Bugacov, B.C. Gazen, B. Koel, A. Madhukar, T.R. Ramachandran, R. Resch, and P. Will. Nanorobotic assembly of two-dimensional structures. In *Proc. IEEE Int. Conf. Robotics and Automation*, pages 3368–3374, Leuven, Belgium, May 1998.
- [25] L.T. Hansen, A. Kuhle, A.H. Sorensen, J. Bohr, and P.E. Lindelof. A technique for positioning nanoparticles using an atomic force microscope. *Nanotechnology*, 9:337–342, 1998.
- [26] G. Binnig, C.F. Quate, and C. Gerber. Atomic force microscope. *Phys. Rev. Lett.*, 56:930–933, 1986.
- [27] Guangyong Li, Ning Xi, Heping Chen, Craig Pomeroy, and Mathew Prokos. Videolized atomic force microscopy for interactive nanomanipulation and nanoassembly. *IEEE Trans. on Nanotechnology*, 4:605–614, September 2005.
- [28] G.Y. Li, N. Xi, and M. Yu. Development of augmented reality system for afm based nanomanipulation. *IEEE/ASME Trans. on Mechatronics*, 9:199–211, June 2004.
- [29] S.C. Terry, J.H. Jerman, and J.B. Angell. A gas chromatographic air analyzer fabricated on a silicon wafer. *IEEE Trans. Electron Devices*, ED:1880–1886, 1979.
- [30] M.J. Zdeblick, P.W. Barth, and J.A. Angell. Microminiature fluidic amplifier tech. *Digest IEEE Solid-State Sensor and Actuator Workshop*, 1986.
- [31] E. Bassous, H.H. Taub, and L. Kuhn. Ink jet printing nozzle arrays etched in silicon. *Appl. Phys. Lett.*, 31:135–137, 1977.
- [32] K.E. Pertersen. Fabrication of an integrated planar silicon ink-jet structure. *IEEE Trans. Electron Devices*, ED:1918–1920, 1979.
- [33] K.E. Pertersen. Silicon as a mechanical material. *Proc. IEEE*, pages 420–457, 1983.
- [34] Jerry Ok, Milton Chu, and C.-J. Kim. Pneumatically driven microcage for micro-objects in biological liquid. In *Proc. IEEE Micro Electro Mechanical Systems Workshop*, pages 459–463, Orlando, Florida, USA, February 1999.
- [35] Junghoon Lee and C.-J. Kim. Surface-tension-driven microactuation based on continuous electrowetting. *Microelectromechanical Systems*, 9:171–180, 2000.

- [36] Ching-Yao Chen and Eckart Meiburg. Miscible displacement in capillary tubes: Influence of Korteweg stresses and divergence effects. *Journal of Fluid Mechanics*, 14:2052–2058, 2002.
- [37] A. Hatch, A.E. Kamholz, G. Holman, P. Yager, and K. F. Böhringer. A ferrofluidic magnetic micropump. *Journal of Microelectromechanical Systems*, 10, June.
- [38] L.J. Yang, T.J. Yao, and Y.C. Tai. Matching velocity of capillary menisci in microchannels. *J. Micromech. Microeng.*, 14:220–225, 2004.
- [39] Sumio Iijima. Helical microtubules of graphitic carbon. *Nature*, 354:56–58, 1991.
- [40] Toshio Fukuda, Fumihito Arai, and Lixin Dong. Assembly of nanodevices with carbon nanotubes through nanorobotic manipulations. *Proceedings of the IEEE*, 91:1803–1818, 2003.
- [41] Norikazu Arima and Akihito Matsumuro. High-aspect-ratio nanofabrication using carbon nanotube probe in scanning tunneling microscope. In *Proc. IEEE International Symposium on Micro-NanoMechatronics and Human Science*, pages 175–180, Nagoya, Japan, November 2005.
- [42] S.S. Wong, A.T. Woolley, T.W. Odom, J.L. Huang, P. Kim, D.V. Vezenov, and C.M. Lieber. Single-walled carbon nanotube probes for high-resolution nanostructure imaging. *Appl. Phys. Lett.*, 73:3465–3467, 1998.
- [43] R. Martel, T. Schmidt, H.R. Shea, T. Hertel, and Ph. Avouris. Single- and multi-wall carbon nanotube field-effect transistors. *Appl. Phys. Lett.*, 73(17):2447–2449, 1998.
- [44] T. Hertel, R. Martel, and Ph. Avouris. Manipulation of carbon nanotubes and their interaction with surfaces. *J. Phys. Chem.*, B:910–915, 1998.
- [45] Sreeja B. Asokan, L. Jawerth, R. Lloyd Carroll, R.E. Cheney, S. Washburn, and R. Superfine. Two-dimensional manipulation and orientation of actin-myosin systems with dielectrophoresis. *Nano Letter*, 3:431–437, 2003.
- [46] X. Duan, Y. Huang, Q. Wei, and C.M. Lieber. Directed assembly of one-dimensional nanostructures into functional networks. *Science*, 291(5504):603–633, January. 2001.
- [47] Maria Dimaki and Perter Bøggild. Dielectrophoresis of carbon nanotubes using microelectrodes: a numerical study. *Nanotechnology*, 15(8):1–8, June 2004.

- [48] K. Yamamoto, S. Akita, and Y. Nakayama. Orientation and purification of carbon nanotubes using ac electrophoresis. *J. Phys. D.*, 31:L34–L36, 1998.
- [49] K. Yamamoto, S. Akita, and Y. Nakayama. Orientation of carbon nanotubes using electrophoresis. *Jpn. J. Appl. Phys.*, 35:L917–L918, 1996.
- [50] F. Wakaya, T. Nagai, and K. Gamo. Position control of carbon nanotube using patterned electrode and electric field. *Microelectronic Engineering*, 63:27–31, 2002.
- [51] X.Q. Chen, T. Saito, H. Yamada, and K. Matsushige. Aligning single-wall carbon nanotubes with an alternating-current electric field. *Appl. Phys. Lett.*, 78:3714–3716, 2001.
- [52] R. Krupke, F. Hennrich, H.B. Weber, D. Beckmann, O. Hampe, S. Malik, M.M. Kappes, and H. von Loehneysen. Contacting single bundles of carbon nanotubes with alternating electric fields. *Appl. Phys. A: Materials Science & Processing*, 76:397–401, 2003.
- [53] L.A. Nagahara, I. Amlani, J. Lewenstein, and R.K. Tsui. Directed placement of suspended carbon nanotubes for nanometer-scale assembly. *Appl. Phys. Lett.*, 80:3826–3828, 2002.
- [54] Blanca H. Lapizco-Encinas, Blake A. Simmons, Eric B. Cummings, and Yolanda Fintschenko. Dielectrophoretic concentration and separation of live and dead bacteria in an array of insulators. *Anal. Chem.*, 76:1571–1579, 2004.
- [55] Ji-Eun Kim and Chang-Soo Han. Use of dielectrophoresis in the fabrication of an atomic force microscope tip with a carbon nanotube: a numerical analysis. *Nanotechnology*, 16(10):2245–2250, 2005.
- [56] Jean-Marc Bonard, Thierry Stora, Jean-Paul Salvetat, Frédéric Maier, Thömas Stöckli, Claus Duschl, László Forró, Walt A. de Heer, and André Chätelain. Purification and size-selection of carbon nanotubes. *Advanced Materials*, 9:827–831, 1997.
- [57] M. Zheng *et al.* Structure-based carbon nanotube sorting by sequence-dependent dna assembly. *Science*, 302:1545–1548, November 2003.
- [58] R. Krupke, F. Hennrich, H.V. Löhneysen, and M.M. Kappes. Separation of metallic from semiconducting single-walled carbon nanotubes. *Science*, 301:344–347, July 2003.
- [59] <http://nobelprize.org/medicine/laureates/1995/press.html>, October 1995.

- [60] G.M. Rubin and E.B. Lewis. A brief history of drosophila's contributions to genome research. *Science*, 287(5461):2216–2218, March 2000.
- [61] G.M. Rubin and M.D. Yandell *et al.* Comparative genomics of the eukaryotes. *Science*, 287(5461):2204–2215, March 2000.
- [62] M.B. Feany and W.W. Bender. A drosophila model of parkinson's disease. *Nature*, 404(6776):394–398, March 2000.
- [63] H.I. Wan, A. DiAntonio, R.D. Fetter, K. Bergstrom, R. Strauss, and C.S. Goodman. Highwire regulates synaptic growth in drosophila. *Neuron*, 26(2):313–329, May 2000.
- [64] <http://ceolas.org/vl/fly/intro.html>, 2005.
- [65] R.W. Bernstein and A. Dragland. Microsurgery on fruit-fly embryos. In *Features, GEMINI 2002/2003, Web Edition*. <http://www.ntnu.no/gemini/2002-06e/40-42.htm>, 2005.
- [66] Y. Kimura and R. Yamagimachi. Intracytoplasmic sperm injection in the mouse. *Biology of Reproduction*, 52(4):709–720, April 1995.
- [67] Y. Sun, Kai-Tak Wan, K.P. Roberts, J.C. Bischof, and Bradley J. Nelson. Mechanical property characterization of mouse zona pellucida. *IEEE Transactions on Nanobioscience*, 2(4):279–286, December 2003.
- [68] A.S. Fiorillo. Design and characterization of a pvdf ultrasonic range sensor. *IEEE Transactions on Ultrasonics, Ferroelectrics, and Frequency Control*, 39:688–692, 1992.
- [69] G.M. Sessler and A. Berraissoul. Tensile and bending piezoelectricity of single-film pvdf monomorphs and bimorphs. *IEEE Transactions on Electrical Insulation*, 24:249–254, 1989.
- [70] Y. Roh, V. V. Varadan, and V. K. Varadan. Characterization of all the elastic, dielectric, and piezoelectric constants of uniaxially oriented poled pvdf films. *IEEE Transactions on Ultrasonics, Ferroelectrics, and Frequency Control*, 49(6):836–846, 2002.
- [71] Deok-Ho Kim, Yu Sun, Seok Yun, Byungkyu Kim, Chang Nam Hwang, Sang Ho Lee, and Bradley J. Nelson. Mechanical property characterization of the zebrafish embryo chorion. In *Proc. of the 26th Annual International Conference of the IEEE EMBS*, pages 5061–5064, San Fransisco, CA, USA, September 2004.

- [72] S. Fahlbush and S. Fatikow. Micro force sensing in a micro robotic system. In *Proc. IEEE Int. Conf. on Robotics and Automation*, pages 3435–3440, 2001.
- [73] Charlotte C.H. Kwong, King W.C. Lai, Ruiguang Yan, and Wen J. Li. Kwong-li probes: Novel nano-probes for biological dissection and injection. In *Proc. of the IEEE/ASME International Conference on Advanced Intelligent Mechatronics*, pages 897–901, Port Island, Kobe, Japan, July 2003.
- [74] X.J. Zhang, S. Zappe, R.W. Bernstein, O. Sahin, C.-C. Chena, M. Fish, M.P. Scott, and O. Solgaard. Micromachined silicon force sensor based on diffractive optical encoders for characterization of micro injection. *Sensors and Actuators A*, 114(2):197–203, April 2004.
- [75] Imad Elhajj, Mengmeng Yu, BooHeon Song, Ning Xi, Wang-Tai Lo, and Yun-Hui Liu. Transparency and synchronization in supermedia enhanced internet-based teleoperation. In *Proc. of the IEEE International Conference on Robotics and Automation*, pages 2713–2718, Washington, D.C., USA, May 2002.
- [76] H. Krupp. Particle adhesion theory and experiment. *Advances in Colloid and Interface Science*, 1:111–239, 1967.
- [77] R.A. Bowling. A theoretical review of particle adhesion. In *K. L. Mittal, editor, Particles on Surfaces 1: Detection, Adhesion and Removal*, 1:129–142, 1988.
- [78] T.B. Jones. *Electromechanics of Particles*. Cambridge University Press, Cambridge, UK, 1995.
- [79] J.N. Israelachvili. The nature of van der waals forces. *Contemp. Physics*, 15:159–177, 1974.
- [80] R.L. Alley, G.J. Cuan, R.T. Howe, and K. Komvopoulos. The effect of release-etch processing on surface microstructure stiction. In *Proc. Solid State Sensor and Actuator Workshop*, pages 202–207, Hilton Head Island, SC, June 1992.
- [81] A. Torii, M. Sasaki, K. Hane, and S. Okuma. Adhesive force distribution on microstructures investigated by an atomic force microscope. *Sensors and Actuators A-Physical*, 42(2):153–158, August 1994.
- [82] Micro total analysis systems. Enschede, The Netherlands, May 2000. Kluwer Academic.
- [83] R. B. Bird. *Transport Phenomena*. John Wiley and Sons, Inc., New York, New York, USA, 1960.
- [84] Stanley Middleman. *An Introduction to Fluid Dynamics*. John Wiley and Sons, Inc., New York, New York, USA, 1997.

- [85] <http://www.udel.edu/pchem/c446/experiments/exp1.pdf>.
- [86] Bruce R. Munson, Donald F. Young, and Theodore H. Okiishi. *Fundamentals of Fluid Mechanics*. John Wiley and Sons, Inc., New York, New York, USA, 1997.
- [87] <http://www.smallparts.com/>.
- [88] <http://www.knf.com/pdfs/nmp05.pdf>.
- [89] H.A. Pohl. *Dielectrophoresis: the behavior of neutral matter in nonuniform electric fields*. Cambridge University Press, Cambridge, UK, 1978.
- [90] Hywel Morgan and Nicolas G. Green. *AC Electrokinetics: colloids and nanoparticles*. Research Studies Press Ltd, Hertfordshire, England, 2003.
- [91] A. Ramos, H. Morgan, N.G. Green, and A. Castellanos. Ac electrokinetics: a review of forces in microelectrode structures. *J. Phys. D: Appl. Phys.*, 31:2338–2353, September 1998.
- [92] H. Morgan, M.P. Hughes, and N.G. Green. Separation of submicron bioparticles by dielectrophoresis. *Biophys. J.*, 77(1):516–525, July 1999.
- [93] Yu-Guo Tao, W.K. den Otter, J.K.G. Dhont, and W.J. Briels. Isotropic-nematic spinodals of rigid long thin rodlike colloids by event-driven brownian dynamics simulations. *J. Chem. Phys.*, 124:1–10, 2006.
- [94] M. Doi and S.F. Edwards. *The Theory of Polymer Dynamics*. Clarendon Press, Oxford, UK, 1986.
- [95] J.K.G. Dhont. *An Introduction to Dynamics of Colloids*. Elsevier, Amsterdam, The Netherlands, 1996.
- [96] Braja M. Das, Aslam Kassimali, and Sedat Sami. *Engineering Mechanics: Statics*. Richard D. Irwin, Inc., Boston, USA, 1994.
- [97] ANS/IEEE Standard, New York, USA. *An American National Standard: IEEE Standard on Piezoelectricity*, September 1987.
- [98] Leonard Meirovitch. *Elements of Vibration Analysis*. McGraw-Hill Education, New York, USA, May 1975.
- [99] Version 1.3 Measurement Computing. <http://www.measurementcomputing.com>, June 2006.

- [100] A. Bicchi and A. Caiti D. Prattichizzo. Dynamic force/torque sensors: Theory and experiments. In *Proc. of the IEEE Conference on Advanced Robotics*, pages 727–732, Monterey, CA, USA, July 1997.
- [101] M.S. Weinberg. Working equations for piezoelectric actuators and sensors. *IEEE Journal of Microelectromechanical Systems*, 8(4):529–533, 1999.
- [102] Measurement Specialties Inc. *Piezo Film Sensors Technical Manual*, newblock internet version edition, August 1998.
- [103] W.H. Bowes, L.T. Russell, and G.T. Suter. *Mechanics of Engineering Materials*. John Wiley and Sons, Inc., New York, New York, USA, 1984.
- [104] Y. Huang and R. Pethig. Electrode design for negative dielectrophoresis. *Meas. Sci. Technol.*, 2:1142–1146, December 1991.
- [105] Capillary tubing. *Data Sheet. L022-D. FHC Inc. www.fh-co.com/010300*, pages 14–15.
- [106] Yu Zhou, Bradley J. Nelson, and Barmeshwar Vikramaditya. Fusing force and vision feedback for micromanipulation. In *Proc. of the IEEE International Conference on Robotics and Automation*, pages 1220–1225, Leuven, Belgium, May 1998.
- [107] Akihito Sano, Hideo Fujimoto, and Toshihito Takai. Human-centered scaling in micro-teleoperation. In *Proc. of the IEEE International Conference on Robotics and Automation*, pages 380–385, Seoul, Korea, May 2001.
- [108] C. K. M. Fung, I. Elhajj, W.J. Li, and N. Xi. A 2-d pvd force sensing system for micro-manipulation and micro-assembly. In *Proc. IEEE Int. Conf. on Robotics and Automation*, pages 1489–1494, Washington D.C., May 2002.
- [109] King Wai Chiu Lai, Ning Xi, and U.C. Wejinya. Automated process for manufacturing single carbon nanotube based nano devices. In *Proc. IEEE Int. Conf. Nanotechnology*, Hong Kong, China, August 2007.
- [110] King Wai Chiu Lai, Ning Xi, U.C. Wejinya, Yantao Shen, and Wen J. Li. Automated robotic deposition system for manufacturing nano devices. In *Proc. IEEE/RSJ Int. Conf. Intelligent Robots and Systems*, San Diego, CA, 2007.

MICHIGAN STATE UNIVERSITY LIBRARIES



3 1293 02956 0525